PONTIFICIA UNIVERSIDAD CATOLICA DE CHILE

ESCUELA DE INGENIERIA

DESIGN OF SOLAR POND FOR WATER PREHEATING USED IN THE COPPER CATHODES WASHING PROCESS AT SPENCE MINE

FELIPE JAVIER GARRIDO GONZALEZ

Thesis submitted to the Office of Research and Graduate Studies in partial fulfillment of the requirements for the Degree of Master of Science in Engineering

Advisor:

JULIO VERGARA AIMONE

Santiago de Chile, (December, 2012)

PONTIFICIA UNIVERSIDAD CATOLICA DE CHILE
ESCUELA DE INGENIERIA

DESIGN OF SOLAR POND FOR WATER PREHEATING USED IN THE COPPER CATHODES WASHING PROCESS AT SPENCE MINE

FELIPE JAVIER GARRIDO GONZALEZ

Members of the Committee:

JULIO VERGARA AIMONE

RODRIGO PASCUAL JIMENEZ

JOSE HERNAN GARCIA

HECTOR JORQUERA GONZALEZ

Thesis submitted to the Office of Research and Graduate Studies in partial fulfillment of the requirements for the Degree of Master of Science in Engineering

Santiago de Chile, (December, 2012)

"The greatest challenge to any thinker
is stating the problem in a way that
will allow a solution."

Bertrand Russell

ACKONWLEDGMENTS

I would like to express my gratitude towards my family and especially my parents, Mario and Silvia, for their love and the unconditional support they have given me throughout this process.

I would like to thank my supervisor, Dr. Julio Vergara, for his wise advise, excellent disposition and for believing in my work. I would like to acknowledge JHG Ingeniería Ltda. for sharing valuable information for the development of this thesis.

And at last but not least, I would also like to thank Fabian Cadiz, Matias Salas, Dennis Dunlop, Mario Abarca, Philipp Kanehl, Juan Guillermo Vidal and Rodrigo Soto for always being there to share a talk, their thoughts on a matter, to aid in moments of difficulty or simply for being my friends.

Felipe Garrido

TABLE OF CONTENTS

ACKNOWLEDGEMENTS **I**

LIST OF TABLES **V**

LIST OF FIGURES **VI**

ABSTRACT **IX**

RESUMEN **X**

1 INTRODUCTION **1**

1.1 Copper extractive processes . . . 2
1.2 Characterization of the energy demand of copper mining in Chile . . . 6
1.3 Electrowon copper cathodes . . . 12
1.4 Spence Mine . . . 12
1.5 Solar pond technology: State of the art . . . 14
1.6 Objectives . . . 18
1.7 Organization of the thesis . . . 19

2 SOLAR POND MODEL **21**

2.1 Insolation . . . 22
2.2 Radiation Absorption . . . 25
2.3 Solar Pond fluid dynamics . . . 26
2.3.1 Balance Equations . . . 28

3 NUMERICAL SOLUTION FOR A ONE-ZONE MODEL **32**

3.1 Boundary conditions . . . 34
3.1.1 NCZ boundary conditions . . . 34
3.1.2 Solar pond boundary conditions . . . 35
3.2 Numerical Modulation . . . 37
3.3 Time and space mesh . . . 39

3.4 Model validation 43
3.5 Model restrictions 44

4 DESIGN PARAMETERS **47**
4.1 Site Selection 47
4.2 Solar pond walls 47
4.3 Bottom and wall lining 50
4.4 Layers thickness 54
4.5 Salt gradient establishment 57
4.6 Salt and water 59
4.7 Heat extraction 60
4.8 Water circulation power 65
4.9 Solar pond monitoring and control 67
4.10 Solar pond maintenance 69
4.10.1 Salt gradient maintenance 69
4.10.2 Wind effects 75
4.10.3 Turbidity effects 76
4.11 Thermal efficiency 79

5 CASE STUDY AND PROPOSED DESIGN **80**
5.1 Case study 80
5.1.1 Internal heat exchanger design 80
5.1.2 Determination of the layers thicknesses 83
5.1.3 Required effective solar collecting surface area 85
5.1.4 Wall angle 86
5.1.5 Thermal insulation 88
5.2 Proposed solar pond design 88
5.2.1 Single versus modular configuration 89

6 RESULTS **92**
6.1 Predicted performance 92

6.2 Economical analysis 93
6.2.1 Investment Cost 93
6.2.2 Maintenance costs 96
6.2.3 Operational costs 97
6.2.4 Discounted cash flows 98
6.2.5 Sensitivity analysis 99

7 CONCLUSIONS 103

BIBLIOGRAPHY 106

APPENDICES 116

LIST OF TABLES

1 Energy consumption of the Chilean copper mining industry in 2010 7
2 Constants for the transmissivity function 26
3 Properties of common materials used for solar pond lining 53
4 Effect of adding an insulating layer to solar ponds close to the water table in the average temperature of the LCZ 53
5 Parameters used for Scanning injection technique at El Paso solar pond 58
6 Cost per meter of PP and PE tubes 65
7 IHE composed by 20 tubes for different diameters 82
8 IHE composed by 20 tubes for different diameters 83
9 Temperature range of the LCZ after the third year of operation for different thicknesses 84
10 Required surface area for different water table depth and outlet temperature for the third year of operation 86
11 Increment of volume and wall area of a solar pond due to slopping walls 87
12 Proposed solar pond design, single configuration, water table at 55 m deep 89
13 Performance of the solar pond design after seven years of operation 92
14 Investment cost of a solar pond with and without thermal insulation for different water table depths 95
15 Life cycle and energy cost of of the current process and with solar pond preheating 98
16 Base case DCF calculation 121
17 Single solar pond, open salt cycle DCF calculation 122
18 Single solar pond, closed salt cycle DCF calculation 123
19 Modular solar pond, open salt cycle DCF calculation 124
20 Modular solar pond, closed salt cycle DCF calculation 125

LIST OF FIGURES

1.1 Chilean refined copper exports by destination 2

1.2 Stages of Pyrometallurgy 3

1.3 Stages of Hydrometallurgy 5

1.4 Energy demand of copper mining in Chile 7

1.5 Chilean copper cathode production between 1995 and 2010 8

1.6 Greenhouse gas emissions and copper production of the Chilean copper mining industry 9

1.7 Daily average of solar radiation in northern Chile 11

1.8 Aerial view of Spence mine 13

1.9 Water heating system for EW cathode washing at Spence mine 14

1.10 Brine stratification in a Solar Pond 15

1.11 The Beith Ha'Arava solar pond, Israel 17

1.12 Solar Pond at El Paso, New Mexico 19

2.1 Phenomena that present in the behavior of a solar pond 21

2.2 Declination angle for an observer in the North hemisphere 23

2.3 The Hour angle 23

2.4 The Zenith or Incidence angle 24

2.5 Simulation of motion in a fluid at rest due to salt-finger phenomena. 27

3.1 Meassured data for Ambient Temperature at Spence for year 2010 and Fourier fitted curve 38

3.2 Solar radiation modeled for a summer and winter day 39

3.3 Discretization of the NCZ used for numerical resolution 40

3.4 Comparison of the simulated and measured LCZ temperature evolution of a solar pond 44

3.5 Predicted and recorded temperature profile of Los Alamos solar pond 45

4.1 Effect of depth of water table on maximum temperature of salt gradient solar pond. 48

4.2 Convective layer generated due to wall heating by Sun exposition 49

4.3 Scheme of angles used to calculate the NRI 49

4.4 Variation of yearly maximum NIP for different latitudes 51
4.5 Lining scheme for solar ponds developed in India 52
4.6 Growth of the upper-convective zone in a solar pond caused by wind and rain . . . 55
4.7 Circular diffuser design 59
4.8 Diffuser design used in the El Paso solar pond 59
4.9 In-pond heat exchanger (IHE) used at Pyramid Hill 61
4.10 Instrumentation tower at El Paso solar pond 68
4.11 Scanner used for monitoring procedures at El Paso solar pond 69
4.12 Evolution of salt concentration profile in the NCZ pond without maintenance . . . 70
4.13 Schematic of flows in a salt recycling system for gradient maintenance 71
4.14 Schematic of flows for gradient maintenance without salt recycling 74
4.15 Schematic view of the pond with three water zones, salt charger and surface washing system 75
4.16 Wind suppressors installed at Pyramid Hill solar pond, Australia 77
4.17 Collection efficiency versus turbidity levels in a solar pond 78
5.1 Interface created to facilitate the supervision of the simulation runs. 81
5.2 Outlet temperature of the water flow for different LCZ thicknesses. 84
5.3 Outlet temperature of the water flow for a 1.1 m thick LCZ. 85
5.4 Outlet temperature of the water flow for different solar pond surface area. 85
5.5 Normalized instability potential of solar pond wall angle at Spence 87
5.6 Proposed site for construction of a solar pond at Spence mine 90
5.7 Proposed modular setup for the solar pond 91
6.1 Prospected energy supply composition with a solar pond preheating stage during lifetime operation 93
6.2 Investment cost composition of single and modular solar pond configuration 95
6.3 LCC of the heating stage with solar pond for different scenarios of water price annual growth 100
6.4 LCC of the heating stage with solar pond for different scenarios of liner replacement frequency 101
6.5 LCC of the heating stage with solar pond for different learning stage lengths 102

A.1 Evolution of the Chilean electrical generation matrix between years 2000 and 2009 117
B.1 Closed and open cycle configurations for in-pond heat extraction method 118
C.1 Solar pond design, single configuration, drained 119
C.2 Solar pond design, modular configuration, filled 120

ABSTRACT

The Chilean copper industry is increasingly dependent on coal-generated electricity and diesel fuel for mining operations and therefore its associated green house emissions have experimented a significant growth in the late years, in addition to scarcity of less polluting energy sources. However, solar energy is breaking through in mining processes that require heating of fluids. At Spence mine, 6% of the national total of fine copper is produced for which 1,400 tonnes of diesel are burnt per year to heat up the water used only to wash the copper cathodes at the end of the electrowinning stage.

Solar ponds are a body of water that collect insolation and store it at the bottom as hot water due to the presence of a density gradient, which can be extracted to provide heat 24 hours per day, making them suitable for application with a constant demand. Considering the insolation conditions at Spence, the use of solar ponds is proposed to preheat the water flow used to wash the copper cathodes. In this thesis a solar pond has been designed taking into account the site conditions and energy demand. The pond resulted with an effective collecting area of 23,240 m^2 and a 1.8 m thick density gradient to prevent convection.

The design is simulated using site weather conditions. The predicted performance shows that it delivers up to 12,300 MWh-year on site, reducing the annual diesel consumption of this process in 77% with a collecting efficiency of 24%. As a result the emission of 3,300 tonnes of CO_2 is avoided and the cost of heat is reduced in 37.7%.

It can be concluded that solar ponds can reduce the fuel dependency and greenhouse emissions of the copper mining industry without compromising competitiveness. Future work should address the study of phenomena not considered in the theoretical model such as biological growth and ground vibrations caused by detonations at the mine.

Keywords: Solar pond, solar thermal energy, renewable energy, process heat.

RESUMEN

La minería chilena del cobre depende cada vez más en combustibles fósiles para la generación eléctrica y térmica y por lo tanto, sus emisiones de gases de efecto invernadero han aumentado significativamente en los últimos años, lo que se suma a la escasez de fuentes energéticas menos contaminantes. Sin embargo, la energía solar se está abriendo paso en procesos mineros que requieren calor de proceso. En la mina Spence, se produce el 6% de del cobre fino del país para lo cual se queman 1,400 toneladas de diésel sólo para calentar el agua con que se lavan los cátodos al final de la etapa de electroobtención.

Las pozas solares son cuerpos de agua que acumulan irradiación solar y la almacenan en el fondo en forma de calor debido a la presencia de un gradiente de densidad, el cual puede ser extraído para proveer de calor 24 horas, haciéndolo útil para procesos con demandas constantes. Considerando las condiciones de radiación solar en Spence, se propone el uso de pozas solares para precalentar el flujo de agua usado para lavar los cátodos. En esta tesis, se ha diseñado una poza, teniendo en cuenta las condiciones de sitio y demanda energética. El área de colección necesaria es de 23,240 m^2.

El desempeño previsto muestra que el diseño es capaz de entregar 12,300 MWh-año, reduciendo el consumo de diésel en 77% con una eficiencia de 24%. Como resultado, se evita la emisión de 3,300 toneladas CO_2 y reducción del costo de energía en 37.7%.

Se cuncluye que las pozas pueden reducir la dependencia de los combustibles y las emisiones de gases de efecto invernadero de la minera chilena del cobre sin comprometer competitividad. Trabajos futuros deberían considerar el estudio de fenómenos no incluídos en este trabajo como formación biológica y vibraciones de suelo producto de detonaciones en la mina.

Palabras clave: Poza solar, energía solar térmica, energía renovable, calor de proceso.

1. INTRODUCTION

Copper and copper-based alloys can be found in a wide range of applications for its multiple properties, some of them known by men for at least 10,000 years. Sumerians, Egyptians, Greeks, Romans and Chinese used copper and its alloys for decorative and utilitarian purposes. Its malleability and formability made it perfect for the production of coins, ornaments and utensils and its antimicrobial effect was no mystery for the Egyptians who used it to treat infections and sterilize water. During the Middle-Ages and Renaissance copper was used in the military for the fabrication of gun cannons and tools, in art for church bells and statuary (Davis, 2001). At the end of the XVIII century, with the discoveries related to electricity and magnetism, copper found new uses and played an important role during the Industrial Revolution. Its excellent current-conductivity makes copper not only the key of nowadays power transmission and generation, but also virtually an exclusive element used in data transmission and widely used in electronics, heat sinks and heat exchangers, automotive industry, plumbing and roofing and in biostatic surfaces (International Copper Study Group, 2010). The important role of copper in modern technology has led to doubling its consumption in the last fifty years totaling 22,000 billion of metric tonnes in 2009 (International Copper Study Group, 2010), positioning it as the third most demanded metal in the world, only behind of aluminum and steel (U.S. Geological Survey, 2010).

Driven by the Asian development and particularly that of China in the last decade (Figure 1.1), the increasing demand of copper has greatly benefited Chile, whose exports raised from 2,411 thousand of tonnes of fine copper (ktF) in 1995 to 5,442 ktF in 2010, positioning the country as the main producer in the world and responsible for one third of the total production (Ocaranza, 2011). Over the years this industry has grown in importance for the Chilean economy, tripling its gross domestic product (GDP) contribution in the last thirty years (Guajardo, 2011), now representing 17% of the total (Ocaranza, 2011).

Copper has been also the engine of development for mining–related manufacture and services sectors. Proof of it is that the regions in the country with copper mining as a main activity have

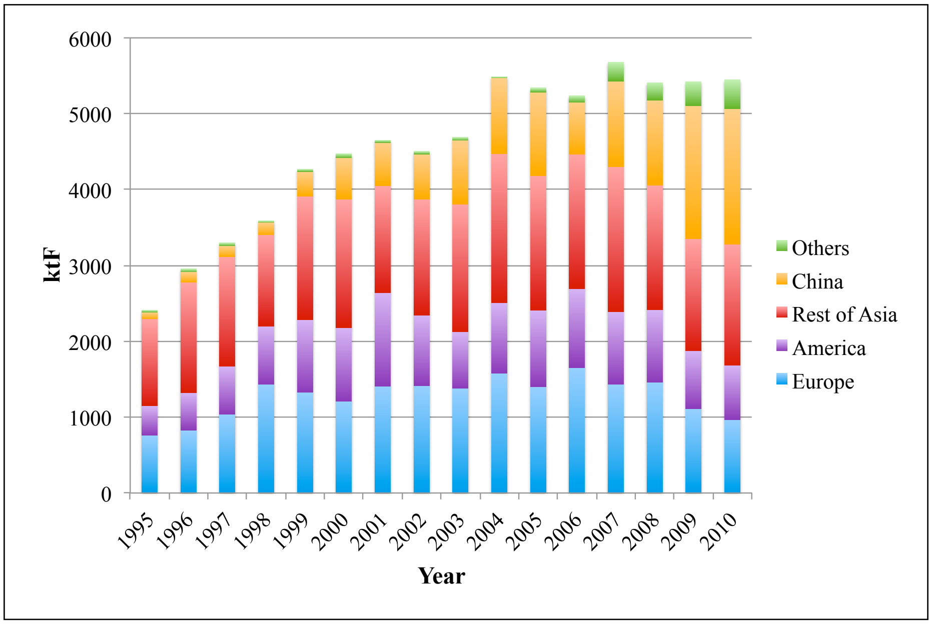

Figure 1.1: Chilean refined copper exports by destination (Ocaranza, 2011).

always been those with the greatest product growth since 1990, over those with manufacturing industry and agriculture as their main activity (Guajardo, 2011).

1.1. Copper extractive processes

Copper is present in nature in very small concentrations (0.5 – 2%) and therefore it has to be benefited to make it suitable for its final uses. The method used to extract the copper depends on the ore composition. The most common are the copper-iron-sulfide and copper-sulfide ores, from which nearly 80% of the world production of copper is obtained through an extraction process known as pyrometallurgy (PM) (Figure 1.2). In it, the concentration of copper is increased progressively by means of three consecutive stages: concentration, smelting and refining.

In the first stage, the Cu is separated from the waste minerals by froth flotation in which a solution of water and crushed ore are mixed in tanks with reagents driving the copper minerals (of about 20-30% purity) to the top and leaving the wastes in the bottom. In the second stage, the concentrate is smelted in a large furnace at 1250°C to obtain a molten high-Cu sulfide phase (50-70% Cu) known as matte. Later, the molten matte is converted (oxidized) in a furnace where iron and sulfur are removed, obtaining molten copper with a 99% concentration, known as impure

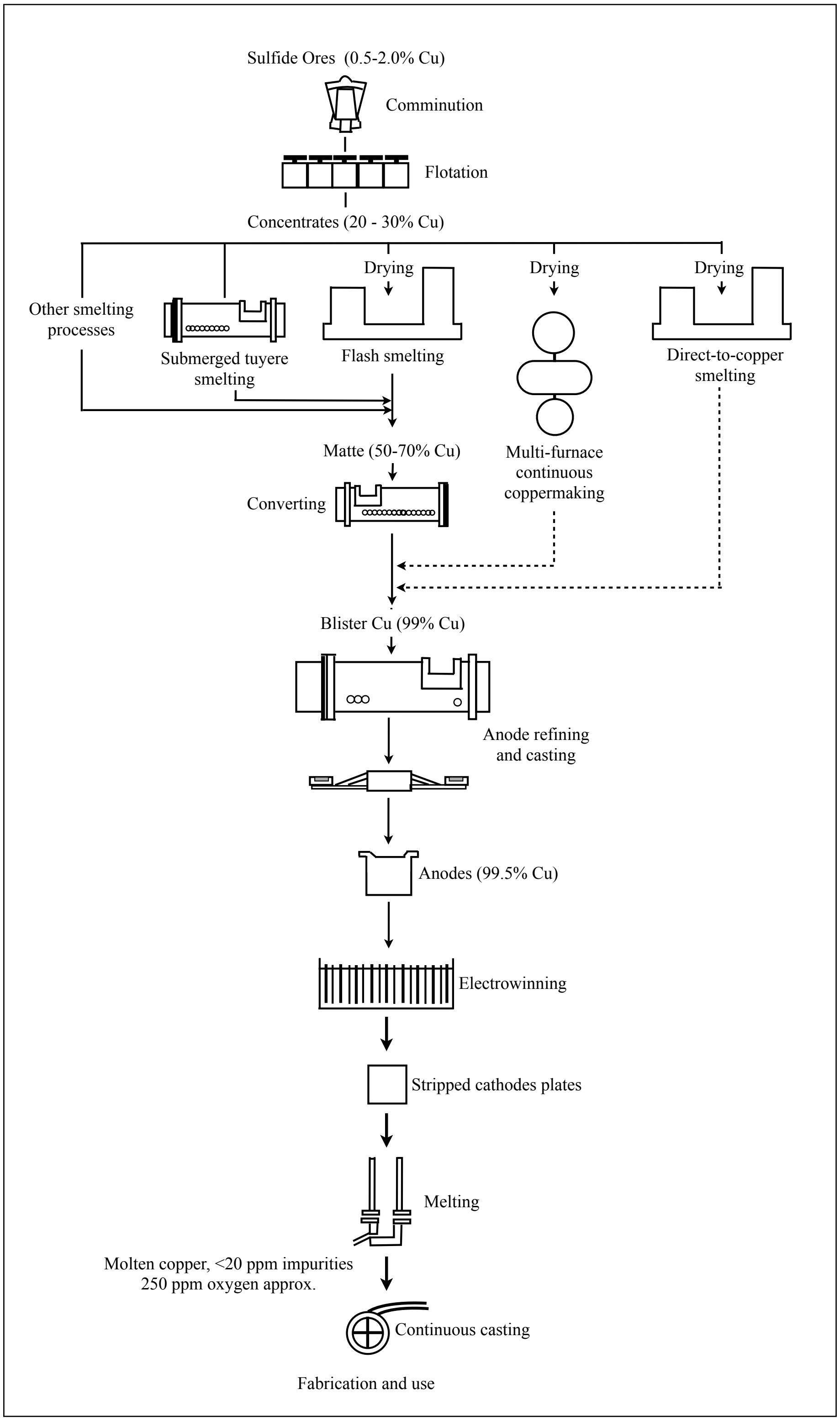

Figure 1.2: Stages of Pyrometallurgy required to extract copper from sulfide ores (Davenport et al., 2002).

copper. In the third stage, the molten blister is converted into flat anodes to be electrochemically refined (ER), obtaining copper cathodes of 99.99%, suitable for commercial use.

Copper can also be found in oxidized ores, from which is obtained the remaining 20% of the world primary production by means of a process known as hydrometallurgy (Figure 1.3). In it, copper is leached in piles and then concentrated and recovered, being the most common methods for the last two mentioned processes the solvent extraction (SX) and electro-wining (EW), respectively. More recently, certain sulfides ores such as chalcocite ores are being extracted using a modified hydrometallurgy process (Davenport et al., 2002).

In the first stage, the crushed ore is pilled in large heaps, where an aqueous-acid solution (commonly sulfuric acid) known as lixiviant, is trickled from the top to dissolve the copper present in the mineral. To dissolve copper from sulfide ores an oxidant is also required, threfore air is injected inside the heap and, to speed up the process to economic rates, the leach is assisted by bacterial action. These bacteria are indigenous to sulfide ore bodies and their aqueous environment and can speed up the leaching up to a million times under certain pH, temperature and nutrients conditions (Davenport et al., 2002).

The copper-pregnant solution is accumulated in tanks outside the leaching heap and then driven by means of gravity to the SX stage, where organic liquid chemicals known as extractants are mixed with the pregnant solution in a tank known as settler, forming two phases that are separated by gravity: an organic Cu-loaded solution which is used to produce the electrolyte for the EW stage and an aqueous Cu-depleted solution (known as raffinatte) that is pumped back to the leaching process to be recycled (Davenport et al., 2002). In the EW stage, an electrical potential is applied between inert anodes (commonly made of lead) and stainless steel cathodes (sometimes also made of copper), electroplating the copper present in the electrolyte on the surface of the cathodes. After this step, the cathodes are washed to remove impurities, then stripped and sent to the market, while the depleted electrolyte is returned to the solvent extraction process for copper replenishment. The purity of the copper obtained from the EW is similar to that of ER obtained

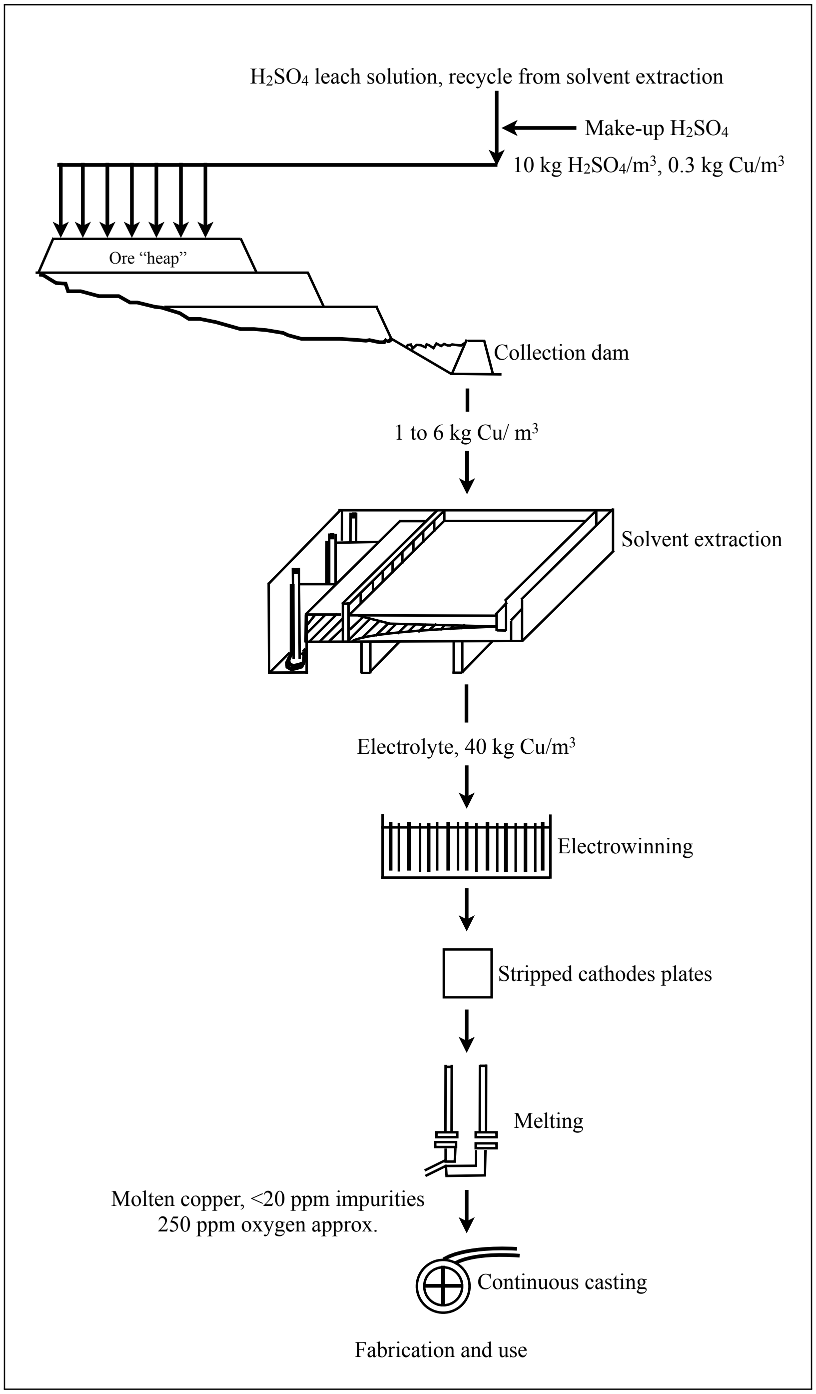

Figure 1.3: Stages of Hydrometallurgy required to extract copper from oxidized ores (Davenport et al., 2002).

copper (Davenport et al., 2002).

The first generation of copper hydrometallurgical processes were developed in 1970 but only in the nineties these became economically viable thanks to several improvements in the SX and EW stages, resulting in low capital and operation cost processes and easier operations and production of cathodes near the mine site made the economics of this process very attractive and interested copper companies, especially in Chile, which in 2010 produced 66% of the copper obtained globally from SX-EW (Ocaranza, 2011). This interest has motivated research efforts in order to improve and develop alternative hydrometallurgic processes suitable for ores that have been traditionally recovered by flotation, smelting and electro-refining (Peacey et al., 2004). EW appears to solve the main disadvantages of PM, such as higher energy requirements, CO_2 and CO emission from carbon oxidation, SO_2 and dioxin emissions (whose treatment involve large capital investments in advanced technologies and equipment) as well as sulfuric acid market saturation, higher capital cost and impurity limitations (Liew, 2008).

1.2. Characterization of the energy demand of copper mining in Chile

The ascending trend of the production of refined copper has been accompanied with an increase in the energy consumption in the industry, however, the composition of such demand has varied through the years due to the employment of new and improved techniques (Figure 1.4). In 2010, the copper production ascended to 5,4 millions of tonnes of copper and demanded around 120,000 TJ, the latter equivalent to 33.7% of the national total, of which 45% corresponded to the fuel used in the exploitation, beneficiation plants and to a lesser extent to stages of hydrometallurgy, whereas the remaining 55% to the electricity used to supply the extractive processes (Table 1).

Whereas the production of ER cathodes has been relatively stable since 1995, the introduction of HM in the nineties has absorbed the increase in the demand of refined copper, almost triplicating its share in 15 years (Figure 1.5) and it is now responsible for 66% of the total production in Chile. One of the reasons for this, is that HM requires 30% less energy to produce a cathode than the one obtained with PM and it is supplied with 23% of fuel and 77% of electricity, compared to the 29% of fuel and 71% electricity composition of the PM energy requirements. This phenomenon

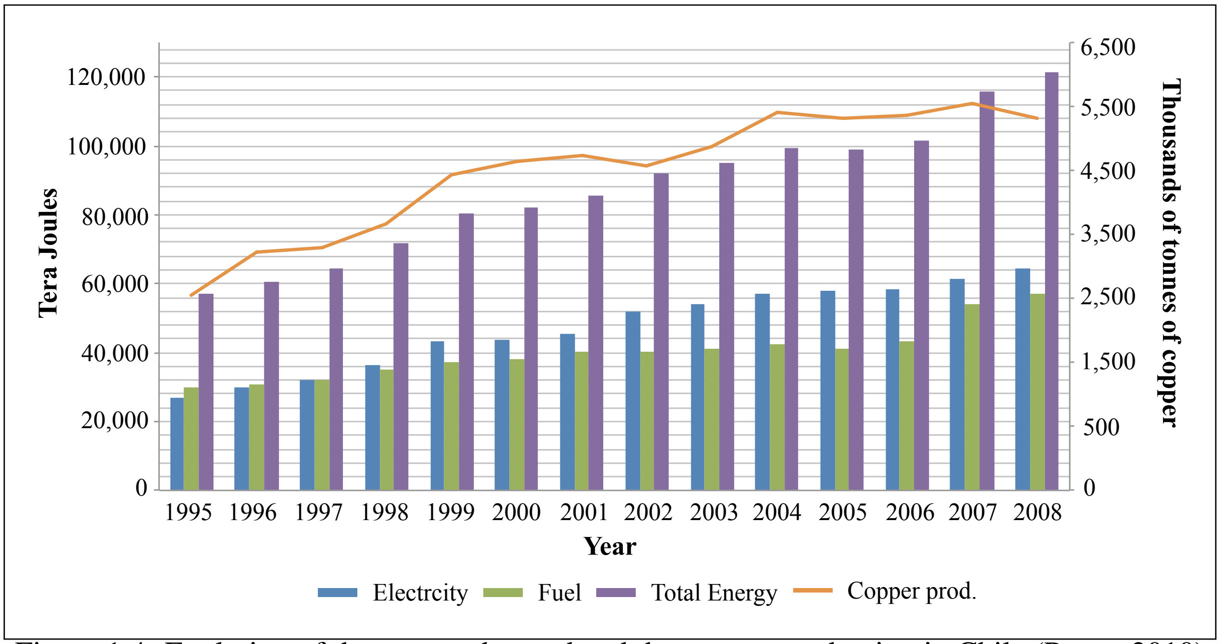

Figure 1.4: Evolution of the energy demand and the copper production in Chile (Perez, 2010).

Table 1: Energy consumption of the Chilean copper mining industry in 2010 (Ocaranza, 2011)

Stage	**Process**	**Production** (ktF)	**Fuel** (MJ/tF)	**Electricity** (MJ/tF)	**Total Consumption** (TJ)
Exploitation	In mine	5,418.9	5,705.9	772.4	37,098.3
	Related Services		367.8	679.7	5,676.3
PM	Beneficiation	2,614.7	206.4	8,945.6	–
	Smelter	1,559.8	4,679.5	3,741	27,409.6
	ER	1,054.9	869.1	1,311.8	20,837.9
HM	LX-SX-EW	2,088.5	3,185.1	10,633.8	28,860.8
				Overall	**119,882.8**

has led the electricity demand to gain importance over fuel (Ocaranza, 2011), as seen in Figure 1.4.

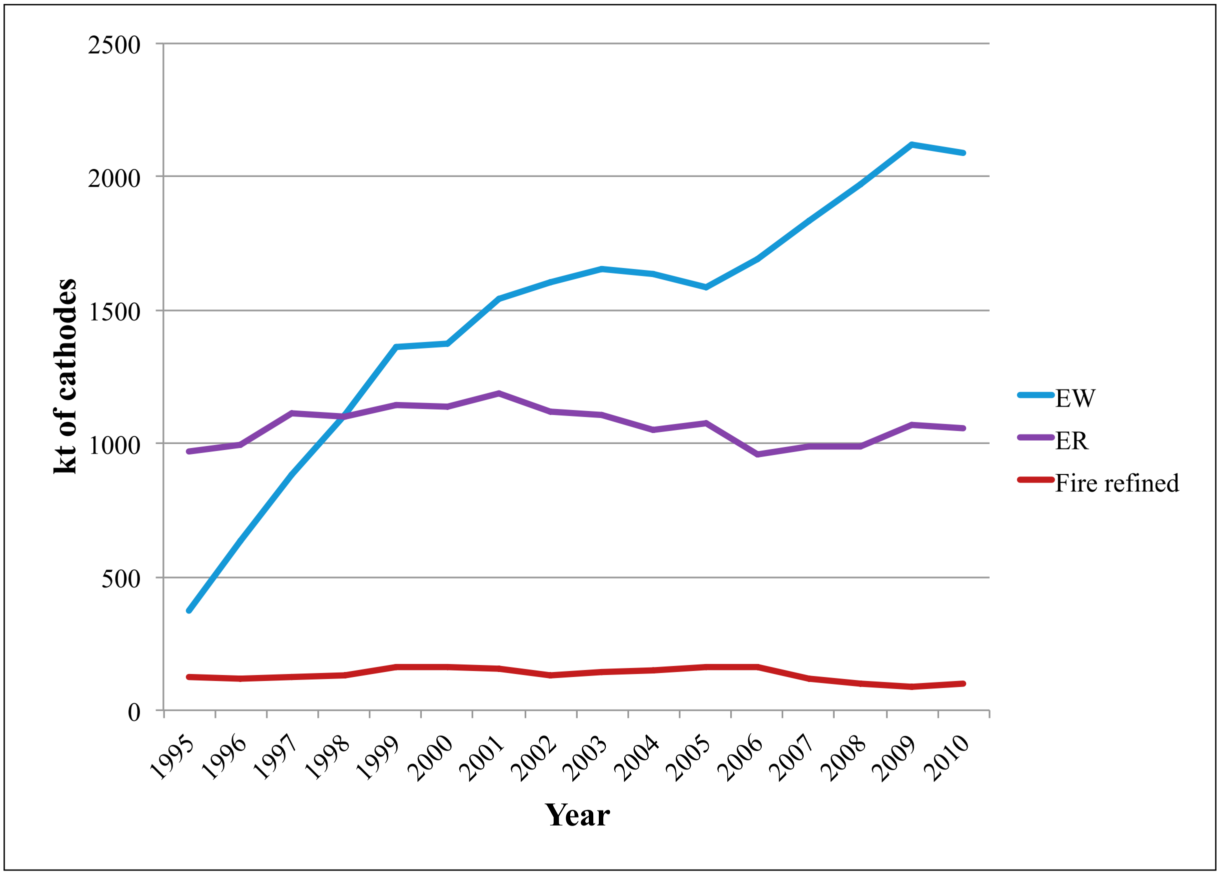

Figure 1.5: Chilean copper cathode production between 1995 and 2010 (Ocaranza, 2011).

The increase in the energy demand by the copper mining industry, as consequence, has incremented its greenhouse gas (GHG) emissions. During the first half of the last decade, this effect was mitigated with the progressive introduction of natural gas to the matrix of electrical energy generation in replacement of diesel and coal at the end of the nineties (Figure A.1), and therefore the CO_2e went from 10.31 millions of tonnes in 2000 to only 11.15 millions of tonnes in 2005 (Ocaranza, 2011). However, in 2006 shortages in the supply of natural gas from Argentina (that in the end would become permanent) reduced its consumption to less than a third and forced the use of oil, coal and coal-petroleum coke mixture instead for power production (Pimentel, 2010). This migration produced an important leap in the greenhouse emissions of an industry increasingly based on electrical energy. It can be noticed in Figure 1.6 that the production of refined copper in 2008 was virtually the same to that in 2005 ($\approx$5.2 millions of tonnes of fine copper) and nevertheless, the GHG emissions were 53% higher.

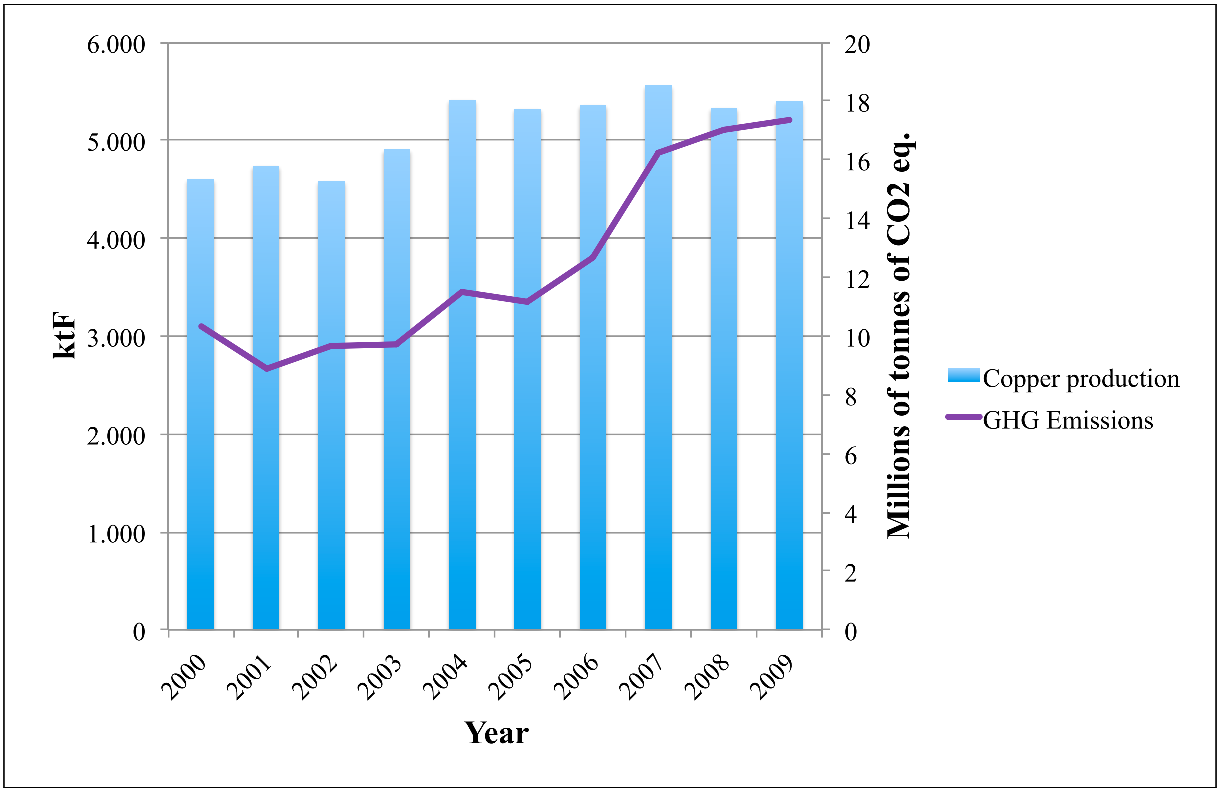

Figure 1.6: Greenhouse gas emissions and copper production of the Chilean copper mining industry (Ocaranza, 2011).

In the context of global warming, this represents one of the major challenges that require the focus of private and governmental organizations, in order to reduce these figures to sustainable levels. The introduction of new and more environmentally friendly energy sources, such as solar, geothermal and wind power appears as an attractive option in the reduction of GHG emissions, however limited by the intermittence of daylight and wind and the required size for a geothermal project.

The majority of the mining operations are located in northern Chile, which according to Perez (2010), together produced in 2010 over 67% of the refined copper (around 3.1 millions of tonnes of fine copper) of which 63% corresponds to EW copper cathodes, equivalent to 92% of the refined copper produced with this technique in Chile. The required fuel for such EW cathodes production ascended to 454,000 tonnes of diesel. However, the high insolation (Figure 1.7) and vast inhabited terrains in the region represent a major opportunity to develop thermal solar projects that can replace part of the supply produced with fossil fuels. Evidence of exploitation of such potential in seeking to reduce GHG emissions of this stage already exists. In May of 2012 Antofagasta Minerals announced the investment of 16 millions of dollars for the construction of a solar field at the El Tesoro mine (with a production of 95 ktF per year), located in the Antofagasta Region, near Sierra Gorda, consisting on 1,280 solar thermal collectors (parabolic troughs) which would deliver 55% of the thermal energy demanded by the SX-EW process, equivalent to 24,850 MWh per year (Cavalli, 2012). Later this year, the state mining company CODELCO announced adjudication of a solar thermal project for the Gaby mine (with a production of 120,000 ktF) to a Chilean-Danish consortium, which seeks to provide heat for the pre-heating of the electrolyte used in the EW as well as heating of service water used in the cathodes wash, avoiding the combustion of 80% of the diesel used in this stage. The solar field will consist on 39,000 m^2 of flat panels collectors and an investment of USD$60 millions for a 10 year operation (El Mercurio, 2012).

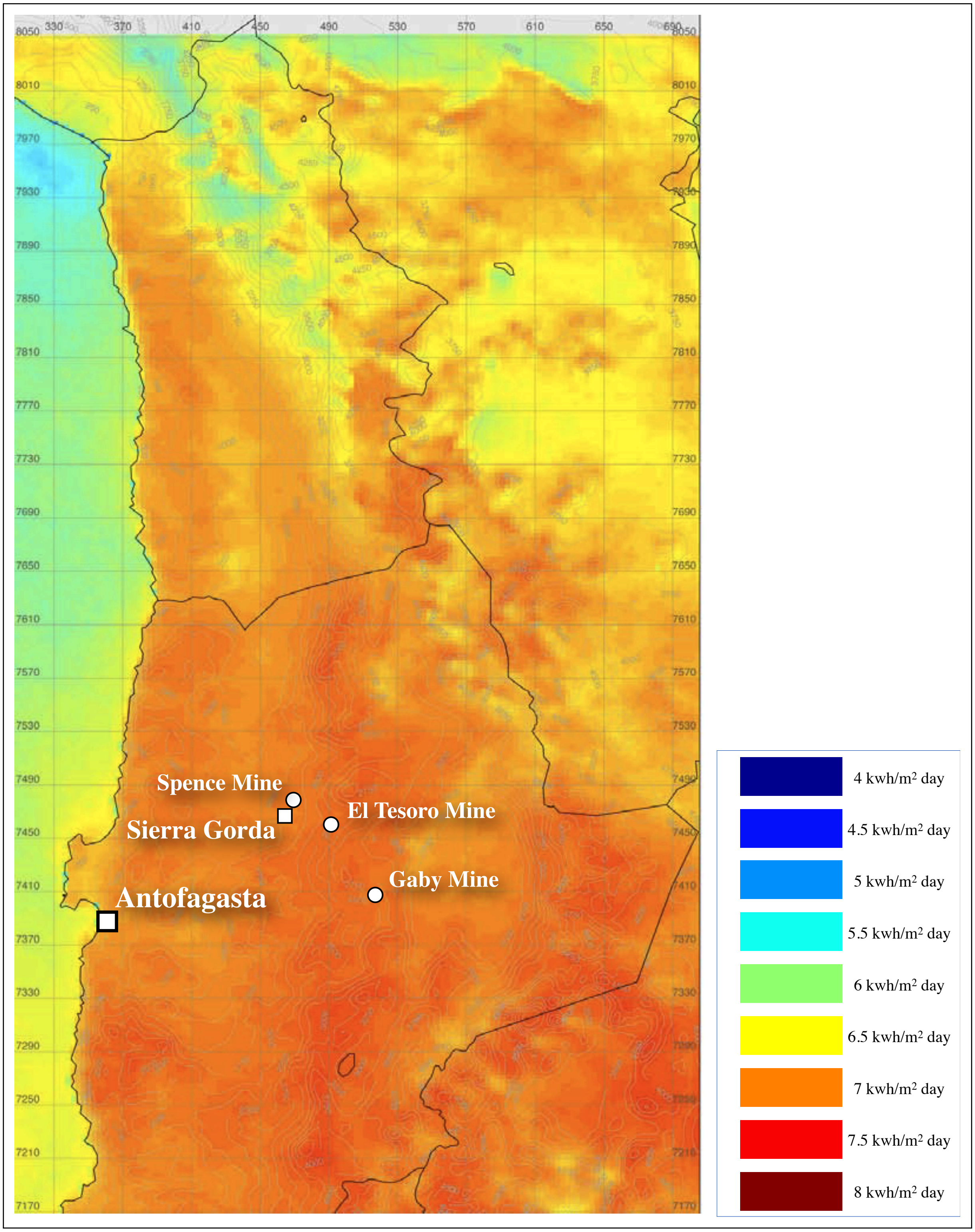

Figure 1.7: Daily average of solar radiation in northern Chile (CNE, 2009).

1.3. Electrowon copper cathodes

At the end of the electrowinning stage, when enough copper has been electrodeposited in both surfaces of the steel cathode to reach a thickness of 3 – 4 cm and the standard weight (usually 40 kg), cathodes are ready to be sent to the stripping process, where copper is removed and sent to the market. But before this, cathodes are washed with pressurized hot water to remove electrolyte remnants, waxes, and other impurities. Water is heated by conventional means, namely diesel water heaters, that consume 9% of the fuel used in the HM process.

1.4. Spence Mine

The Spence mine (Figure 1.8) is an operation of property of BHP Billiton, located 1,700 m above sea level and 150 km north-east of Antofagasta, Chile, that uses hydrometallurgy as extractive process exclusively (Mining Technology, 2011). In 2010 it produced 178 ktF as cathodes (6% of the national production), (Ocaranza, 2011), which placed it as the 19th most producing mine in the world, and the only one that one that uses SX-EW as exclusive extractive process in this list (International Copper Study Group, 2010). The energy demand of this mine ascended in 2010 to around 3,610 TJ of which 68% were intended for the LX-SX-EW stages.

The cathodes washing step in this mine uses 21.45 m^3/h of hot water, 24 hours a day. As seen in Figure 1.9 a flow of water at ambient temperature (that is 15 °C) is stored in a 100 m^3 tank that acts as a buffer. Then, the flow is circulated through a heat exchanger whose hot working fluid is provided by a diesel water heater with ($\eta_t = 84\%$), in order to raise its temperature to 62.3 °C and then returned to the tank. The water, before being used in the cathode washing, is heated up in a second heat exchanger (whose hot working fluid is provided by the same diesel water heater) to raise its temperature to 78.6 °C. The contaminated water resulting from this process is discarded to sinks. The volume of discarded water is constantly replenished to the tank (Arancibia, 2012a). The annual energy consumption of this process is of 13,880 MWh to increase the temperature of the water flow and 2,120 MWh to maintain the temperature in the tank, supplied by 1,600 t of

Figure 1.8: Aerial view of Spence mine (Lobos, 2007).

diesel, emitting 4,270 t of CO_2 eq[1].

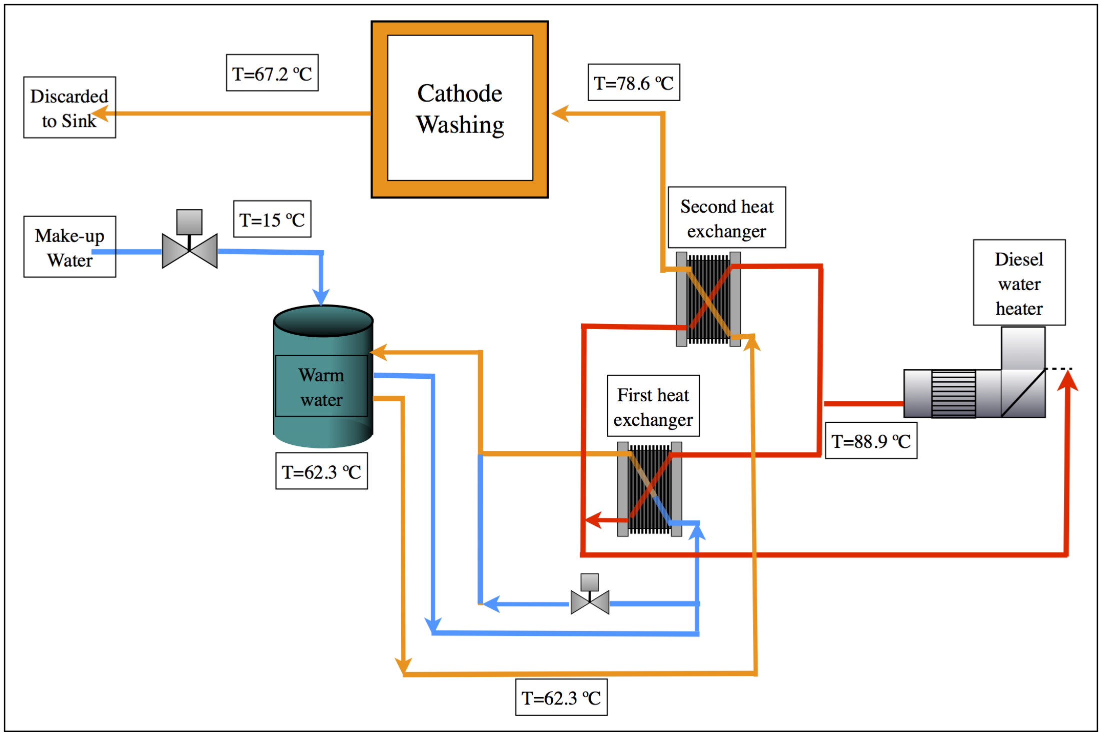

Figure 1.9: Water heating system for EW cathode washing at Spence mine.

1.5. Solar pond technology: State of the art

Solar pond is a type of non-conventional renewable energy source that find application in industrial and commercial applications that require low temperature heat in the range of 45 to 85 °C, as in the water heating for EW cathodes washing. They basically consist of a body of saltwater that acts like a low cost solar collector, absorbing the incident solar radiation and storing it in the bottom as hot water that, with the aid of a heat exchanger, can be extracted for practical use (Srithar and Velmurugan, 2008). Due to the nature of this technology it becomes specially attractive in the context of the mining operations located in the northern regions of Chile, where high insolation and low opportunity cost land are available.

[1]Calculated based on the IPCC emissions factors (Gómez and Watterson, 2006)

The operational principle of solar pond is simple: like any body of water under insolation, they absorb the solar radiation increasing its temperature but unlike oceans or lakes, solar ponds avoid the buoyancy generated by the presence of a hot fluid in the bottom with an artificial salinity gradient that goes from a negligible concentration on top, to around 30% at the bottom (Ouni et al., 2003) assuring a greater density in the lower depths even when heated (Kurt et al., 2000). This prevents the convection currents that otherwise would homogenize its temperature profile due to thermal diffusion, allowing the solar radiation to be absorbed and stored as heat below this gradient. Because of this, the brine stratifies into three layers clearly identifiable (Figure 1.10) of which two are convective, with a constant salinity and temperature. The upper convective zone (UCZ) is usually at ambient temperature and low salt concentration whereas the lower convective zone (LCZ) has a high salt concentration and is where the solar radiation is absorbed and from where the heat is extracted. The third layer is the non convective zone (NCZ) which is where the salt gradient is (therefore its name), the temperature increases with depth through this layer, and due to the low thermal conductivity of water, acts as a transparent insulation for the hot layer below (Leblanc et al., 2011). In order to maintain this stratification and the solar pond functionality in time, the gradient has to be preserved by means of maintenance routines that take care of the salt that migrates from the LCZ to the UCZ due to diffusion.

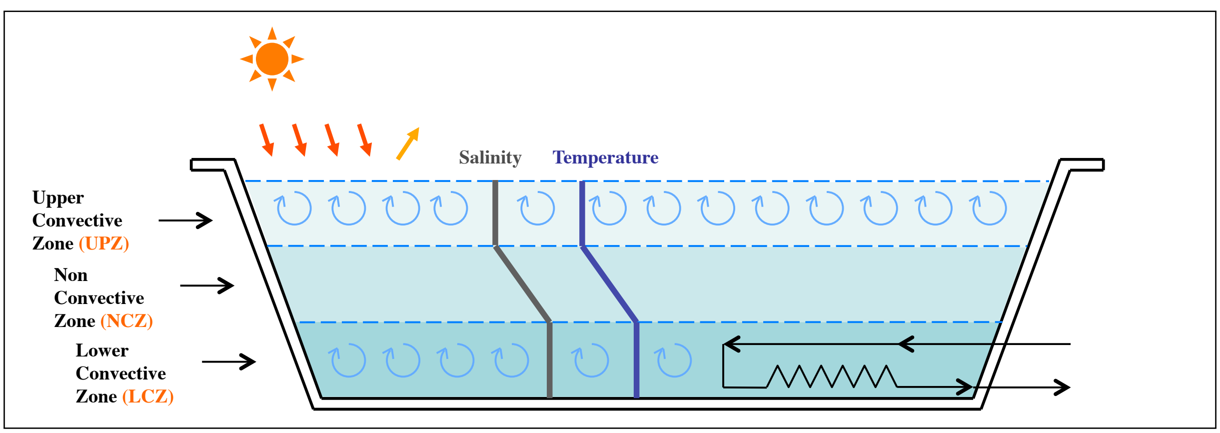

Figure 1.10: Brine stratification and characteristics of each layer in a Solar Pond.

This phenomena has existed in nature for a long time, though it has only been noticed and studied recently. The first recorded reference date back to early XX century, in which temperatures of up to 70°C were measured in the bottom of the Medve Lake in Transylvania, Romania (Mills,

2001) though the effect of factors that could cause these temperatures such as biological activity, chemical heating, hot springs or geothermal gradients under the lake were not detected (Abdel-Salam and Probert, 1986). However, the presence of salt leaching at the bottom of the lake and the supply of fresh water at the top were noticed (Kaushika, 1984). Similar observations have been reported from lakes in Oroville WA, Eilat in Israel and Lake Vanda in Antarctica (Kurt et al., 2000).

Such findings led Dr. Rudolph Bloch to the idea of creating artificial solar ponds that could collect solar energy more effectively than solar lakes in nature, and deliver it as useful energy. An extensive research on the key aspects of the behavior of solar ponds, including the development of analytic models, experimental testing and economic analysis was carried out (Srithar and Velmurugan, 2008) with particular emphasis in Israel. After 8 years of hiatus the R & D was restarted in 1974 when development of this technology was declared ”national project”. With the idea that solar ponds could produce low calories already accepted, the Israeli effort in the development of this technology focused primarily on proving that these moderate–temperature calories could be converted into electrical and mechanical power. Needed for the conversion to mechanical power a suitable organic vapor Rankine cycle turbine was developed. Several small solar ponds (of up to 1,000 m^2) for the collection of data and three demonstration solar ponds of 1,500, 7,000 and 40,000 m^2 to prove their practical use to produce electric power where built (Tabor, 1981). The encouraging results obtained motivated the construction of the largest solar pond built so far (of 210,000 m^2) at Beith Ha'Arava (Figure 1.11) in 1982, which was able to deliver 5 MW_e to the electric grid with a 65% load factor, operating with a bottom temperature of up to 96°C. The It remained operative until 1988 as the power generation cost was higher than the existing electricity price of that time(Tabor and Doron, 1990).

Following the Israeli experience, the Commonwealth Scientific and Industrial Research Organization (CSIRO), Australia started the research on solar pond technology in 1964 focused in the use of the technology for the production of salt. However, deficiencies in the operation (turbidity and algae control) led to poor results and the program was terminated in 1966. In 1998, solar ponds re-gained interest when the Royal Melbourne Institute of Technology (RMIT) started a solar pond program led by Dr. Aliakbar Akbarzadeh to develop this technology. A 53 m^2 experimental

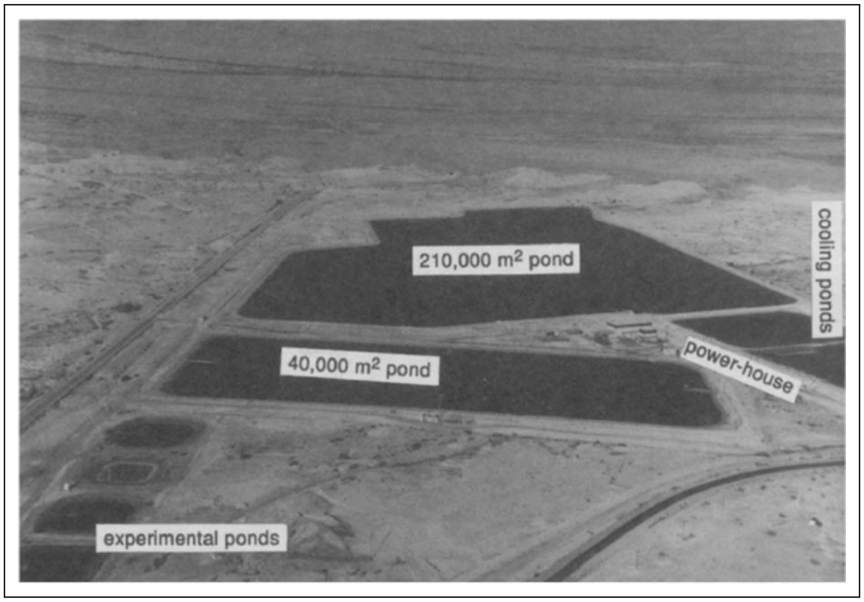

Figure 1.11: Aerial picture of the installations at Beith Ha'Arava solar pond, Israel (Tabor and Doron, 1990).

salinity-gradient solar pond was built at the Renewable Energy Park of the School of Aerospace, Mechanical and Manufacturing Engineering at RMIT, primarily to aid in the validation of mathematical models. In 2000, fruit of the collaboration between RMIT, Pyramid Salt Pty Ltd. and Geo-Eng Australia Pty Ltd. a 3,000 m^2 solar pond was built at Pyramid Hill, Victoria to demonstrate and commercialize a solar pond system as an innovative, cost-effective method of capturing and storing solar energy for a range of applications. The solar pond is currently used to provide hot air (at 45°C) necessary for the crystallization phases of the salt production at Pyramid Salt, equivalent to 60 kW. It has also been used to demonstrate its performance as an autonomous desalination for in-land brines, where the by products (low concentration brines) are used as make up water for the solar pond. The current cost of the heat produced with Pyramid Hill solar pond is of US$ 12.7 per GJ, and it is projected that with further improvements the cost could decrease to US$ 9 per GJ (Leblanc et al., 2011). The Australian program has also participated in the development of other solar ponds outside the country, such as the Solvay-Martorell solar pond in Granada, Spain, which was designed and built in 2007, in conjunction with Universitat Politècnica de Catalunya and Solvay Minerals. The solar pond is currently tested for the desalination of water (Valderrama et al., 2011).

Significant development has also been made in the USA since 1974, when researchers from Ohio State University proposed that solar ponds could be used for energy storage. The first two experimental solar ponds were built a year later to test their suitability for space heating, obtaining encouraging results (Tabor, 1981). Three years later, a 2,020 m^2 was built in Miamisburg to heat up an outdoor swimming pool in summer and a building in winter. In 1985, a 3,000 m^2 multi purpose experimental solar pond was put into operation at El Paso, New Mexico (Figure 1.12), that in 1986 became the first solar pond electric power generating facility in USA, and a year later, became the first solar pond powered water desalination facility in the country. After 18 years of operation, in which numerous developments were achieved such as new durable insulating liners, an automated system for control and monitoring, operation strategies and improved heat extraction systems, the project was shut down in 2003 (Leblanc et al., 2011). Based on the performance of this solar pond economical projections were made. It was noticed that bigger the solar pond, the cheaper was the industrial heat produced. The leveled cost of energy cost (LEC) at temperatures between 50 – 90°C ranges from US$6.6 per GJ for a 1 hectare solar pond to US$1.3 per GJ for a 100 hectares solar pond, making it very competitive against heat produced from natural gas or coal (Lu et al., 2004).

Since the discovery of the thermal inversion in solar lakes due to the presence of a salinity gradient, more than 60 pilot projects have been realized in countries (besides of the already mentioned) such as Argentina, India, Canada, Portugal, the Russian Federation, Kuwait, Turkey among others to test the technical and economical performance of this technology in commercial uses with positive results (Kurt et al., 2000).

1.6. Objectives

Main objective

Design a solar pond to be coupled to the current water heating system used in the copper cathodes washing step and evaluate its performance in reducing the fuel consumption at the Spence mine.

Figure 1.12: El Paso solar pond, New Mexico (Leblanc et al., 2011).

Secondary objective

Study the solar pond working principle and identify the design parameters that determine its performance.

1.7. Organization of the thesis

The thesis begins describing the energy context in which the copper industry operates and how solar energy is breaking through as a way to reduce the dependency on fossil fuels in processes that require hot water. The working principle of solar ponds was presented and was proposed, as an alternative to flat panels and parabolic through collectors, to provide process heat for the copper cathodes washing at the Spence mine.

In section two the phenomena to which a solar pond is subject are described and their mathematical formulation is given to model the behavior if this technology. In chapter three the numerical methods chosen, as well as the assumptions used to facilitate model solution are presented.

Validation of the model against operational records of a solar pond is presented.

In chapter four, the main parameters that determine the performance of a solar pond are detailed. In section five, results of the iterative process carried out considering the parameters previously presented and the site conditions to design the solar pond are presented. Performance of the solar pond is predicted using numerical solution of the model and potential reduction in diesel consumption by preheating the water flow used to wash cathodes with the designed solar pond is exposed. An economic analysis that estimates cost of investment, operation and maintenance of the solar pond is given to estimate the cost of energy of water heating system with a solar pond preheating step. The economic analysis also includes the sensitization of key parameters. Finally, in chapter six, main conclusions are presented.

2. SOLAR POND MODEL

In order to design a solar pond it is needed first to identify and understand the phenomena under study (Figure 2.1). When solar radiation reaches the surface of the pond, part of it is reflected back or scattered and the rest penetrates through the water layers. In its way through the pond, a fraction of this radiation is refracted and the rest is attenuated due to turbidity and therefore it does not reach the LCZ. The solar radiation that does reach the LCZ heats up the water at such depth, induces a temperature gradient between the water body and the ground and causing the loss of part of this heat through the bottom. The remaining energy is available to be withdrawn by a heat extraction system. The presence of a density gradient created by the addition of salt, counters the buoyancy of the hot fluid, preventing it from reaching the surface and dissipating the heat to the atmosphere. At the same time, that gradient causes migration of salt from the higher concentration layer (LCZ) to the lower concentration zone (UCZ) due to simple diffusion mechanism, which is very slow, but that over time tends to homogenize that salinity profile in the pond. Therefore, in order to maintain the inherent feature of solar ponds to store thermal energy, the density gradient has to be preserved in time. Also, surface water is evaporated mostly by the action of wind, relative humidity and temperature differences between the UCZ and the ambient.

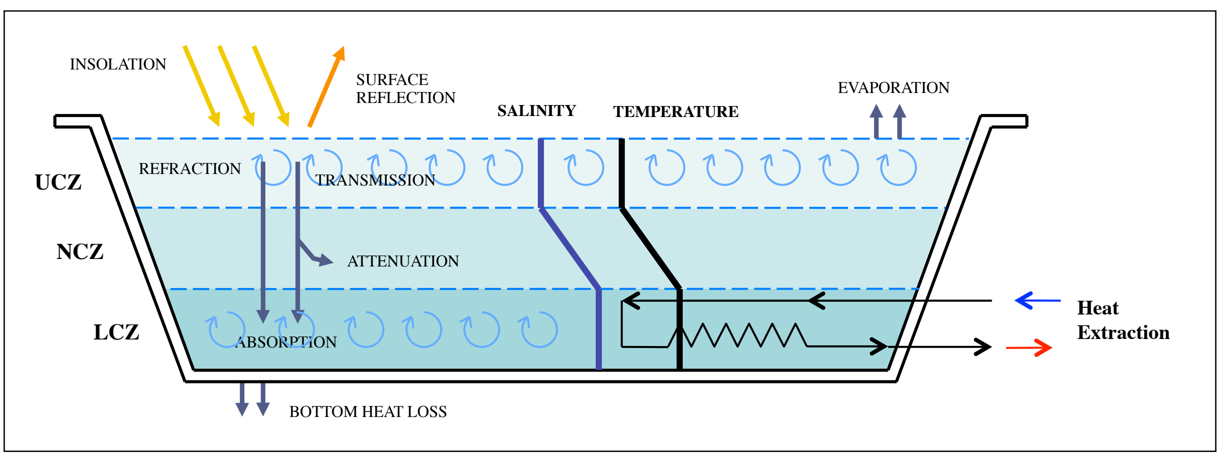

Figure 2.1: Phenomena present in the behavior of a solar pond.

The development of mathematical models for these phenomena, allow the prediction of the behavior of a solar pond under different conditions and design configurations. Weinberger (1964) was the first to give a mathematical formulation of a solar pond. Later, Rabl and Nielsen (1975), expanded the one-zone model proposed by Weinberger into a two-zone model of a solar pond. Akbarzadeh and Ahmadi (1981) studied the attenuation of the solar radiation in a solar pond, caused by salt concentration, biological formation, radiation propagation, bottom and wall reflection. Kishore and Joshi (1984) studied the heat losses to the ambient and the efficiency of solar ponds. A lot of effort has been put into modeling the heat and salt diffusion, and its numerical solution, field in which Hull (1980), Rubin and Benedict (1984), Liao (1987), Dah et al. (2005), Karim et al. (2010) and other authors have made important contributions (Busquets et al., 2012).

2.1. Insolation

The thermal performance of solar pond is determined by the amount of solar radiation that reaches the LCZ, which is a small portion of the total incident radiation on the surface of the pond. The fraction of solar radiation that is reflected back to the atmosphere can be estimated with the Fresnel Law and the position of the sun referred to the location of the pond, or more specifically, the zenith (or incident) and refraction angle (Wang and Akbarzadeh, 1983). The refraction angle is calculated with the zenith and, at the same time, the latter is determined by the hour angle, declination angle and latitude. Therefore, prior to the study of the radiation absorption in a solar pond, it was essential to understand how these angles describe the position of the sun. To do so, notions given by Duffie and Beckman (2006) were used and herein presented.

The declination of the Sun is the angle between the an incident ray and the plane of the equator in the Earth (Figure 2.2) and It is calculated (in degrees) with expression equation (2.1.1):

$$\vartheta_{DE} = 23.45\ sin\left(\frac{360\ (284+n)}{365.25}\right) \tag{2.1.1}$$

where *23.45* is the inclination angle of the axis of the Earth respect of the vertical and *n* is the day of the year, being *n=1* equivalent to January 1st.

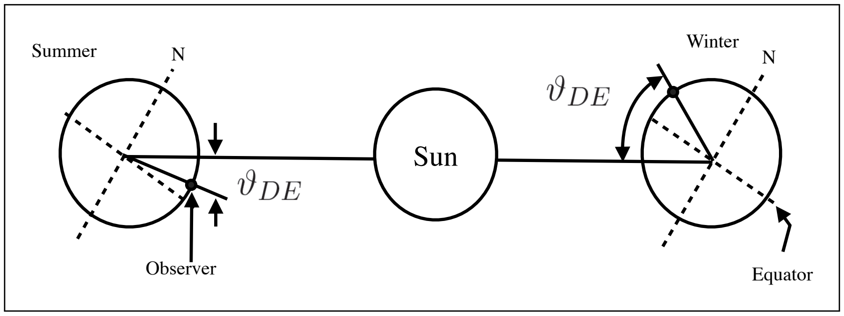

Figure 2.2: Declination angle for an observer in the North hemisphere.

The hour angle is the angular displacement of the Sun, east or west of the local meridian and is due to the rotation of the Earth on its axis at 15° per hour (Figure 2.3) and is given by:

$$\vartheta_{HA} = 2\,\pi \frac{(h - 12)}{24} \tag{2.1.2}$$

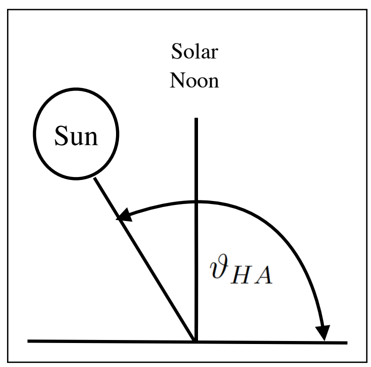

Figure 2.3: The Hour angle.

where *h* is the local hour of the day.

The zenith angle or incidence angle is the angle of the Sun relative to a line perpendicular to the surface of the Earth at the observer location (Figure 2.4) and it is calculated with the expression:

$$cos\vartheta_i = cos\vartheta_{DE}\; cos\varphi\; cos\vartheta_{HA} + sin\vartheta_{DE}\; sin\varphi \tag{2.1.3}$$

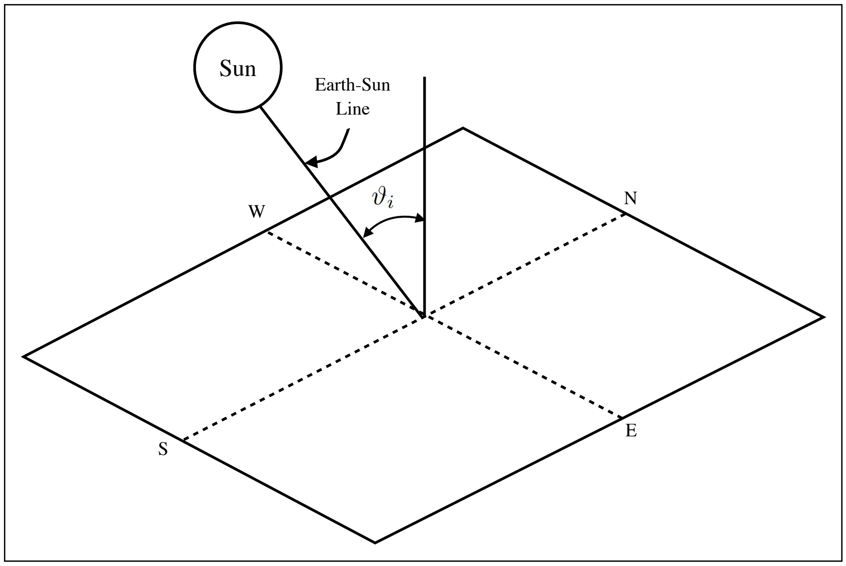

Figure 2.4: The Zenith or Incidence angle.

where φ is the latitude angle. The azimuth angle is the relative position of the Sun to the north-south axis of the Earth, and it is calculated by the expression:

$$cos\vartheta_{AZ} = \frac{cos\vartheta_i \; sin\varphi - sin\vartheta_{DE}}{sin\vartheta_i \; cos\varphi} \tag{2.1.4}$$

The length of the day can be estimated by:

$$L_D = \frac{24}{\pi} \, \vartheta_{ssh} \tag{2.1.5}$$

where ϑ_{ssh} is the sunset hour angle, which can be determined with:

$$\vartheta_{ssh} = cos^{-1}(tan\vartheta_{DE} \; tan\varphi) \tag{2.1.6}$$

With this set of equation it was possible to describe the movement of the Sun throughout the year, and its influence in the performance of a solar pond.

2.2. Radiation Absorption

Viskanta and Tabor (1978) proposed the following expression to quantify the solar radiation absorbed by the solar pond:

$$Q_I(Z,t) = \frac{-dI(Z,t)}{dZ} \tag{2.2.1}$$

where *I(Z,t)* is the direct radiation flux at depth *Z* of the pond and time *t*. This flux is a fraction of the total incident on the surface. Wang and Akbarzadeh (1983) proposed the use of the Fresnel Law of reflection for a smooth surface water body to calculate the portion of solar radiation that is reflected back to the atmosphere as follows:

$$R = \frac{1}{2}\left[\frac{sin^2(\vartheta_i - \vartheta_r)}{sin^2(\vartheta_i + \vartheta_r)} + \frac{tan^2(\vartheta_i - \vartheta_r)}{tan^2(\vartheta_i + \vartheta_r)}\right] \tag{2.2.2}$$

where ϑ_r is the angle of refraction, which can be obtained as follows (Rezachek, 1993):

$$sin\vartheta_r = 0.752\ sin\vartheta_i \tag{2.2.3}$$

The flux of solar radiation in the pond is attenuated by the effect of turbidity caused by algae formation, by bottom and side wall reflectivity and propagation through the water layers. Akbarzadeh and Ahmadi (1980) summarized all the effects of radiation reduction factors in a coefficient of $\theta' = 0.83$ and Jaefarzadeh (2004) proposed the use of $\theta' = 0.85$ if the reflection is calculated with equation (2.2.2), as shown in (2.2.5).

A penetrating flux of solar radiation into a body of water decays exponentially with depth, as fluid layers absorb energy. The rate of decay (or transmissivity) in a solar pond was studied by Rabl and Nielsen (1975) and proposed the following expression, function of the wavelength of the radiation for the whole spectrum, to calculate it:

$$\sum_{j=0}^{4} \eta_{cj}\ exp\left(\frac{-\mu_{cj}\ Z}{cos\vartheta_r}\right) \tag{2.2.4}$$

where η and μ are coefficients for the main wavelengths of solar radiation that can be found in the following table:

Table 2: Constants for the transmissivity function

Wavelength of the refracted radiation (μm)	η_c	μ_c (m^{-1})
0.2–0.6	0.237	0.032
0.6–0.75	0.193	0.45
0.75–0.9	0.167	3
0.9–1.2	0.179	35

Then, $I(Z,t)$ can be expressed as:

$$I(Z,t) = (1-R)\,\theta'\,cos\vartheta_i\,I_0 \sum_{j=0}^{4} \eta_{cj}\,exp\left(\frac{-\mu_{cj}\,Z}{cos\vartheta_r}\right) \tag{2.2.5}$$

where I_0 is the incident solar measured in the site (García, 2012).

2.3. Solar Pond fluid dynamics

In order to model the thermo-dynamics in a body of water, a one-dimensional analysis of the heat conduction equation across the concentration gradient layer of the pond is usually used. However this approach neglects effects of heat convection as well as thermohaline double diffusion present in a solar pond.

Heat convection within a fluid generates non-diffusive fluid motions and it is responsible for heat and mass transfer. In order to illustrate this effect, portions of a warm salty fluid at rest that overlies a fresh cold layer of water will sink due to local changes of temperature and density, driving convection movements (Figure 2.5). Such phenomenon is called “salt-finger” (Shigeta et al., 2009).

A solar pond is considered stable if the induced salt gradient is preserved in time. If defining:

$$F_s = \frac{1}{\rho}\,\frac{d\rho}{dz} \tag{2.3.1}$$

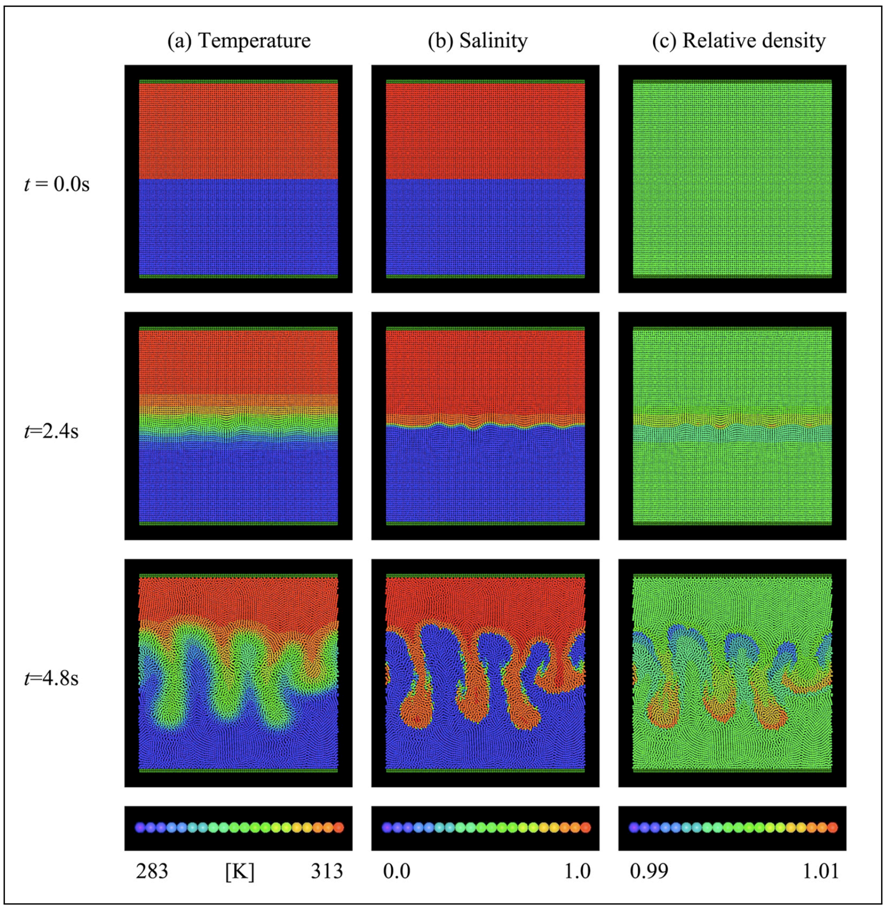

Figure 2.5: Incompressible Smoothed Particle Hydrodynamics (SPH) Simulation of the motion in a fluid at rest due to salt-finger phenomena (Shigeta et al., 2009).

as a factor of stability, with the depth z equal to zero at the bottom and positive upwards, it is clear that the pond will remain stable if $F_s < 0$ at all time. Considering that in a solar pond, the density at a certain depth z is a function of the salinity S and temperature T (Pande and Chaudhary, 1984). Then, applying the chain rule to the right hand side of equation (2.3.1) results:

$$F_s = \frac{1}{\rho}\,\frac{d\rho}{dz} = \frac{1}{\rho}\,\left[\left(\frac{\partial \rho}{\partial S}\right)\left(\frac{\partial S}{\partial z}\right) + \left(\frac{\partial \rho}{\partial T}\right)\left(\frac{\partial T}{\partial z}\right)\right] \tag{2.3.2}$$

Therefore, it can be seen the stability condition ($F_s < 0$) is satisfied when:

$$\frac{\partial T}{\partial z} < \frac{\beta}{\alpha}\left(\frac{\partial S}{\partial z}\right) \tag{2.3.3}$$

where α is the thermal expansion coefficient and β is the salinity expansion coefficient (Mamaev, 1975), given by:

$$\alpha = \frac{1}{\rho}\,\frac{\partial \rho}{\partial T}$$

$$\beta = -\frac{1}{\rho}\,\frac{\partial \rho}{\partial S}$$

2.3.1. Balance Equations

In order to predict the dynamic temperature distribution in the solar pond, balance equations for the gradient layer as well as at singular faces at the bottom and sides of the pond were used. The Navier-Stokes equations for incompressible fluids in 3 dimensions consist of 6 balance equations, which can be solved numerically with the aid of suitable boundary and initial conditions.

The differential form of the general balance equation for an arbitrary physical quantity ϕ can be derived by applying the Gauss theorem to the Reynolds transport theorem for an infinitely small volume moving with a fluid (Henningson and Berggren, 2005), which results in:

$$\frac{\partial}{\partial t}(\rho\,\phi) + \frac{\partial}{\partial x_i}(J_i) = S_\phi \tag{2.3.4}$$

where J_i represents the flux vector of the quantity ϕ and S_ϕ its external source. The flux vector is composed of convection and conduction fluid motion components:

$$J_i = (\rho\ u_i\ \phi)_{convection} + \xi_{conduction} \tag{2.3.5}$$

where $\xi_{conduction}$ is the non-convective flow. By substituting (2.3.5) in (2.3.4) results in:

$$\frac{\partial}{\partial t}(\rho\ \phi) + \frac{\partial}{\partial x_i}(\rho\ u_i\ \phi) + \frac{\partial}{\partial x_i}\xi_{conduction} = S_\phi \tag{2.3.6}$$

which is the expression used to obtain the balance equations by replacing ϕ with the relevant physical quantities.

• Continuity equation

The continuity equation of mass for an incompressible fluid ($\nabla \cdot u = 0$) is obtained by replacing $\phi = 1$ in (2.3.4), resulting in:

$$\frac{\partial \rho}{\partial t} + u_i \frac{\partial \rho}{\partial x_i} = 0 \tag{2.3.7}$$

It can be noticed that the source term (S_ϕ) disappears since no mass can be generated.

• Momentum conservation

In order to obtain the momentum conservation equation of an incompressible Newtonian fluid (with constant viscosity μ), ϕ in (2.3.4) is replaced by the components of convection velocity u as follows:

$$\frac{\partial}{\partial t}(\rho\ u_j) + \frac{\partial}{\partial x_i}(\rho\ u_i\ u_j) + \frac{\partial}{\partial x_i}(-\sigma_{ij}) = \rho\ g_j \tag{2.3.8}$$

where g is the external accelerations vector due to gravity and σ_{ij} is the simplified stress tensor for a Newtonian fluid, and equal to:

$$\sigma_{ij} = -p\ \delta_{ij} + \mu\ (\frac{\partial u_i}{\partial x_j} + \frac{\partial u_j}{\partial x_i}) \tag{2.3.9}$$

being p the pressure and δ_{ij} the Kronecker delta. Replacing (2.3.9) in (2.3.8), considering that the fluid is incompressible and simplifying the results gives this:

$$\frac{\partial u_j}{\partial t} + u_j \frac{\partial u_j}{\partial x_i} = \frac{1}{\rho}\left[\frac{\partial}{\partial x_i}\left(\mu \frac{\partial u_j}{\partial x_i}\right) - \frac{\partial p}{\partial x_i}\right] + g_j \tag{2.3.10}$$

• **Energy conservation**

In order to obtain the energy conservation equation the quantity ϕ in (2.3.4) is replaced by the internal energy U_{int}, the source term S_ϕ is replaced by the solar radiation flux $I(z,t)$ derived in (2.2.5), $\xi_{conduction}$ by the conducting heat flux in the fluid (q_i) and the continuity equation (2.3.7) is also taken into account, resulting:

$$\rho \frac{\partial U_{int}}{\partial t} + \rho\, u_i \frac{\partial U_{int}}{\partial x_i} + \frac{\partial}{\partial x_i} q_i = \sigma_{ij} \frac{\partial u_i}{\partial x_j} + \frac{\partial I_(x_3,t)}{\partial_{x_3}} \tag{2.3.11}$$

being the direction coordinate x_3 the z direction coordinate. The conducting heat flux can be substituted by Fourier law of heat conduction:

$$q_i = -k \frac{\partial T}{\partial x_i} \tag{2.3.12}$$

where k is the heat conductivity of the fluid. Considering that in ideal fluids the variation of internal energy is proportional to the change of temperature:

$$C \frac{\partial T}{\partial x_i} = \frac{\partial U_{int}}{\partial x_i} \tag{2.3.13}$$

with C as the heat capacity of the fluid. Replacing (2.3.12) and (2.3.13) in (2.3.11) results:

$$\rho\, C \frac{\partial T}{\partial t} + \rho\, u_i\, C \frac{\partial T}{\partial x_i} = \frac{\partial}{\partial x_i}\left(k \frac{\partial T}{\partial x_i}\right) + \sigma_{ij} \frac{\partial u_i}{\partial x_j} + \frac{\partial I(x_3,t)}{\partial x_3} \tag{2.3.14}$$

• **Salinity conservation**

The vertical motion due to convection leads to salt migration to upper zones of the pond, jeopardizing the insulating function of the salt gradient in the NCZ and therefore, the study of salinity conservation in a solar pond is of most importance. Hence, another equation is added to the set of balance equations, by replacing ϕ in (2.3.4) by the salinity S, which results in:

$$\rho \frac{\partial S}{\partial t} + \rho \, u_i \, \frac{\partial S}{\partial x_i} = -\frac{\partial}{\partial x_i} \left(D \, \rho \frac{\partial S}{\partial x_i} \right) + s_i - s_0 \tag{2.3.15}$$

where D represents the coefficient of salt diffusion, s_i represents the incoming salt per time unit of makeup brine required to maintain the salt profile and s_0 represents the salt lost due to surface evaporation or brine withdrawal.

3. NUMERICAL SOLUTION FOR A ONE-ZONE MODEL

The general mathematical model presented in the previous section was solved with the aid of numerical methods executed with Matlab™. Also, special assumptions specific for solar ponds were used to simplify the Navier-Stokes equations solution.

The balance equations for the physical quantities have been derived for a 3 dimensional space, necessary to describe phenomena like convective vortices that occur naturally when, for example, a fluid is heated from below (like in a stove) which, at first, decreases its density locally. The convective motions generated inside the fluid lead to very fast transport of mass and therefore ensure that the salinity and temperature are distributed homogeneously throughout the fluid. However, in solar ponds and in particular inside the non-convective zone these convective motions are countered by the presence of a salinity gradient that increases with depth. The transport of thermal energy and salinity are then limited to diffusive motions, which occur over a much longer period of time. This time scale makes possible the preservation of the salinity gradient by replenishing the LCZ with salt at the same rate as it diffuses upward and maintain the functionality of a solar pond.

The solution of the equations that describes the dynamics of the non-convective zone was as follows. The absence of convective motions in the NCZ led to the assumption that the velocity profile was zero in the three axis and therefore the momentum conservation could be reduced to:

$$0 = \frac{1}{\rho}\left[\frac{\partial p}{\partial x_j}\right] + g_j \tag{3.0.16}$$

which means that the pressure increases linearly with depth. The internal energy balance equation was reduced to:

$$\rho\, C\, \frac{\partial T}{\partial t} = \frac{\partial}{\partial x_i}\left(K\, \frac{\partial T}{\partial x_i}\right) + \frac{\partial I_R}{\partial x_3} \tag{3.0.17}$$

which corresponds to the heat conduction equation. Since the irradiation term I_R is function of x_3 and not of any other coordinate, and in the absence of phenomena like vortices, made a three-dimensional analysis unnecessary and therefore the problem was simplified to an uni-dimensional analysis. Also, the salinity conservation can be written as follows:

$$\frac{\partial c}{\partial t} = \frac{\partial}{\partial x_i}\left(D\frac{\partial c}{\partial x_i}\right) \tag{3.0.18}$$

where c is the concentration of salt obtained with

$$c = S \times \rho$$

The set of equation that describe the dynamics in the NCZ for an uni–dimensional analysis with respect of the depth of the pond then becomes

$$\rho\, C\, \frac{\partial T}{\partial t} = \frac{\partial}{\partial z}\left(K\, \frac{\partial T}{\partial z}\right) + \frac{\partial I_R}{\partial z} \tag{3.0.19}$$

$$\frac{\partial c}{\partial t} = \frac{\partial}{\partial z}\left(D\, \frac{\partial c}{\partial z}\right) \tag{3.0.20}$$

The physical properties of sodium chloride brines were calculated with empirical correlations, which are function of temperature and salt concentration (Jaefarzadeh, 2004):

$$C(c) = 4180 + 4.396\, c + 0.0048\, c^2 \tag{3.0.21}$$

$$\rho(c,T) = 998 + 0.65\, c - 0.4\, (T - 10) \tag{3.0.22}$$

$$K(c,T) = 0.5553 - 0.0000813\, c + 0.0008\, (T - 10) \tag{3.0.23}$$

$$D(c,T) = (8.16 + 0.255\, T + 0.00254\, T^2 - 0.00025\, c) \times 10^{-10} \tag{3.0.24}$$

3.1. Boundary conditions

3.1.1. NCZ boundary conditions

As for the upper and lower convection zones, the salinity and temperature were considered constant with respect to depth, based on the fact that thermal convective motions presence in these layers tend to homogenize the salinity and temperature throughout the layers. To make the numerical model representative of a three-zones solar pond, it was assumed that the UCZ and LCZ acted as storage for salt and thermal energy and interacted with the NCZ by means of specified boundary conditions. The absence of convective motions in the NCZ implies that the heat transfer between this layer and the interfaces (UCZ-NCZ, LCZ-NCZ, sidewalls-NCZ) are only due to conduction and can be described with the aid of Fourier Law of heat conduction. Therefore the boundary conditions for the NCZ are as follows:

• **NCZ-LCZ interface**

$$K_{NCZ} \left. \frac{\partial T(z,t)}{\partial z} \right|_{z=\delta_{LCZ}} = h_{LCZ} \ \left[T_{LCZ}(t) - T_{NCZ}(z = \delta_{LCZ}, t)\right] \tag{3.1.1}$$

• **NCZ-UCZ interface**

$$-K_{NCZ} \left. \frac{\partial T(z,t)}{\partial z} \right|_{z=\delta_{LCZ}+\delta_{NCZ}} = h_{UCZ} \ \left[T_{UCZ}(t) - T_{NCZ}(z = \delta_{LCZ} + \delta_{NCZ}, t)\right] \tag{3.1.2}$$

where $z = 0$ at the bottom of the pond and positive upwards, K_{NCZ} is the conductivity of the NCZ, h_{LCZ}, h_{UCZ} correspond to the heat transfer coefficients of the LCZ and NCZ, respectively, δ_{LCZ}, δ_{NCZ} and δ_{UCZ} corresponds to the thickness of the LCZ, NCZ and UCZ, respectively. The values for h_{UCZ} and h_{LCZ} have been obtained from Sodha et al. (1981).

The boundary conditions used for mass transfer at the interfaces where proposed by Alagao (1996), and are as follow:

•NCZ-LCZ interface

$$D_{NCZ}\,\frac{\partial c(z,t)}{\partial z}\bigg|_{z=\delta_{LCZ}} = \nu\ c_i \tag{3.1.3}$$

where left hand side of the equation corresponds to the Fick's Law of diffusion for the NCZ characteristics and the right hand side is the rate of make-up salt injection expressed in terms of brine velocity (ν) and brine concentration (c_i). This implies that the LCZ is being replenished with salt as it diffuses to upper layers.

•NCZ-UCZ interface

$$c_{NCZ,UCZ} = c_{UCZ} \tag{3.1.4}$$

where $c_{NCZ,UCZ}$ is the concentration of the NCZ at the boundary with the UCZ, and c_{UCZ} is the concentration of the UCZ.

3.1.2. Solar pond boundary conditions

It was assumed that the interaction between the solar pond and its environment was by means of heat transfer only, and therefore no salt was loss through any interface. The results of the energy balances between the pond and the environment are as follow:

•Sidewalls heat losses

The heat loss through the sidewalls are given by:

$$Q_s = K_{NCZ}\ \left[T_{NCZ}(z,t) - T_w\right] = K_w\left[T_w - T_g\right] \tag{3.1.5}$$

where T_w is the mean temperature of the wall, K_w is the conductivity of the wall and T_g is the temperature of the ground, far from the interface.

• Bottom heat losses

The heat losses through this interface are given by:

$$Q_b = (1 - R_b)\ I_{LCZ,b} + h_{LCZ,b}(T_{LCZ} - T_b) = K_b \frac{\partial T}{\partial z} \tag{3.1.6}$$

where R_b is the reflectivity of the bottom, $I_{LCZ,b}$ is the solar radiation that reaches that reaches the bottom of the LCZ, $h_{LCZ,b}$ is the heat transfer coefficient due to natural convection for the LCZ water-boundary interface and K_b is the thermal conductivity of the bottom.

•Surface heat losses

The heat loss through the of the solar pond consists of heat loss due to evaporation, black body radiation and convection. The latter has been already considered in the balance equations, but to account for the losses due to radiation and evaporation the following empirical models proposed by Kishore and Joshi (1984) were used to represent the real behavior of the solar pond.

• Heat loss due to radiation

This empirical model assumes that the bottom of the solar pond acts as a black body and therefore the surface of the pond will emit both short and long wave radiation, respectively. The heat flow due to radiation can thus be described with the aid of the Boltzmann Law:

$$Q_{rad} = \varepsilon\ \sigma\ (T_s^4 - T_{sky}^4) \tag{3.1.7}$$

where ε is the emissivity of the surface, σ the Stefan-Boltzmann constant and T_S is the surface temperature of the pond. The atmospheric temperature T_{sky} was approximated with the following correlation:

$$T_{sky} \approx\ T_a\ (0.55 + 0.61\sqrt{P_a})^{\frac{1}{4}} \tag{3.1.8}$$

where T_a is the ambient temperature and P_a is the partial pressure (in mm Hg) of water vapor in the air.

• Heat loss due to evaporation

The heat loss due to evaporation was estimated with this expression (Mansour et al., 2004):

$$Q_{ev} = \frac{\lambda\ h_c}{1.6\ C_s\ P_t}(P_s - P_a) \tag{3.1.9}$$

where, λ is the latent heat of evaporation of water, C_s the humid heat capacity of air, P_t the atmospheric pressure (in mm Hg). The wind convective heat transfer coefficient h_c can be estimated with:

$$h_c = 5.7 + 3.8\ V_w \tag{3.1.10}$$

where V_w is the wind velocity at the surface of the pond. The vapor pressure (in mm Hg) evaluated at the surface of the pond P_s is given by:

$$P_s = exp\left(18.403 - \frac{3885}{T_s + 230}\right) \tag{3.1.11}$$

where T_s is the temperature of the surface of the pond. The partial pressure (in mm Hg) of water vapor in ambient air P_a can be estimated with:

$$P_a = RH\ exp\left(18.403 - \frac{3885}{T_a + 230}\right) \tag{3.1.12}$$

where T_a is the ambient temperature.

3.2. Numerical Modulation

In order to obtain a representative behavior of a solar pond at the site from the numerical model, the simulation are run with weather data measured at the Spence mine. The data for temperature, humidity, wind speed, evaporation and insolation corresponding to the year 2010 has been provided (García, 2012) and used to realistically model the respective conditions. Since the weather data available is for only one year, a periodic behavior has been assumed. A Fourier analysis was used to generate continuous data from the discrete measurements and for each quantity the coefficients of a fifth order Fourier expansion of the shape

$$Y(t) = \sum_{i=0}^{5} (a_i sin\ i\omega t + b_i cos\ i\omega t) \tag{3.2.1}$$

was computed and then fitted to the data, as presented in Figure 3.1 were the measured data and the Fourier fit for ambient temperature.

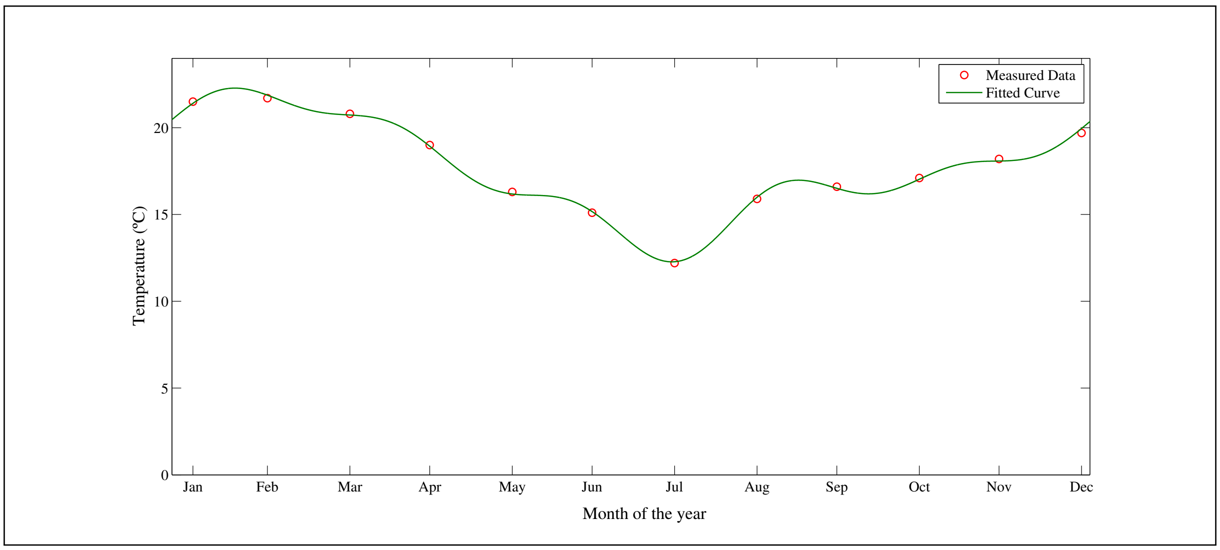

Figure 3.1: Meassured data of ambient temperature for year 2010 and Fourier fitted curve.

The insolation has been modeled with the solar angles and length of day functions presented in section 3.1 and modulated with discrete radiation measures taken in site[2]. The result is a model able to generate continuous insolation data and to illustrate a Figure 3.2 shows the solar radiation that reaches the surface of the pond for two different days of the year, one in summer and the other in winter.

[2]Data provided by JHG Ingeniería Ltda.

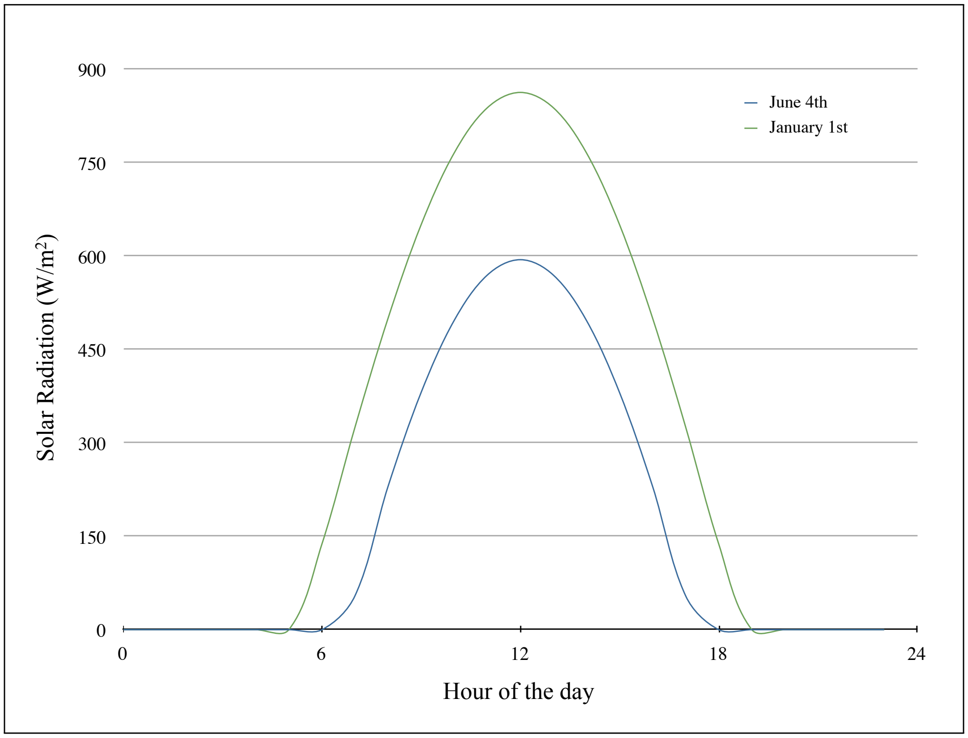

Figure 3.2: Solar radiation modeled for a summer and winter day.

3.3. Time and space mesh

To solve the partial derivatives of the mathematical model the finite differences method has been chosen, due to its simplicity in implementation, particularly when the space grid and its boundaries have no complex geometry like in a solar pond. The interior spatial derivatives were solved using a second order, centered finite difference approximation as follows:

$$\frac{du_i}{dx} = \frac{u_{i+1} - u_{i-1}}{2\,\Delta\,x} + O(\Delta x^2) \tag{3.3.1}$$

At the interfaces, three point forward and backward approximations were used for the upper and lower boundary, respectively as follows:

$$\frac{du_i}{dx} = \frac{-u_{i+1} + 4\,u_i - 3\,u_{i-1}}{2\,\Delta\,x} + O(\Delta x^2) \tag{3.3.2}$$

$$\frac{du_i}{dx} = \frac{u_{i+1} - 4\,u_i + 3\,u_{i-1}}{2\,\Delta\,x} + O(\Delta x^2) \tag{3.3.3}$$

This method approximates a partial differential equation by linear combinations of function values for grid points. The more grid points used to calculate a derivative the higher the accuracy, however, at a higher numerical costs. Therefore, the NCZ is discretized into N points (Figure 3.3) whereby the results of the model of salinity and temperature are available only for these points. The finite length corresponding to the non-convective zone is:

$$\Delta z = \frac{h_{NCZ}}{N-1} \tag{3.3.4}$$

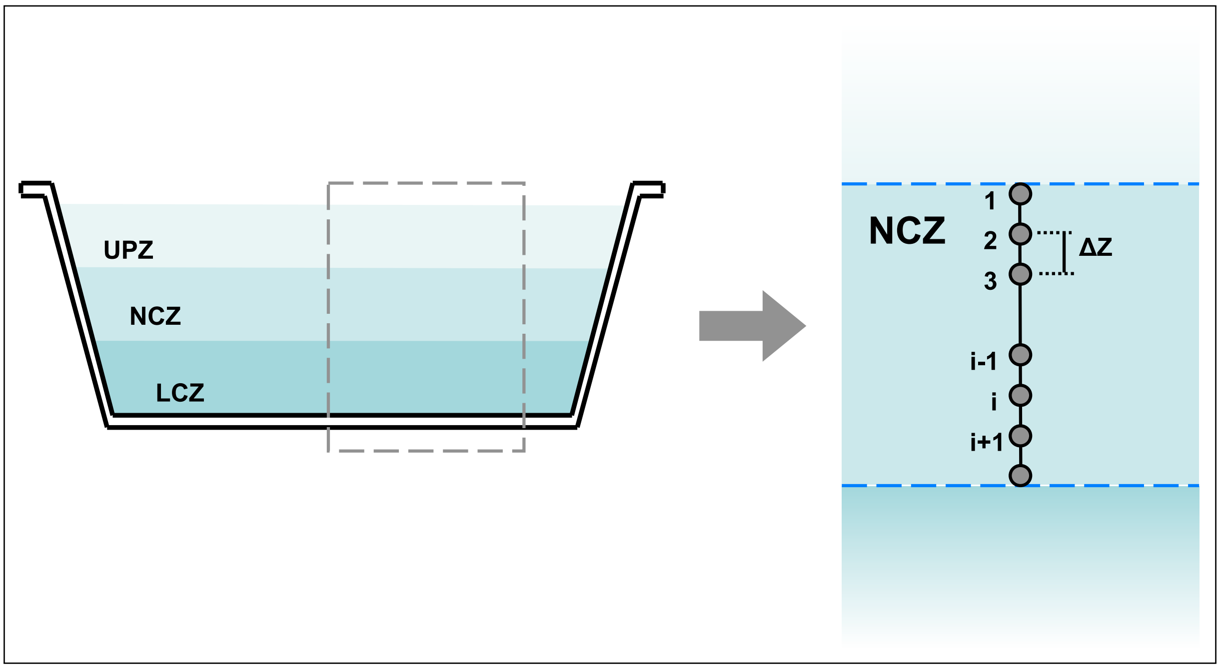

Figure 3.3: Discretization of the NCZ used for numerical resolution of the spatial derivatives.

Then, the derivative of a temperature array of N points, can be calculated with the following matrix multiplication

$$\frac{\partial T}{\partial z} \approx \frac{1}{2\Delta z} \begin{pmatrix} -3 & 4 & -1 & & & & \\ -1 & 0 & 1 & \cdots & & 0 & \\ 0 & -1 & 0 & \cdots & & & \\ \vdots & \vdots & \vdots & \ddots & & \vdots & \\ & & & & 0 & 1 & 0 \\ & 0 & & & -1 & 0 & 1 \\ & & & & 1 & -4 & 3 \end{pmatrix} \begin{pmatrix} T_0 \\ T_1 \\ T_2 \\ \vdots \\ T_{N-2} \\ T_{N-1} \\ T_N \end{pmatrix} = \sum_i D_{ij}\, T_i \tag{3.3.5}$$

being D_{ij} the central difference derivative matrix. The heat conductive equation can then be rewritten as:

$$\frac{\partial T_k}{\partial t} = \frac{1}{\rho_k\, C_k} \left[\sum_j D_{jk} \left(K_j \sum_i D_{ij}\, T_i \right) + I_k \right] \tag{3.3.6}$$

whereas the equation for salt concentration can be rewritten as:

$$\frac{\partial c_k}{\partial t} = \sum_j D_{jk} \left(D_j \sum_i D_{ij}\, T_i \right) \tag{3.3.7}$$

For equations (3.3.6) and (3.3.7), the respective Neumann boundary conditions exist at the upper and lower interface, which control the flow from the LCZ to the NCZ and from the NCZ to the UCZ. It was assumed that both the LCZ and UCZ layers were constantly in motion due to convection and therefore, mass and heat fluxes get equally distributed in the layer in a short period of time, and therefore presented a uniform temperature and salinity profile. Numerically both layers act as a storage whose capacity instantly changes as the influx changes. In order to determine the flow,Fourier Law is used for the temperature, whereas Fick Law is used for the salt concentration. With T_{LCZ} and c_{LCZ} as the temperature and salinity of the lower convection zone respectively, the applicable boundary conditions are:

$$\dot{Q} = K_{N+\frac{1}{2}}\, \frac{T_N - T_{LCZ}}{\Delta z} \tag{3.3.8}$$

$$J_R = D_{N+\frac{1}{2}}\ \frac{c_N - c_{LCZ}}{\Delta z} \tag{3.3.9}$$

In order to study the evolution in time of concentration c and temperature T in the NCZ, the time derivatives in the balance equations (3.0.19) and (3.0.20) have to be solved and integrated for each discretized point of the NCZ. To do so, the explicit Runge–Kutta of fourth order method (also known as RK4) has been chosen:

$$\frac{\partial T}{\partial t} = \frac{1}{\rho\, C}\left[\frac{\partial}{\partial z}\left(K\,\frac{\partial T}{\partial z}\right) + \frac{\partial I_R}{\partial z}\right] = f(c, T, t) \tag{3.3.10}$$

$$\frac{\partial c}{\partial t} = \frac{\partial}{\partial z}\left(D\frac{\partial c}{\partial z}\right) = g(c, T, t) \tag{3.3.11}$$

The method executes the following steps at each grid point, for a time step Δt

$$\alpha_i = f(c_i^n, T_i^n, t)$$

$$\varepsilon_i = g(c_i^n, T_i^n, t)$$

$$\beta_i = f(c_i^n + \frac{\varepsilon_i}{2}, T_i^n + \frac{\alpha_i}{2}, t + \frac{\Delta t}{2})$$

$$\epsilon_i = g(c_i^n + \frac{\varepsilon_i}{2}, T_i^n + \frac{\alpha_i}{2}, t + \frac{\Delta t}{2})$$

$$\gamma_i = f(c_i^n + \frac{\epsilon_i}{2}, T_i^n + \frac{\beta_i}{2}, t + \frac{\Delta t}{2})$$

$$\zeta_i = g(c_i^n + \frac{\epsilon_i}{2}, T_i^n + \frac{\beta_i}{2}, t + \frac{\Delta t}{2})$$

$$\delta_i = f(c_i^n + \zeta_i, T_i^n + \gamma_i, t + \Delta t)$$

$$\eta_i = f(c_i^n + \zeta_i, T_i^n + \gamma_i, t + \Delta t)$$

And the evolution in time of T and c are given by:

$$T_i^{n+1} = T_i^n + \Delta t \frac{1}{6}(\alpha_i + 2\beta_i + 2\gamma_i + \delta\delta_i) \tag{3.3.12}$$

$$c_i^{n+1} = c_i^n + \Delta t \frac{1}{6}(\varepsilon_i + 2\epsilon_i + 2\zeta_i + \eta i) \tag{3.3.13}$$

The evolution in time of these quantities is complemented with the study of the stability in the NCZ using the criteria presented in (2.3.3).

3.4. Model validation

In the absence of empirical data obtained from a pilot, the validation was carried out with operational data measured in 1982 of a 232 m^2 solar pond at the Los Alamos National Laboratory, whose objective was to study pond hydrodynamics with the aid of an underwater pyranometer. The pond was built in a ground whose geology is composed of a soft volcanic rock known as tuff, which has an approximate thermal conductivity of $\lambda = 0.05$ W/m^2C. The layers thicknesses were of 1.2 m for the LCZ and a salinity of 22%, whereas the NCZ and UCZ a thickness of 1.2 m and 0.1 m respectively. On the other hand, initial water temperature and makeup water temperature were measured at about 25°C (Jones et al., 1983). Because the performance of a solar pond depends directly on weather conditions, such data was also required to recreate the behavior of the solar pond with the model. However, only incomplete records for the year 1982 were found and so, weather data from the year 1985 (Weather Underground, 2012) and historical insolation records (Morris et al., 1985) were used in the simulation instead.

The temperature evolution record in the lower convective zone of the solar pond started on August 4^{th}, which was the day after the gradient zones was formed and ended on October 17^{th}, hence sets the time frame for the simulation. The radiation attenuation factor (θ') was set to 0.8, a value that has been used to model ponds of similar characteristics (Jaefarzadeh, 2004). The numerical results were then compared to the experimental ones (Figure 3.4) from which it could be observed that the model did indeed provide reasonably accurate results.

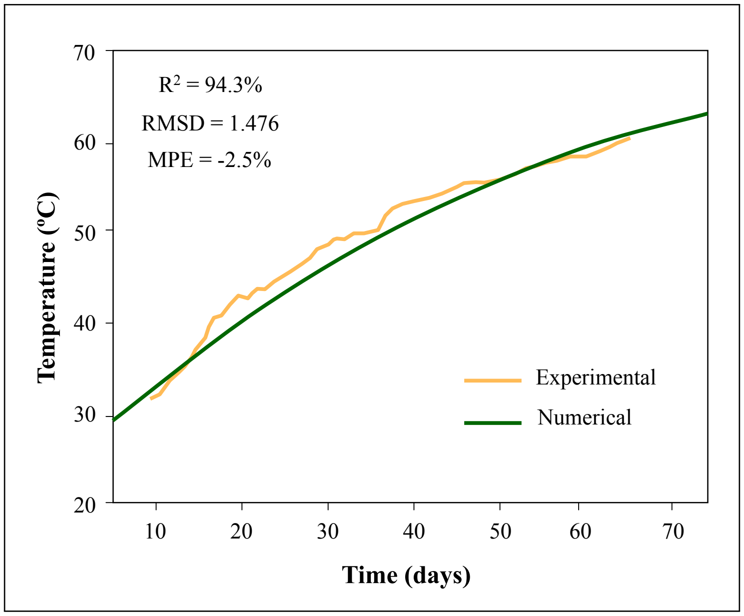

Figure 3.4: Comparison of the simulated and measured LCZ temperature evolution of the solar pond built at El Paso National Laboratory

In addition, the evolution of the entire temperature profile for the three layers were also estimated and compared (Figure 3.5). Even though the numerical results resemble the actual salinity profile, discrepancies in the LCZ and UCZ were observed. The fact that numerical results were considered for the noon, whereas the factual time of measurement is unknown and that the simulation was run with weather data different of 1982 can explain the the divergences for the UCZ temperature, which is strongly influenced by the ambient temperature. The deviation of in the LCZ can be attributed to a higher solar radiation penetration than presumed or to deviation from perfect black body behavior at the bottom.

3.5. Model restrictions

The one zone model presented is able to simulate conductive and radiation absorption processes over a long period of time and can approximate heat losses and heat extraction. However, next to linearization, discretization and averaging several other assumptions and simplifications were made to formulate the theory and they are as follows:

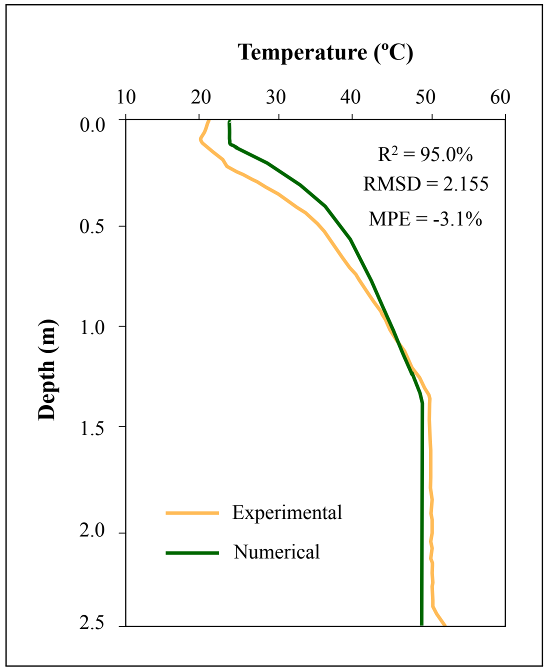

Figure 3.5: Predicted and recorded temperature profile of Los Alamos solar pond on September 3rd

- No vertical fluid motion exist inside the non-convective zone.
- Infinitely fast homogenization inside the convective layers (time steps Δ t>>1 s), therefore temperature and salinity profiles are constant in such regions.
- The boundaries between the convective and not convective layers do not move, therefore the NCZ does not grow with salt diffusion. This is equivalent to assume that perfect maintenance to the gradient is performed.
- The bottom of the solar pond behaves like a perfect black body, and therefore no radiation is reflected back to the water body.
- Modulation of density, diffusivity, conductivity and heat capacity are valid for temperatures ranging from 5 to 100°C and salinity ranging from 0 to 25%.
- The heat exchanger tubes extract heat equally throughout the lower convective zone, and therefore no horizontal gradients occur.
- Because the model is uni-dimensional, the effect of walls could not be included. However, if the surface of the bottom of the solar is large compared to surfaces of the sides of the pond

and therefore the heat losses through this interface are small compared to those through the bottom.

The time step has been set to 1 hour to ensure numerical stability and homogeneous distribution of temperature and salt concentration in the convective layers. As a result events in shorter periods of time cannot be described. Also, during times when there is no heat withdrawal, temperatures in the storage zone can raise above 100°C at which, the model becomes unreliable.

Improvements for the model would be the implementation of side walls, which would lead to additional heat losses and the separate investigation of convective motions, in order to determine the degree of homogenization and its effect (degradation) on adjacent interfaces.

4. DESIGN PARAMETERS

In this section, different parameters regarding to site conditions that condition performance as well as considerations for a proper maintenance and operation of a solar pond are reviewed in order to provide a design that addresses their effect.

4.1. Site Selection

There are parameters that make a site suitable to place a solar pond that should be considered. Solar ponds are a low energy density technology and therefore require of large areas. Knowing this, it should be situated on a land with no other potential uses, namely low mineral importance and relatively sterile. It should also be as flat as possible in order to maintain land-works to a minimum. The underlying geophysical structure should be homogeneous and free of stresses, strains and fissures. Special attention should be put into the latter, for temperature increase caused by the solar pond will lead to differential thermal expansions that can result in earth movements (Tabor, 1980).

At a certain depth below the solar pond exists an underground region where the soil or rocks are permanently saturated with water due to the presence of underground waters, which is known as water table. The presence of underground waters not only represents a threat of accidental pollution due to leakage but also it has been noticed that this layer acts as a heat sink that lowers the thermal performance of the solar pond. Saxena et al. (2009) studied the effect of the depth of the water table on the thermal performance of a solar pond, and noted that the deeper the water table is, the higher the temperature achieved in the LCZ but does not affect the time that takes to the solar pond to achieve its maximum operational temperature.

4.2. Solar pond walls

Usually solar ponds are not built by digging out the whole volume of earth, unless they are very small solar ponds, but instead they are constructed by flattening the ground with conventional land-machinery and the removed earth is used to build the walls, generally with an angle to avoid the use of wall supports and to facilitate the digging for the machinery because they can easily go

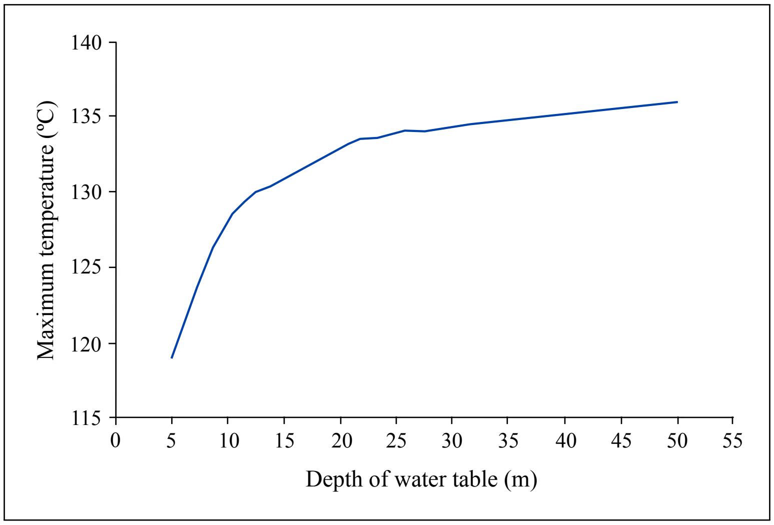

Figure 4.1: Effect of depth of water table on maximum temperature of salt gradient solar pond (Saxena et al., 2009).

in out of the excavation site, reducing the associated costs (Tabor, 1981).

Experience gained in experimental solar ponds show that walls can be a source of instability in solar ponds. Akbarzadeh (1989) observed that solar pond walls heated by insolation, after a period of time, generate convective layers on its surface (Figure 4.2) product of horizontal density and temperature gradients. These gradients would then cause variations of pressure spreading the convective layers horizontally through the pond and hence enhancing the upward salt transfer and therefore resulting in faster erosion of the salt gradient (Akbarzadeh, 1988).

In further studies, Akbarzadeh and Golding (1992) studied the influence of wall angle in the stability of the salt gradient and described its effects. To do so, they defined the normalized radiation on the inclined wall (NRI) as a measure of the enhancement of the flux of solar radiation that reaches the inclined wall by deviation from the vertical, which is written as:

$$NRI = \frac{q_i}{q_v} = sin\psi + cos\psi \sqrt{\frac{n^2}{sin^2\vartheta_i} - 1} \tag{4.2.1}$$

where ψ is the inclined wall angle with respect of the horizontal (Figure 4.3).

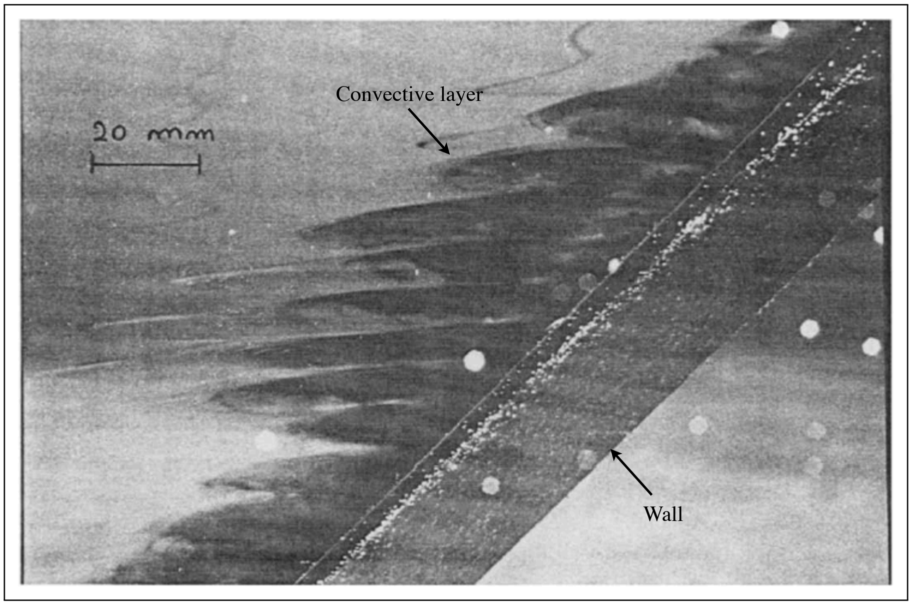

Figure 4.2: Convective layer generated due to wall heating by Sun exposition (Akbarzadeh, 1989)

Akbarzadeh and Golding (1992) noticed that most of the values of equation (4.2.1) are greater than one, and therefore concluded that any deviation from the vertical enhance the absorption of solar radiation by the wall.

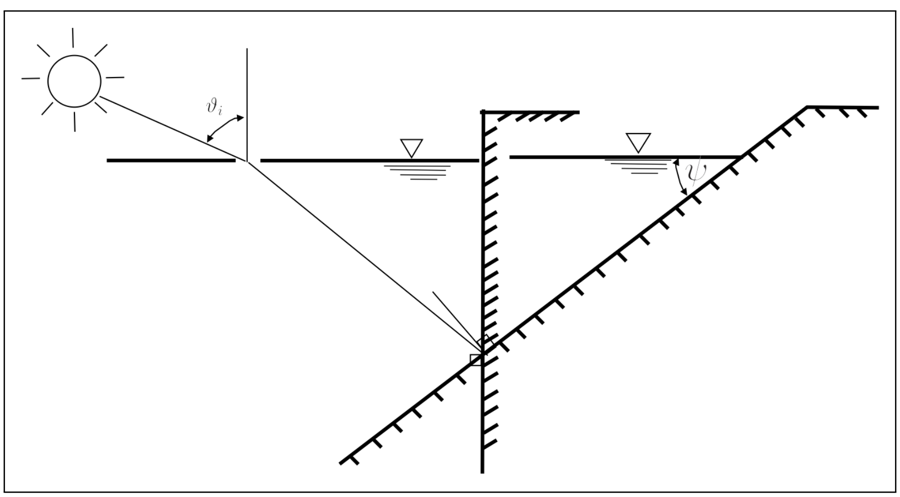

Figure 4.3: Scheme of angles used to calculate the NRI

Previously, Chen and Skok (1974) studied the effect in the stability of the temperature difference of a wall and a stratified fluid, concluding that for the same temperature difference the system becomes more stable as it deviates from the vertical, mainly to an attenuated effect of gravity.

Considering the fact that this effect opposes the effect of the absorbed radiation at the surface of a slopping wall, Akbarzadeh and Golding (1992) defined the normalized instability potential (NIP) that combines both effects as follows:

$$NIP = NRI \times sin\psi \tag{4.2.2}$$

where $\sin\psi$ is the the effect of the slope on improving the stability by reducing the gravity along the inclined wall. Combining (4.2.1) and (4.2.2) results in:

$$NIP = \left(sin\psi + cos\psi \sqrt{\frac{n^2}{sin^2\vartheta_i} - 1} \right) sin\psi \tag{4.2.3}$$

The NIP then can be used as a parameter to compare an inclined wall with a vertical wall and its potential effect of destabilization. They also noted that (4.2.2) maximizes when:

$$\psi = \frac{1}{2} \arctan \left(-\sqrt{\frac{n^2}{sin^2\vartheta_i} - 1} \right) \tag{4.2.4}$$

and can be therefore considered as the wall angle of least stability and must be considered in the design of a solar pond. It is important to mention that this angle varies with respect of the local latitude (φ), starting with about 54° in the equator and decreasing to 45° for a latitude of 23.45° (Figure 4.4).

4.3. Bottom and wall lining

The main function of the lining system in a solar pond is to prevent the leakage of hot brine between the LCZ and the ground soil, which would result in the loss of heat and salt as well as groundwater contamination. The materials used for such purpose then have to be robust, impermeable, resistant to UV radiation, tolerant to temperatures up to 90°C and to aggressive aqueous media such as brine near saturation. Most of the experimental solar ponds built so far have relied in the use synthetic liners such as high density polyethylene (HDPE), Hypalon, interpolymer alloys (such as XR-5) (Raman and Kishore, 1990) and propylene which can also be found in landfills and water containments. The estimated lifetime of these geomembranes is of approximately 20 years under temperatures of up to 160°C and high insolation; however, a lining used at El Paso solar pond

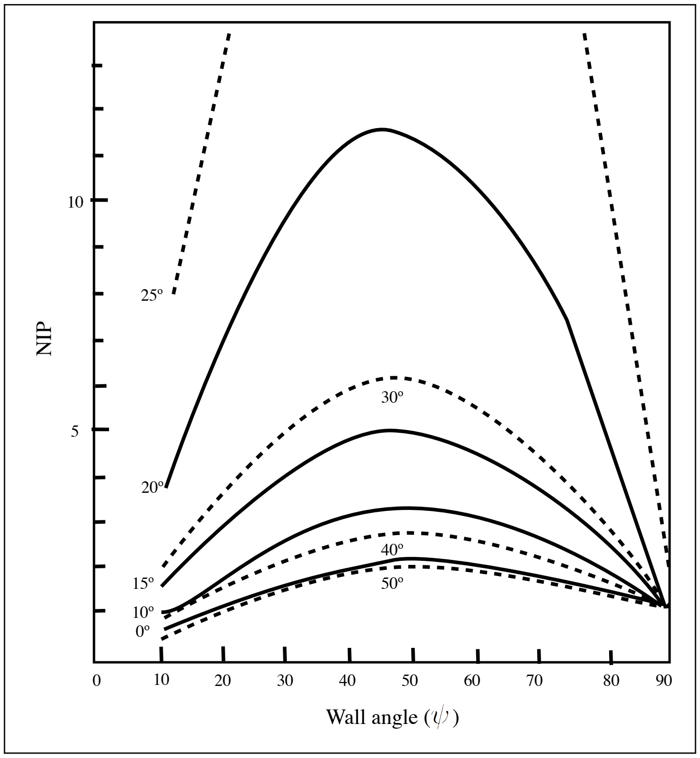

Figure 4.4: Variation of yearly maximum NIP as a function of wall angle for different latitudes (Akbarzadeh and Golding, 1992)

consisting of a cover layer of XR-5 and Hypalon layer, failed after 7 years of operation when hundreds of holes where found due to an increased brittleness in the material. The liner was replaced by a polypropylene (PP) layer which was used until the end of the project, in 2003 (Lu et al., 2004).

An important disadvantage of the synthetic liners is their high cost, that in the case of El Paso solar pond, accounted for 26% of the initial investment (Raman and Kishore, 1990). Hence, new inexpensive and effective lining techniques needed to be developed for the construction of larger solar ponds such as the Beith Ha'Arava, where a scheme consisting on polyethylene layers in a "sandwich" filled with locally available compacted clay (Tabor and Doron, 1990) was used. This new lining method reduced the cost per square meter from the US$ 42 spent in previous projects to only US$ 12 [3]. This scheme has been improved by Kumar and Kishore (1999), which developed a cost–effective system for a 6,000 m^2 solar pond in Kutch, India (Figure 4.5). Such results motivated the study by Silva and Almanza (2009), who analyzed in depth the performance of several

[3] 1990 dollars in present value

types of compacted clays (CCL) under solar pond conditions, and concluded that some can be impermeable enough to work even without a synthetic layer, whereas others where not suitable for lining. The attractiveness of clay liners, however, underlies mostly in the cost of the material which is very site-specific, being cheap if available nearby and expensive if not (ANCID, 2004), for they are difficult to build, have to be thicker and require more land work than using geosynthetic membranes (Silva and Almanza, 2009). Clays have also been used in geosynthetic clay liners (GCL), which are a mixture of clay and synthetic membranes that are easy to install and are cost attractive. They were tested also at El Paso solar pond, however with discouraging results due to low UV resistance and manufacturing defects, failing only two years after its installation.

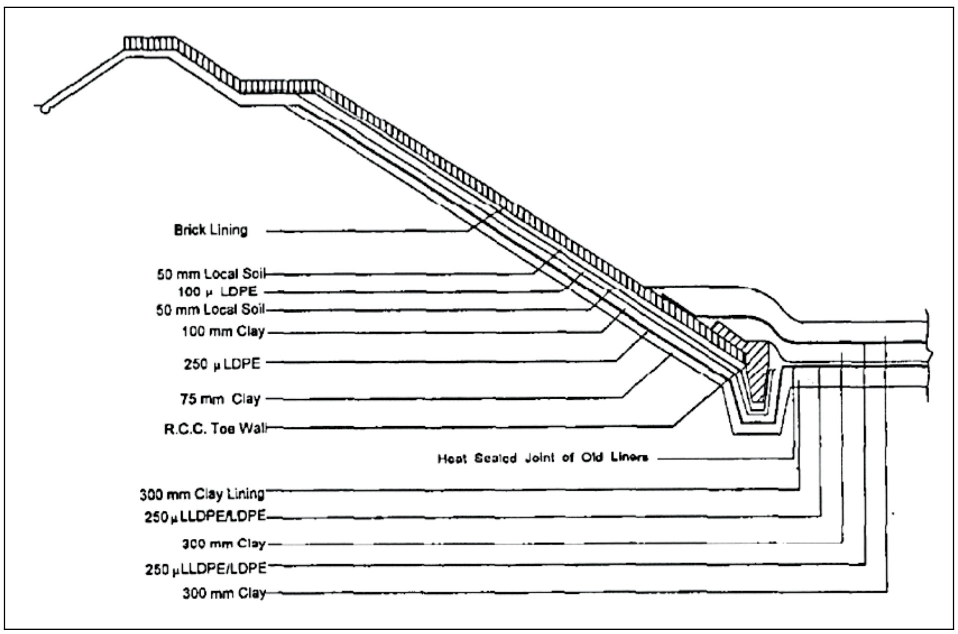

Figure 4.5: Lining scheme for solar ponds developed in India (Kumar and Kishore, 1999)

Some properties of lining materials and costs (material and installation) have been provided by Garrido (2012b), senior engineer at Environmental Information and Logistic (EIL), LLC [4] (except for the bentonite CCL) and are presented in Table 3.

[4]http://www.eilllc.com

Table 3: Properties of common materials used for solar pond lining

Material	Thickness (mm)	k (W/m°C)	Permeability	Cost US$/m^2
HDPE	1.5	0.46-0.52	–	5.2
LDPE	1	0.3-0.34	–	3.2
Bontomat CL (GCL)	6.7	0.17	2.32 (cm s^{-1})$\times 10^{-11}$	5.8
Bentonite (CCL)	600	0.6	1.4 (cm s^{-1})$\times 10^{-7}$	5-22 *

*Depending on availability (Silva and Almanza, 2009)

In certain cases, the lining not only works as a hydraulic barrier, but can also work as a thermal insulation layer to reduce the heat losses through conduction between the LCZ and the ground. This results useful in cases where the soil has a relatively high thermal conduction or the water table is located near to the surface. Zhang and Wang (1990) studied the effect of adding an insulating layer to a solar pond where the water table is located at 5.5 m below the bottom of the solar pond and compared it to the same solar pond without thermal insulation and with a solar pond where the water table is located 20.5 m below (Table 4). They noticed that the insulation layer not only helped to increase the average temperature of the LCZ in almost 20 °C compared to the pond without it, but also to reach a higher temperature to that of the solar pond with a lower water table. Zhang and Wang (1990) proposed the inclusion of polystyrene foam (XPS) layers as insulation to the lining, for its low thermal conductivity ($\approx$ 0.035) and durability.

Table 4: Effect of adding an insulating layer to solar ponds close to the water table in the average temperature of the LCZ

Water table depth	20.5 m	5.5 m	
Thermal Insulation	No	No	0.4 m XPS
Years	Average LCZ temperature (°C)		
1	68.3	66.2	82.2
2	93.6	84.0	102.8
3	98.4	84.4	103.0
4	100.7	84.5	103.2
5	102.0	84.5	103.3

The thermal performance of the lining insulation to be used solar pond can be assessed by calculating the heat losses through the ground. To do so, firstly the overall heat transfer coefficient has to be estimated as follows:

$$\frac{1}{U_g} = \frac{1}{h_{LCZ}} + \frac{t_i}{K_i} + \frac{l_{sink}}{K_g} \tag{4.3.1}$$

where h_{LCZ} is the heat transfer coefficient due to natural convection in the LCZ that research by Sodha et al. (1981) determined to be 78,92 W/m^2°C. Also, t_i corresponds to the thickness of the insulation, K_i is the thermal conductivity of the insulation, l_{sink} is the depth of the water table and K_g is the thermal conductivity of the ground. Then, the heat losses through the ground per square meter are given by:

$$Q_g = U_g\left(T_{LCZ,t} - T_{sink}\right) \tag{4.3.2}$$

where $T_{LCZ,t}$ is the temperature of the of the LCZ at time t and T_{sink} is the temperature of the water table.

4.4. Layers thickness

As mentioned before part of the solar radiation that reaches the surface of the solar pond is absorbed, reflected back to the atmosphere and scattered by the UCZ and the NCZ before it can be absorbed by the LCZ and be available for its extraction. Therefore, to collect the maximum amount of energy it is necessary to let as much solar radiation as possible to reach the bottom. The thicker the UCZ and NCZ are, the less solar radiation is absorbed by the LCZ (Peinan and Hongfei, 1994).

The presence of the UCZ at the top of a solar pond is product of wind mixing, penetrative convection and the action of salt diffusion. This layer grows at expense of the NCZ thickness (FIgure 4.6), which reduces the conductive insulation hence increasing the heat losses to the atmosphere (Punyasena et al., 2003). Also, about one third of the total solar radiation incident on the surface of the pond is absorbed by this layer and then lost to the atmosphere, thus reducing the thermal efficiency (Akbarzadeh et al., 1983). Then, it is desirable that the UCZ is kept as thin as possible, preferably in the range of 5 cm (Tabor, 1980) and at a maximum of 20 cm (Shladow, 1984), by counteracting the aforementioned phenomena.

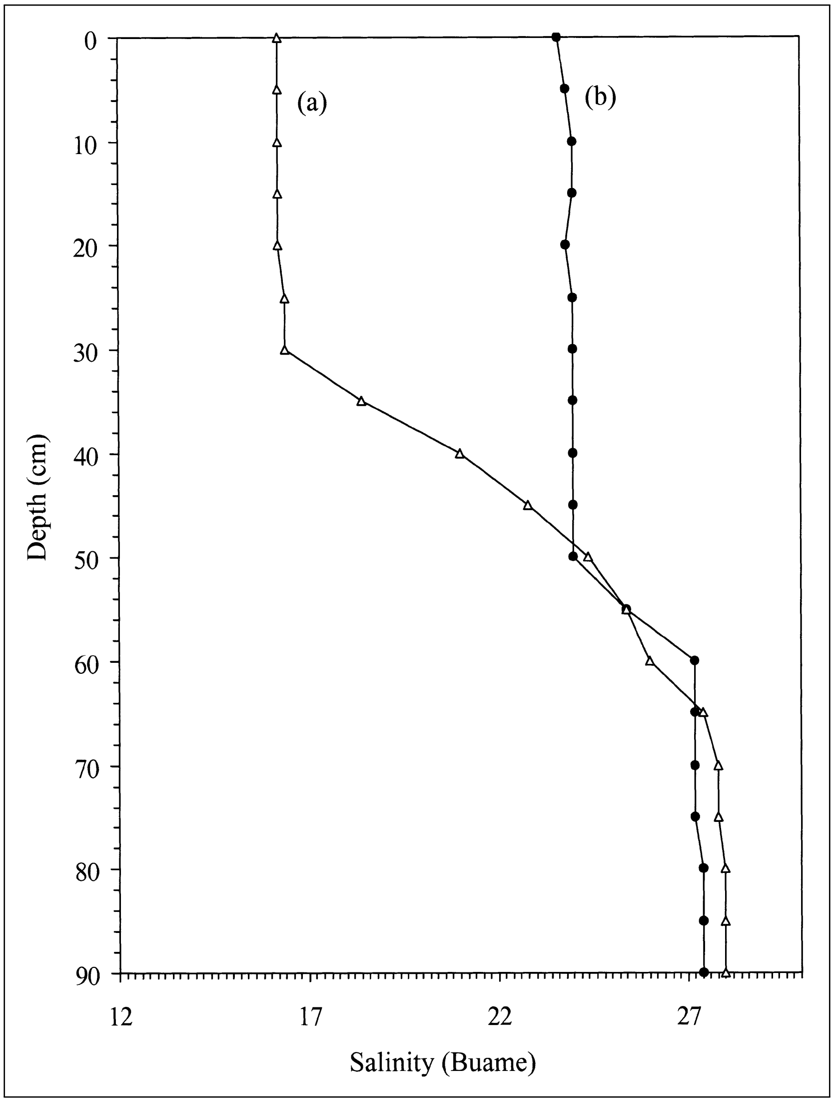

Figure 4.6: Initial salinity profile (a) and growth of the UCZ (b) by the action of wind and rain registered in a solar pond in Sri Lanka (Punyasena et al., 2003)

When the remnant energy is stored in the LCZ, part of it is scattered or lost through walls and bottom, but if they are adequately insulated, then the heat is lost mostly by conduction through the NCZ. If such is the case, the NCZ plays an important role as a thermal insulation layer, and therefore cannot be too thin. Peinan and Hongfei (1994) proposed a method to optimize the size of this layer to obtain a better thermal performance. By assuming that the initial temperature of both the UCZ and NCZ equal to the ambient temperature, that the stratification of the layers is clear and that the temperature within the NCZ increases gradually from top to bottom, they proposed that the useful energy in the LCZ is:

$$Q_u = \bar{p}\, \bar{I}_0 \left[a - b\, ln\left(\frac{\delta_{UCZ} + \delta_{NCZ}}{cos\vartheta_I}\right)\right] - \left(\frac{k\, \Delta T}{\delta_{NCZ}}\right) - Q_w \tag{4.4.1}$$

where, $\bar{p}$ is the average weighted coefficient of direct and diffuse irradiation, $\bar{I}_0$ is the average surface solar irradiance,a and b are constants ($a = 0.36$, $b = 0.08$), δ_{UCZ} and δ_{NCZ} are the thicknesses of the UCZ and NCZ respectively, ϑ_I is the refraction angle, ΔT is the temperature difference between the ambient temperature and the objective temperature and Q_w is the heat lost by conduction through walls and bottom. By optimizing (4.4.1) with respect of δ_{NCZ} results:

$$\frac{dQ_u}{d\delta_{NCZ}} = \frac{-b\, \bar{p}\, \bar{I}_0}{\delta_{UCZ} + \delta_{NCZ}} + \frac{k\, \Delta T}{\delta_{NCZ}} = 0 \tag{4.4.2}$$

and solving:

$$\delta^*_{NCZ} = k\, \Delta T\, \frac{\Gamma}{2\, b\, \bar{p}\, \bar{I}_0} \tag{4.4.3}$$

where $\Gamma = 1 + \sqrt{1 + (4\, x_1\, \bar{p}\, \bar{I}_0/k\Delta t)}$ and δ^*_{NCZ} is the thickness of the NCZ that maximizes the energy that penetrates through the layer below. As for the LCZ, this layer is responsible for one of the distinguishing features of the solar pond, that is having a built-in seasonal energy storage whose capacity is proportional to the thickness of this layer (Prasad and Rao, 1996). However, as the LCZ consists of nearly saturated brine, an increase in the thickness of the LCZ increases the salt requirements and hence the cost of the pond. Therefore the thickness of the pond should be the minimum necessary to meet the energy requirements, considering energy losses. Also, the heat withdrawal from this layer induces temperature variations that can lead to the erosion of the NCZ if the LCZ does not have the adequate thickness. The end-use of the energy determines the heat withdrawal pattern and the minimum acceptable temperature at the LCZ, whereas the maximum temperature is limited by the boiling point of the brine (Prasad and Rao, 1996).

4.5. Salt gradient establishment

The salt gradient in the NCZ is the key element of a solar pond whose establishment is not trivial. In earlier ponds, the gradient was established with a highly time demanding and expensive technique, in which progressively less dense brine were superposed. This method required an additional pond in which the batches of decreasing salinity were prepared and then pumped and injected into the pond with a diffuser to avoid stirring of the layers that was usually suspended over the pond or floating on the rising surface (Zangrando, 1980).

Zangrando (1980) proposed a simpler method that did not require additional mixing tanks or ponds and that was suitable for solar ponds of any size. The procedure consisted basically in filling partially the pond with high salinity brine and then inject fresh water at low speed with a diffuser immersed in the upper portion of the brine, which progressively dilutes the brine above it creating the gradient. Because the level of water increases in the pond, the diffuser has to be raised either in a continuous motion or in discrete steps of 5 cm each (determined from experience) with such timing that when the water reaches the desired level the diffuser reaches the surface.

An improved variation of this method was developed in 1995 at the El Paso solar pond named "Scanning injection technique" (Lu et al., 2004), in which the diffuser, instead of staying fixed in each step, it continuously goes up and down (scans) within a preset region during each step of injection (scanning region). In this method, the steps are of 5 cm and the scanning region is set to 20 cm. The volume of fresh water injected in each step is determined by:

$$V_{inj} = (V_z)_i \left[\frac{c_{z,i} - c_{z,f}}{c_{z,f}} \right] \tag{4.5.1}$$

where V_{inj} is the volume of fresh water added, $c_{z,i}$ is the initial concentration of the brine at step z and $c_{z,f}$ is the desired concentration of the brine after the injection of water at step z.

At the El Paso solar pond, 990 t of salt were used to develop a LCZ of 120 cm with brine at near saturation concentration and a NCZ of 150 cm thick in about one week. The water injection was carried out in 30 steps (Table 5), in which the flow rate ranged from 7.6 to 9.5 l/s at a velocity of 2.5 to 2.9 m/sec. The scanning speed of the diffuser was set to 10 cm/min for the downward movement and 7 cm/min for the upward movement.

Table 5: Parameters used for Scanning injection technique at El Paso solar pond

Step	Scan Range (cm)	Volume Injected (m^3)	Flow rate (l/s)
1	120–140	36.8	9.5
1	125–145	36.8	9.5
.	.	.	.
24	235–255	41.8	9.1
25	240–257	45.4	9.1
26	245–259	41.6	9.1
27	250–261	47.1	8.2
28	260	47.4	7.6
29	265	49.1	7.6
30	270	Level of pond is completed adding water onto the top	

Both the fixed level and scanning injection techniques have been used at El Paso solar pond, which Lu et al. (2004) compared and concluded that the scanning injection technique is able to create a smoother gradient, with less labor and in 50% of the time. Therefore, the latter is the method that should be used to construct the gradient.

The diffuser has also been subject of improvement at El Paso solar pond. Prior to 1995, the design of diffusers consisted of two circular plates with a small gap between them (Figure 4.7), however this type of design had difficulties when placed near the banks or the instrumentation tower. The new technique for the construction of the salt gradient also considered an improved design of PVC diffuser (Figure 4.8) of tubular shape with 12 slots from where the water exits at a design velocity of 2.8 m/s and flow rate of 0.57 m^3/min. The injection diffuser is driven by a computer software controlled DC motor and a drum-cable system (Lu et al., 2004).

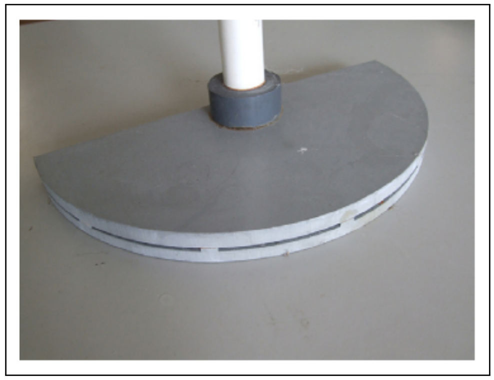

Figure 4.7: Circular diffuser design (Leblanc et al., 2011)

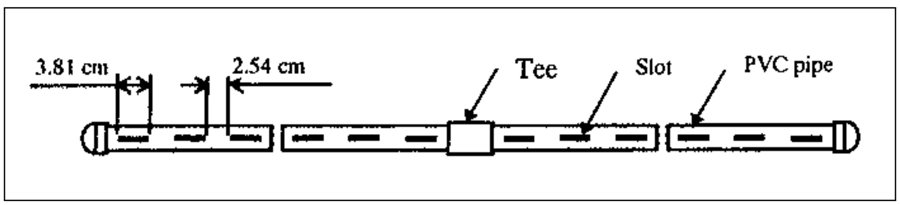

Figure 4.8: Diffuser design used in the El Paso solar pond (Lu et al., 2004)

4.6. Salt and water

In principle, any inorganic salt can be used to establish the density gradient in a solar. However, aspects such as cost, availability, pollution risk and solubility without significant solar radiation attenuation limit the range. Therefore, most solar ponds are built in places where water and salt are already available. Such is the case of the El Paso solar pond that used salt from an underground salt mine used to store nuclear wastes and the Beith Ha'Arava solar pond was filled with Dead Sea compounds (Mehta et al., 1988). The most commonly used salts are sodium chloride (known also as common salt) and magnesium chloride obtained from the evaporation of seawater (Kaushika, 1984). Hassairi et al. (2001) studied the use of natural brines and compared its performance against a sodium chloride solar pond, noticing that the latter had a better thermal performance.

4.7. Heat extraction

In a solar pond, the heat is usually withdrawn from the LCZ and this has been achieved with two different approaches. In the first one, hot brine is pumped out of the LCZ, circulated through a heat exchanger and then pumped back at a lesser temperature into the lower layer. In the second, a heat exchanger is placed inside the LCZ, hence known as internal heat exchanger (IHE), in which a cold flow (usually of water) is passed through and heated up. Alternatively, the flow can be circulated through the IHE and a secondary external heat exchanger in a closed loop configuration to heat up a different cold flow (Appendix B.1). The brine withdrawal approach was used at the El Paso solar pond and the second is currently used at the Pyramid Hill solar pond (Leblanc et al., 2011).

Based on the experience of a solar pond built in Miamisburg, OH that employed both approaches in two stages of operation, Sabetta et al. (1985) identified the main problems of each. The hot brine withdrawal requires heat transfer equipment withstand corrosion, which can significantly increase the cost of the system (twice the cost of an in-pond heat exchanger). Secondly, the extraction of hot brine has to be carried out at low velocities to avoid the erosion of the NCZ for which large diffusers are used. However, at the Miamisburg solar pond, it was found that most of the flow was suctioned within the inital 10% of the dffuser pipe length, resulting in much larger than predicted velocities and constant gradient erosion.

With regard to the internal heat exchanger Sabetta et al. (1985) indicate that the IHE is subject to corrosion and therefore commonly used materials for heat transfer cannot be used. For maintenance and repairing, the internal heat extraction may have to be removed, rendering the solar pond useless. This method can also generate a non uniform temperature distribution in the UCZ if the solar pond is large compared to the IHE. The main advantage of the IHE over the hot brine withdrawal is that it has a negligible effect on the gradient stability and therefore (Sabetta et al., 1985) suggest that the employment of the internal heat exchanger is preferable if corrosion and maintenance issues can be avoided, no matter the size of the solar pond.

To avoid all of the aforementioned issues of an internal heat exchanger, the IHE used at the Pyramid Hill solar pond was entirely made of polyethylene, whose low thermal conductivity was compensated with a larger heat transfer area. As it can be seen in Figure4.9, it consists of a discharge manifold that distributes a water flow to a mesh of evenly separated tubes that transversely crosses the pond, right below the NCZ-LCZ interface to facilitate convection, and connects to a return manifold that collects the hot water (Leblanc et al. (2011)).

Figure 4.9: In-pond heat exchanger (IHE) used at Pyramid Hill (Leblanc et al., 2011)

To design an IHE that withdraws the heat from the LCZ at temperature T_{LCZ}, and raise the inlet temperature T_{in} of a constant mass flow to an outlet temperature T_{out}, first the heat exchange rate between the LCZ and a differential volume of the tube has to be characterized as follows:

$$d\dot{Q} = U_{HX}\ (T_{LCZ} - T)\ dA_{s,HX} \tag{4.7.1}$$

where U_{hx} is the overall heat transfer coefficient, dA_{HX} is the infinitesimal surface area of a tube that composes the IHE. As a result, the temperature of the fluid inside the tube will increase its temperature as follows:

$$U_{HX}\ dx\ p_{c,HX}\ (T_{LCZ} - T)\ dt = dx\ A_{c,HX}\ \rho\ C\ dT \tag{4.7.2}$$

where dx is an infinitesimal length of one of the tubes that composes the IHE, $p_{c,HX}$ and $A_{c,HX}$ are the cross section perimeter and area of one of the tubes respectively whereas ρ and C

are the density and specific heat of the fluid inside the tube. The left hand side of equation (4.7.2) corresponds to the heat that goes into the infinitesimal section of the tube during dt whereas the right hand side corresponds to the increase in the energy of the flow in the section during dt. Rearranging equation (4.7.2) it gives:

$$\frac{d(T - T_{LCZ})}{T - T_{LCZ}} = \frac{U_{HX}\ p_{c,HX}}{\rho\ C\ A_{c,HX}}\ dt \tag{4.7.3}$$

Integrating equation (4.7.3), it yields:

$$ln\frac{T(t) - T_{LCZ}}{T_{in} - T_{LCZ}} = \frac{U_{HX}\ p_{c,HX}}{\rho\ C\ A_{c,HX}}\ t \tag{4.7.4}$$

Isolating T(t) in equation (4.7.4), results:

$$T(t) = T_{LCZ} - (T_{LCZ} - T_{in}) \exp\left(-\frac{U_{HX}\ p_{HX}}{\rho\ C\ A_{c,HX}}\ t\right) \tag{4.7.5}$$

Equation (4.7.5) provides the temperature of the pumped water in the tube over time. Using it to replace T in equation (4.7.1), the resultant equation yields the energy transfer as follows:

$$d\dot{Q} = (T_{LCZ} - T_{in}) \exp\left(-\frac{U_{HX}\ p_{HX}}{\rho\ C\ A_{c,HX}}\ t\right) U_{HX}\ p_{HX}\ dx \tag{4.7.6}$$

Assuming that the mass flow moves at a constant velocity $W = x/t$ through a heat exchanger composed by N tubes equation (4.7.6) gives:

$$d\dot{Q} = (T_{LCZ} - T_{in}) \exp\left(-\frac{U_{HX}\ p_{HX}}{W\ \rho\ C\ A_{c,HX}}\ x\right) U_{HX}\ p_{HX}\ dx \tag{4.7.7}$$

Integrating equation (4.7.7) through the length of the tube results:

$$\dot{Q} = \ W\ A_{c,HX}\ \rho\ C\ (T_{LCZ} - T_{in})\ \left(1 - \exp\left(-\frac{U_{HX}\ p_{HX}\ L}{W\ A_{cHX}\rho\ C}\right)\right) \tag{4.7.8}$$

where L is the length of a single tube. The surface area of each tube corresponds to $A_{s,HX} = p_{HX}\ L$ and $\dot{m} = W\ A_{c,HX}\rho$. Equation (4.7.8) can be re written as:

$$\dot{Q} = \ \dot{m}\ C\ (T_{LCZ} - T_{in})\ \left(1 - \exp\left(-\frac{U_{HX}\ A_{s,HX}}{\dot{m}\ C}\right)\right) \tag{4.7.9}$$

Equation (4.7.9) provides the energy extracted from the LCZ by one tube. If the IHE is compossed by N tubes, then $\dot{m}$ corresponds to the N$^{\text{th}}$ part of the total mass flow that has to be heated up, namely the water used to wash cathodes.

The outlet temperature of the flow is then calculated with

$$T_{out} = T(L/W) = T_{LCZ} - (T_{LCZ} - T_{in})\ \exp\left(-\frac{U_{HX}\ A_{s,HX}}{\dot{m}\ C}\right) \tag{4.7.10}$$

And the required heat exchange surface area to achieve T_{out} is given by:

$$A_{s,HX} = \frac{\dot{m}\ C}{U}\ \ln\left(\frac{T_{LCZ-T_{in}}}{T_{LCZ} - T_{out}}\right) \tag{4.7.11}$$

The overall heat transfer coefficient (U_{HX}) is given by

$$\frac{1}{U_{HX}} = \frac{d_e}{d_i}\left(\frac{1}{h_i}\right) + \frac{d_e}{2\ K_{HX}}\ \ln\left(\frac{d_e}{d_i}\right) + \frac{1}{h_e} \tag{4.7.12}$$

where h_i is the heat transfer coefficient due to forced convection inside the tube, d_e and d_i are the external and internal diameters of the tube and K_{HX} is the conductivity of the tube and h_e is the heat transfer coefficient due to natural convection outside the tube. The determination of h_i depends of the geometry of the tubes and type of flow, namely laminar or turbulent and are given by:

$$h = \frac{K_w}{d_i}\ Nu \tag{4.7.13}$$

where K_w is the conductivity of the internal flow and Nu is the Nusselt number, whose calculation varies with the type of fluid. For laminar flow it can be assumed that $Nu = 3.66$ (Jaefarzadeh, 2006) whereas for turbulent flow the Nusselt number can be calculated with the Dittus-Boelter correlation:

$$Nu = 0.023\ Re^{0.8}\ Pr^{0.4} \tag{4.7.14}$$

where Re is the Reynolds number, which is given by:

$$Re = \frac{\rho_w \; v \; d_i}{\mu_w} \tag{4.7.15}$$

and Pr is the Prandtl number, calculated with:

$$Pr = \frac{C_w \; \mu_w}{K_w} \tag{4.7.16}$$

where ρ_w is the density, v is the mean velocity, μ_w is the dynamic viscosity and C_w is the specific heat of the fluid running inside the tube that in this case is water. To calculate h_e, the following correlation for a long pipe under external natural convection is used (Kern, 1950):

$$h_e = \frac{0.53 \; K_{LCZ}}{d_e} \left[\left(\frac{d_e^3 \; \rho_{LCZ,f}^2 \; g \; \beta \; (T_w - T_{LCZ})}{\mu_{LCZ,f}^2} \right) \left(\frac{C \; \mu_{LCZ,f}}{K_{LCZ}} \right) \right] \tag{4.7.17}$$

where K_{LCZ} is the thermal conductivity ρ is the density, g is the gravity acceleration, β is the volumetric expansion coefficient,ν is the kinematic viscosity, α is the linear thermal expansion coefficient, T_w is the temperature of the external wall of the tubes and the subscript "LCZ, f" means that the properties are evaluated for LCZ brine at film temperature. The film temperature is the defined as:

$$T_f = \frac{T_w + T_{T_{LCZ}}}{2} \tag{4.7.18}$$

As mentioned above, corrosion represents a major threat for the IHE. Hence, they are usually designed with materials resistant to saturated brine at moderately high temperatures such as polypropylene (PP) or polyethylene (PE) compounds (Leblanc et al. (2011); Sabetta et al. (1985)). These materials are usually used for piping and not for heat exchange and hence the low thermal conductivity of PP (0.22 W/m °C) and PE (0.38 W/m °C) (Simona AG, 2011a), which results in large heat exchange areas and proportionally large lengths of tubes. Table 6 shows the cost per meter of pressure tubes made of PP-H AlphaPlus® (Simona AG, 2011b) and PE-100 (Simona AG, 2011a) for various commercial diameters and thicknesses:

Table 6: Cost per meter of PP and PE tubes

	PP-H AlphaPlus®		PE-100	
Diameter mm	Thickness mm	US$/ m	Thickness mm	US$/ m
32	1.8	3	1.9	2.6
50	2.9	4.8	3	3.9
75	4.3	10.2	4.5	7,0
90	5.1	14.3	5.4	9.1

From Table 6, both the PE and PP have been used in in-pond heat extraction systems with good results, but PE-100 not only has a 72% higher thermal conductivity than the PP-H but from Table 6 it can be noticed that it is also cheaper, making it more suitable for the purpose of the solar pond and is therefore chosen for the design.

4.8. Water circulation power

To circulate the water through the heat extraction system it is necessary to use a pump to overcome the pressure loss due to friction inside the tubes and intake and discharge height differences. The power required by the pump can be calculated as follows:

$$P_p = \frac{\dot{m}_{cw}\ w_p}{\eta_p} \tag{4.8.1}$$

where $\dot{m_{cw}}$ corresponds to the water flow used to wash the cathodes, w_p is the specific work of the pump and η_p is the efficiency. The specific work of the pump can be calculated with (ASHRAE, 2009):

$$w_p = \frac{\Delta p_t + \Delta p_{\Delta p}}{\rho_w(T)} \tag{4.8.2}$$

where Δp_t is the pressure loss due to the friction inside the tubes of the heat exchanger, $\Delta p_{\Delta p}$ is the pressure loss due to height difference between the intake and point of discharge and $\rho_w(T)$

is the density of the water flow inside the tubes at temperature T. The pressure loss due to friction in a circular pipe can be calculated with the Darcy-Weisbach equation:

$$\Delta p_t = f_t \left(\frac{L_t}{D_i}\right) \frac{\rho_w(T)\, V_w^2}{2} \tag{4.8.3}$$

where f_t is the friction factor of the tubes, L_t is the length of the tubes composing each heat exchanger, D_i is the internal diameter of the tubes and V_w is the average velocity of the water flow. The friction factor can be either determined with the Moody chart or calculated with the Churchill equation, which is valid for any value of the Reynolds number and not iterative (Menon and Menon, 2010):

$$f_t = 8\left[\left(\frac{8}{Re_t}\right)^{12} + (A+B)^{-\frac{3}{2}}\right]^{\frac{1}{12}} \tag{4.8.4}$$

where the parameters A and B are calculated as follows:

$$A = \left[2.457\; ln\left(\left(\frac{7}{Re_t}^{0.9}\right) + 0.27\frac{\varepsilon_t}{D_i}\right)\right]^{16}$$

$$B = \left(\frac{37530}{Re_t}\right)^{16}$$

where ε_t is the absolute roughness in the interior of the tubes and Re_t is the Reynolds number for the water flow inside the tubes, which is given by:

$$Re_t = \frac{D_i\; V_w\; \rho_w(T)}{\mu_w(T)} \tag{4.8.5}$$

where $\mu_w(T)$ is the dynamic viscosity of water at temperature T. The pressure loss in the discharge manifold can be calculated with (Green and Perry, 2008):

$$\Delta p = \left(\frac{4fL}{3D} - 2K\right) \frac{\rho V_i^2}{2} \tag{4.8.6}$$

where Δp is the net pressure loss over the length of he manifold distributor, L is the length of the manifold, D is the diameter of the manifold, f is the Fanning friction factor and V_i is the manifold inlet velocity. The factor K represents the losses due to momentum recovery, which for discharge manifolds is usually 0.5. The pressure loss in the return manifold can be calculated with (Green and Perry, 2008):

$$\Delta p = \left(\frac{4fL}{3D} + 2K \right) \frac{\rho V_i^2}{2} \tag{4.8.7}$$

For return manifolds, the factor K is usually very close to 1.

The pressure loss due to height difference between the intake and discharge point can be calculated with the following relationship:

$$\frac{\Delta p_{\Delta p}}{\rho_w(T)\ g} = \Delta z - \frac{1}{\rho_w(T)} \left(\frac{\Delta z}{2}\ \left[\rho_w(T_i) + \rho_w(T_o) \right] \right) \tag{4.8.8}$$

where g is he gravity acceleration, Δz is the height difference between the intake and outlet point, $\rho_w(T_i)$ is the density of the water flow at intake temperature and $\rho_w(T_o)$ is the density of the water flow after being heated up.

4.9. Solar pond monitoring and control

The efficient operation of a solar pond requires the establishment of a density gradient of a determined thickness, the maintenance of its stability, and the clarity of the brine and the early detection and solution of any undesired phenomena so the performance of the pond can be kept as predicted. It is therefore necessary to count with monitoring procedures for the measurement of key parameters in the thermal performance of a solar pond such as brine clarity, temperature and salinity distribution to estimate the shape of both the density and temperature gradients in order to asses the stability of the pond with the criteria presented in (2.3.3)) in a regular basis by means of reliable instrumentation.

One of the many developments achieved during the operation of El Paso solar pond was an automated instrumentation system (Lu et al., 2004) that consisted of a DC motorized drum-cable scanner with a sensor head and two thermocouples, a sample pump mounted on the deck of an instrumentation tower (Figure 4.10), an ”U” tube density meter, pH probe, turbidimeter and cooling heat exchanger mounted on the same enclosure on the pond bank near the instrumentation tower. This integrated configuration allowed the simultaneous measurement of temperature, salinity and brine clarity for the entire depth of the pond in 3 hours.

The polypropylene sensor head (Figure 4.11) withdrew small samples of brine at each step and flowed them through the cooling heat exchanger to decrease their temperature, before sending them to the turbidimeter, density meter and pH probe. The thermocouples were aligned and mounted in opposite sides of the scanner and provided of redundant information of the temperature. To ensure a smooth downward movement and to avoid the buoyancy of the scanner in the high density brine a counter weight was attached to the bottom of the sensor head.

Figure 4.10: Instrumentation tower at El Paso solar pond (Leblanc et al., 2011)

The measurement of salinity, pH and turbidity could be performed on a weekly basis, since changes of these parameters occured very slowly. However, temperature measurement has to be taken on a daily basis. The spatial steps for temperature and salinity measurement should be of 5

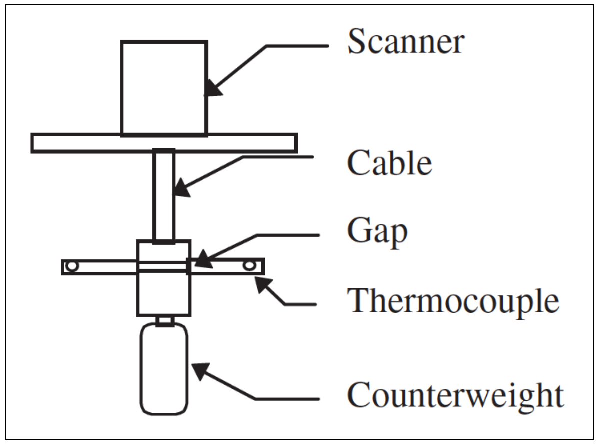

Figure 4.11: Scanner used for monitoring procedures at El Paso solar pond (Leblanc et al., 2011)

cm or less, in order to ensure a resolution capable of detect gradient breakdowns, whereas turbidity should be performed in steps of 10 cm (Lu et al., 2004).

4.10. Solar pond maintenance

4.10.1. Salt gradient maintenance

The optimal operation of a solar pond requires measures to counteract the action of salt diffusion in order to maintain the design thicknesses, concentrations of the layers and expected thermal performance. If no maintenance is carried out to the gradient in the NCZ, the three layers stratification and the salt gradient will eventually disappear, resulting in a pond filled with a homogeneous brine without any of the characteristics of a solar pond (Figure 4.12). This is because of the mass diffusion of the salt from the bottom to top, caused by both molecular and thermo diffusion tend to homogenize or flatten the concentration profile of the pond (Angeli and Leonardi, 2005). The phenomenon decreases the concentration in the LCZ and simultaneously increases the concentration in the UCZ, therefore in order to preserve the gradient in the NCZ the concentration in both layers has to be re-established by adding salt or concentrated brine in the bottom and fresh water at the top. The rate of this diffusion process depends on the molecular diffusivity of the salt, the salt concentration gradient, and the induced mass eddy diffusivity, caused by surface waves or other perturbations. Different rates of upward salt diffusion have been estimated and they can range from approximately 27 to 200 g/m^2 per day if the pond is located in an area subject to high wind velocities (Akbarzadeh and Ahmadi, 1981).

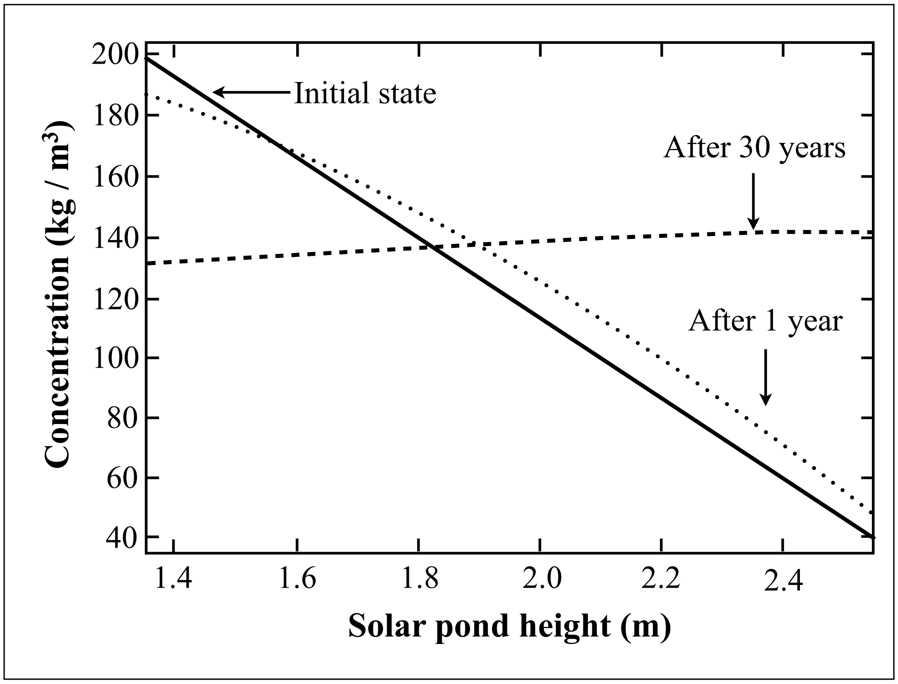

Figure 4.12: Evolution of salt concentration profile in a solar pond without maintenance after 1 year and 30 years (Angeli and Leonardi, 2005).

To re-establish the concentration in both convective zones, there are two general approaches. The first one considers the recycling of the extracted brine from the top of the UCZ by pumping it back into the lower convective zone after a concentration process. The second implies that part of the water from the UCZ is discarded after it has reached a certain concentration of salt and replaced with fresh water, while new concentrated brine is added at the bottom convective zone (Alagao et al., 1994).

Alagao et al. (1994) proposed a theoretical model to determine the size of the evaporation pond required to concentrate the brine extracted from the top to be then re-injected at the bottom. To do so, two main assumptions were made:

1. Volume flow rates and other parameters are taken as average values over a particular period. Annual averages are preferred because of the extreme variation of some parameters like rainfall and evaporation.

2. The system is assumed to undergo a steady state, steady flow process.

Figure 4.13 shows the flows associated with the operation of solar pond with a salt recycling system for salt gradient maintenance, where Q_1 is the make-up water in, Q_2 is the water lost by evaporation from the pond, Q_3 is the rainfall over the solar pond in m^3/year, Q_4 is the overflow sent to the evaporation pond, Q_5 is the rainfall over the evaporation pond in, Q_6 is the evaporation from the evaporation pond and Q_7 is the saturated brine injected at the bottom of the solar pond, being all these quantities in m^3/year, whereas C_1, C_4, C_7 correspond to salt concentrations (kg/m^3), A_{sp} and A_{ep} are the areas of the solar pond and evaporation pond respectively in m^2 and ST is the total salt diffused from the bottom to top in kg/m^2 per year.

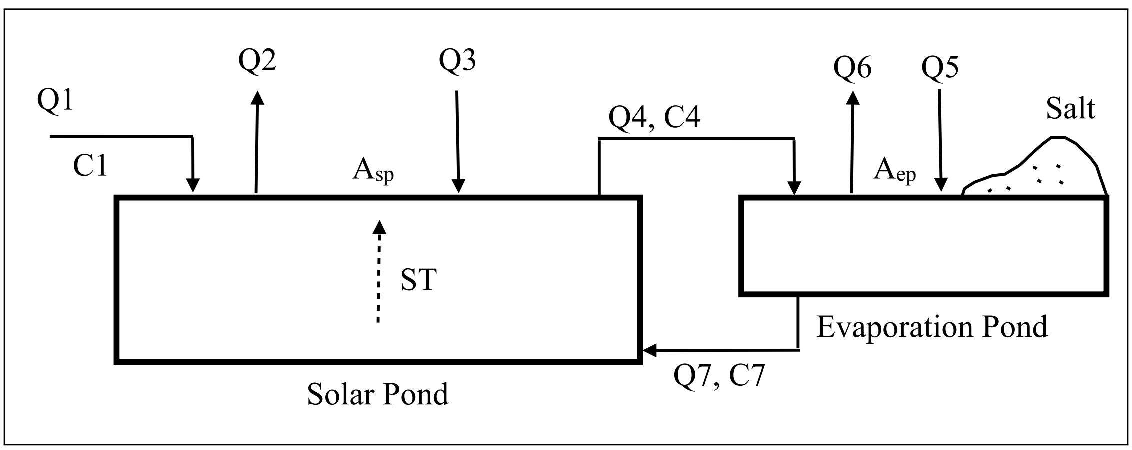

Figure 4.13: Schematic of flows in a salt recycling system for gradient maintenance (Alagao et al., 1994).

To calculate the rate of make-up water Q_1, first the volume balance over the solar pond has to be considered, which yields:

$$Q_4 = Q_1 + (Q_3 - Q_2) + Q_7 \tag{4.10.1}$$

To maintain the salt balance in the SP, the amount of brine re-injected must equal the total salt transport to the surface, which can be expressed as:

$$C_7\, Q_7 = A_{sp}\, ST \tag{4.10.2}$$

Knowing that:

$$Q_3 - Q_2 = A_{sp}\,(R - E_{sp}) \tag{4.10.3}$$

where R and E_{sp} are rainfall and evaporation rates at the solar pond in m/year. Combining (4.10.1), (4.10.2) and (4.10.3) gives:

$$Q_4 = Q_1 + A_{sp}\,(R - E_{sp}) + \frac{A_{sp}\, ST}{C_7} \tag{4.10.4}$$

The salt balance at the solar pond can be expressed as:

$$Q_1\, C_1 + Q_7\, C_7 = Q_4\, C_4 \tag{4.10.5}$$

Combining (4.10.1), (4.10.4) and (4.10.5) and rearranging gives:

$$Q_1 = A_{sp}\, \left[ST \left(\frac{1}{C_4} - \frac{1}{C_7} \right) + (E_{sp} - R) \right] \left[\frac{C_4}{(C_4 - C_1)} \right] \tag{4.10.6}$$

which corresponds to the volume of make-up water needed for a known SP size. Considering that $E_{sp} = V_{sp\ evap}\, A_{sp}^{-1}$, where $V_{sp\ evap}$ is the total volume of water evaporated from the solar pond in a year, and that if fresh water is used as make-up water ($C_1 = 0$), (4.10.6) can be reduced to:

$$Q_1 = A_{sp}\, ST \left(\frac{1}{C_4} - \frac{1}{C_7} \right) + V_{sp\ evap} \tag{4.10.7}$$

It can be noticed that the expression (4.10.7) corresponds to the amount of water necessary to compensate the evaporation in the solar pond and the fraction of water removed from the UCZ, sent to the evaporation pond, and lost during the process of re concentration. Therefore, the amount of water lost in the evaporation pond corresponds to:

$$V_{ep\,evap} = A_{sp}\,ST\left(\frac{1}{C_4} - \frac{1}{C_7}\right) \tag{4.10.8}$$

To determine the size of the evaporation pond, first the balance in its control volume has to be considered, which is given by:

$$Q_4 = (Q_6 - Q_5) + Q_7 \tag{4.10.9}$$

Equation (4.10.9) can be rewritten by considering that:

$$Q_6 - Q_5 = A_{ep}\,(E_{ep} - R) \tag{4.10.10}$$

where E_{ep} is the evaporation at the evaporation pond surface in m/year, which gives:

$$A_{ep} = \frac{Q_4 - Q_7}{E_{ep} - R} \tag{4.10.11}$$

If the overflow and injected brine at the bottom of the pond rates are known, then equation (4.10.11) can be used to determine the required area of the evaporation pond to provide enough replenishment brine. If these are not known, combining (4.10.1), (4.10.3), (4.10.7) and (4.10.11) gives:

$$A_{ep} = \frac{A_{sp}\left[\frac{1}{C_4} - \frac{1}{C_7}\right]\;\left[\frac{C_4}{(C_4 - C_1)}\right] + (E_{sp} - R)\left[\frac{C_1}{(C_4 - C_1)}\right]}{E_{ep} - R} \tag{4.10.12}$$

Assuming again that the make-up water is fresh water ($C_1 = 0$), total absence of rain ($R = 0$) and $E_{sp} = E_{ep}$, (4.10.12) is reduced to:

$$A_{ep} = \frac{A_{sp}\,ST\;\left(\frac{1}{C_4} - \frac{1}{C_7}\right)}{E_{sp}} \tag{4.10.13}$$

A similar model can be derived for the case in which the UCZ overflow is simply discarded and new salt is added to compensate the diffused salt with the aid of Figure 4.14:

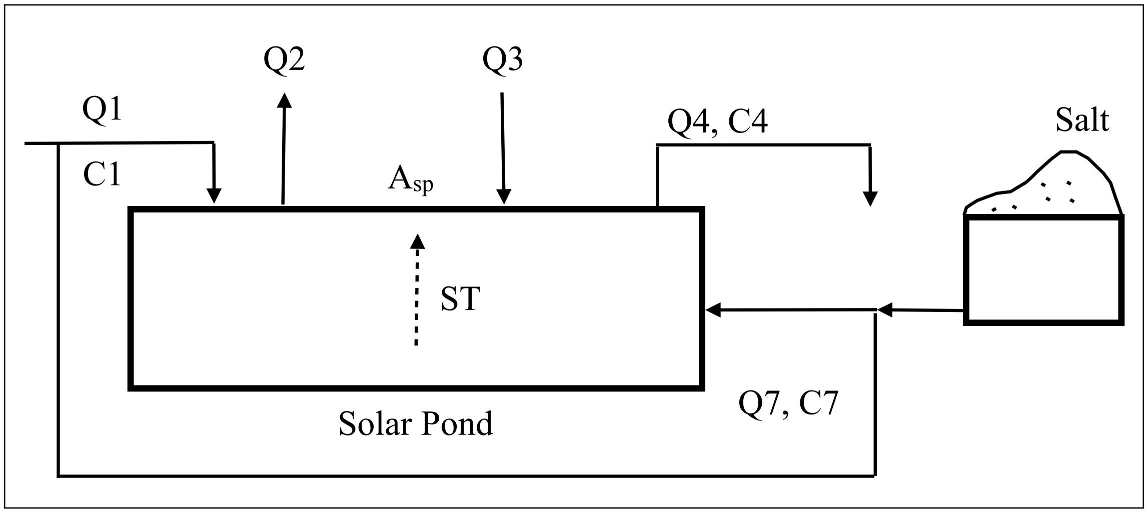

Figure 4.14: Schematic of flows for gradient maintenance without salt recycling (Alagao et al., 1994).

The rate of make-up water can be calculated by considering again the control volume balance over the solar pond, which is:

$$Q_1 - Q_7 = Q_2 + Q_4 - Q_3 \tag{4.10.14}$$

By neglecting the rain ($Q_3 = 0$) and expressing Q_4 in terms of concentration, equation (4.10.14) can be reduced to:

$$Q_1 + Q_7 = V_{sp\ evap} + \frac{A_{sp}\ ST}{C_4} \tag{4.10.15}$$

where the terms on the left hand side represent the total amount of make-up water required to compensate for the water that has evaporated and the water that has been extracted. Therefore, the extracted volume can be calculated as:

$$V_{extracted} = \frac{A_{sp}\ ST}{C_4} \tag{4.10.16}$$

The required salt to re establish the concentration in the LCZ is simply given by:

$$required\ salt = A_{sp}\ ST \tag{4.10.17}$$

The process of salt replenishment requires different equipment and procedures if the salt is added as concentrated brine or if it is granular, no matter if the salt is recycled or not. If the salt is to be added as brine, the same scanning injection system used to establish the salt gradient, has been proved to be very effective to inject the brine with the diffuser and re establish the design-concentration profile in the solar pond (Lu et al., 2004). Moreover, if the salt is to be added in granular form, the use of salt chargers (Figure 4.15) distributed in the perimeter of the pond has been proved to be efficient in maintaining the concentration and thickness of the LCZ by Jaefarzadeh and Akbarzadeh (2002).

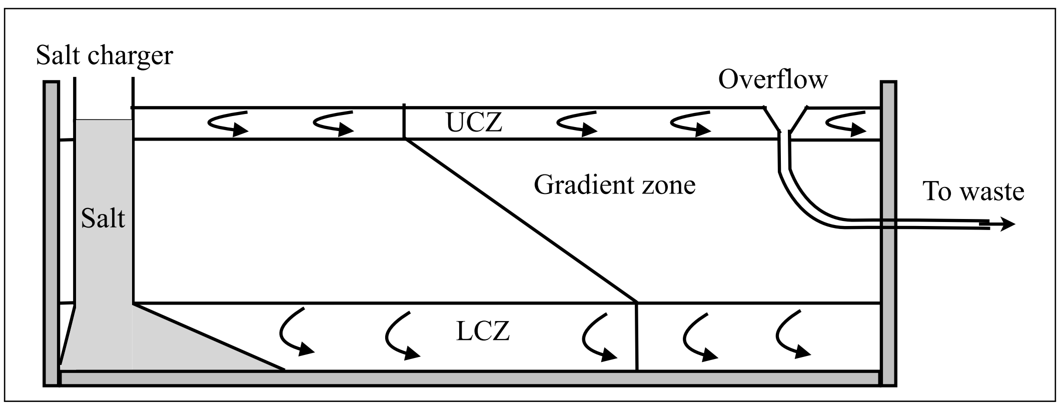

Figure 4.15: Schematic view of the pond with three zones, salt charger and surface washing system used in RMIT solar pond, Melbourne (Jaefarzadeh and Akbarzadeh, 2002).

4.10.2. Wind effects

The thickness of the UCZ is another important factor that limits the efficiency of a solar pond. This is because around one third of the solar heat that reaches the surface, is absorbed by this layer and then dissipated back to the atmosphere, and the thicker this layer is, the more radiation it will absorb rather than facilitating the LCZ heat collection. Therefore, it is desirable to maintain this layer as thin as possible. The formation of this layer is mainly caused by two factors (Akbarzadeh et al., 1983):

1. The absorption of solar radiation in the first few centimeters depth of the water causes a large temperature gradient, which results in the development of a convective current. The depth of this layer varies with the intensity of the solar radiation and therefore, decrements of up to 50% in the thickness of the UCZ can be experienced between day and night.

2. Wind causes mixing in the top region of solar ponds whose action can be separated into two effects: surface waves and wind-driven currents. Waves cause turbulence and induce eddy diffusivity that erode the salt gradient in the NCZ, which in time may result in convection in this region. Wind shear effect also generates currents at the surface that creates circulation in the vertical plane resulting in layer mixing and erosion of the top surface of the density gradient layer.

To counter the harmful effects of wind in the thickness of the UCZ and stability of the salt gradient, the use of floating rings (Figure 4.16) as wave suppressors that reduce the fetching area of wind, has been successfully tested in experimental solar ponds, in which the average thickness of this layer decreased in 50% compared to the operation without the wind suppression system (Akbarzadeh et al., 1983). Tang and Hassab (1990) also noted that the use of wind suppressors not only helps to avoid the formation of wind-induced localized convective zones in he NCZ, but also to overcome these perturbations. They carried out several experiments where artificially induced convective layers were created in the gradient of a small solar pond with and without wind suppressors. In the presence of the latter, the perturbations in the gradient were self-repaired after a few days without any direct action by the operators.

4.10.3. Turbidity effects

Turbidity is another important factor in the thermal performance of a solar pond because it reduces the penetration of solar radiation into the storage zone and high turbidity levels could impede the storage of energy. Temperatures registered in a solar pond with significant presence of turbidity (1 nephelometric turbidity units or NTU) are much lower than in a pond with clear water (0.3 NTU) under same conditions of heat extraction (Figure 4.17) (Wang and Seyed-Yagoobi, 1995). This undesirable phenomena in a solar pond can be caused mainly by the growth of algae,

Figure 4.16: Wind suppressors installed at Pyramid Hill solar pond, Australia (Leblanc et al., 2011).

bacteria and the presence detritus. Therefore, in order to maintain the design efficiency of solar radiation collection , monitoring and maintenance of the clarity of the pond is necessary.

In presence of phosphorus (P) and with increasing salinity, certain halotolerant species, such as the *Dunaliella* can grow and subsist in a solar pond (however, cannot withstand temperatures greater than 45°C) (Sherman and Imberger, 1991). Common sources of P are water, soil, rocks and also airborne sources, such as leafs, bird excreta and windblown dust and soil. So far, several techniques to counter turbidity have been tested in working solar ponds. The main approach has been the use of chemicals in order to make the brine incapable of sustaining any biological activity. These chemicals methods include chlorination, coagulation/flocculation, precipitation, peroxidation, algacide addition and acidification (Hull, 1990). Also, natural control methods have been tested, such as the use of brine shrimps *Artemia salina*, which feed of algal population and detritus and excrete dense fecal pellets that sink to the bottom of the pond. The growth and survival of the

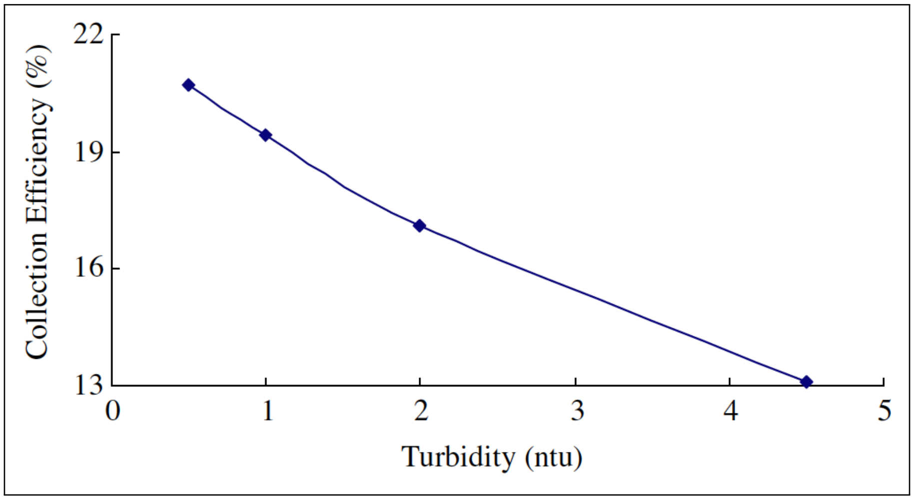

Figure 4.17: Collection efficiency versus turbidity levels in a solar pond (Li et al., 2010).

shrimp population is influenced by temperature and salinity, commonly in the range of 19-25°C and 35-110 ppt respectively, and are therefore useful for turbidity control of the upper region of the pond (Jaefarzadeh and Akbarzadeh, 2002).

While shrimps can control the growth of algae and maintain a reasonable transparency in the solar pond, Hull (1990) proposes the use of alum ($Al_2(SO_4)_3$) as phosphate control, in order to completely avoid the occurrence of algae growth. Alum not only precipitates phosphate (in the form of Al-P that is relatively sterile) without impairing the pond transparency but also its coagulant effect increases the settling rate of suspended particles. After years of operation of the 1,000 m^2 Argonne National Lab solar pond, IL, and the test of several combinations of chemicals for clarity control with relative success, Hull (1990) found out that the use of modest doses of granulated alum (< 5 g m^{-2} per year) in addition to chlorine (2.8 g m^{-2} per year) can effectively maintain a transparency such that the bottom was easily visible below 4 m of brine throughout the year, result that should be achievable in any sodium chloride solar pond.

4.11. Thermal efficiency

Beniwal and Singh (1987) define the thermal efficiency of a solar pond as the effective available heat stored in the LCZ q_{eff} over the average insolation $\overline{I}$, which can be expressed as:

$$\eta = \frac{q_{eff}}{\overline{I}} \tag{4.11.1}$$

The effective available heat is defined as the total absorbed heat by the LCZ minus the losses. It can be expressed as follows:

$$q_{eff} = (1 - R)\, \theta'\, \overline{I} - U_L\, \Delta T - U_g\, \Delta T \tag{4.11.2}$$

where R is the fraction of solar radiation reflected to the atmosphere, θ' is the attenuation factor given by turbidity and other effects, U_L is the heat loss coefficient given by the losses by the convective and radiation losses to the atmosphere, U_g is the heat loss coefficient to the ground. Therefore, the equation 4.11.1 can be rewritten as:

$$\eta = (1 - R)\, \theta' - \frac{U_{Lg}\, \Delta T}{\overline{I}} \tag{4.11.3}$$

which resembles the Hottel-Whillier-Bliss equation for flat panel solar collectors. It can be seen that the efficiency decreases when ΔT increases, and therefore it can be concluded that the hotter the solar pond is, the less efficient it becomes.

5. CASE STUDY AND PROPOSED DESIGN

The design of a solar pond is as determined by the site conditions (i.e. solar radiation, ground, wind, etc.) as by its purpose. This section is divided in two subsections; the first corresponds to the case study, where the design parameters where evaluated under site conditions and according to the energy demand of the cathode washing process at Spence. In the second subsection, a design is provided.

With exception of the IHE design, all the values herein presented were obtained by means of simulation routines carried out using MATLAB™ that solved the numerical model presented in Section 3, for various input parameters. The software provides "real time" information with a graphic interface of the status of the simulated solar pond, such as temperature profile, salinity profile, stability and also information related to the thermal performance or any other desired information (Figure 5.1).

The simulations assumed that the salt gradient is already formed at $t = 0$ (January 1st, at 12 pm) and therefore, did not consider the necessary time to establish it. Also, a two month period was assigned to heat up the solar pond and therefore, no heat is extracted during that time. Due to model restrictions, the thicknesses of the layers do not vary in time. This is equivalent to assume that adequate maintenance is carried out and enough water was being supplied to make up for evaporation and surface flushing as well as diffused salt was either being re-injected (if closed salt loop is used) in the LCZ or replaced by new salt (open salt loop). Finally, all the simulations were carried out taking care that the stability criterion ($F_s<0$) was fulfilled at all times.

5.1. Case study

5.1.1. Internal heat exchanger design

The working principle of the IHE to be used is similar to the one used at the Pyramid Hill solar pond, namely the distribution of the flow with manifolds and passed through a mesh of tubes located in the LCZ. In this case, the circulated fluid corresponds to the water used for the cathodes

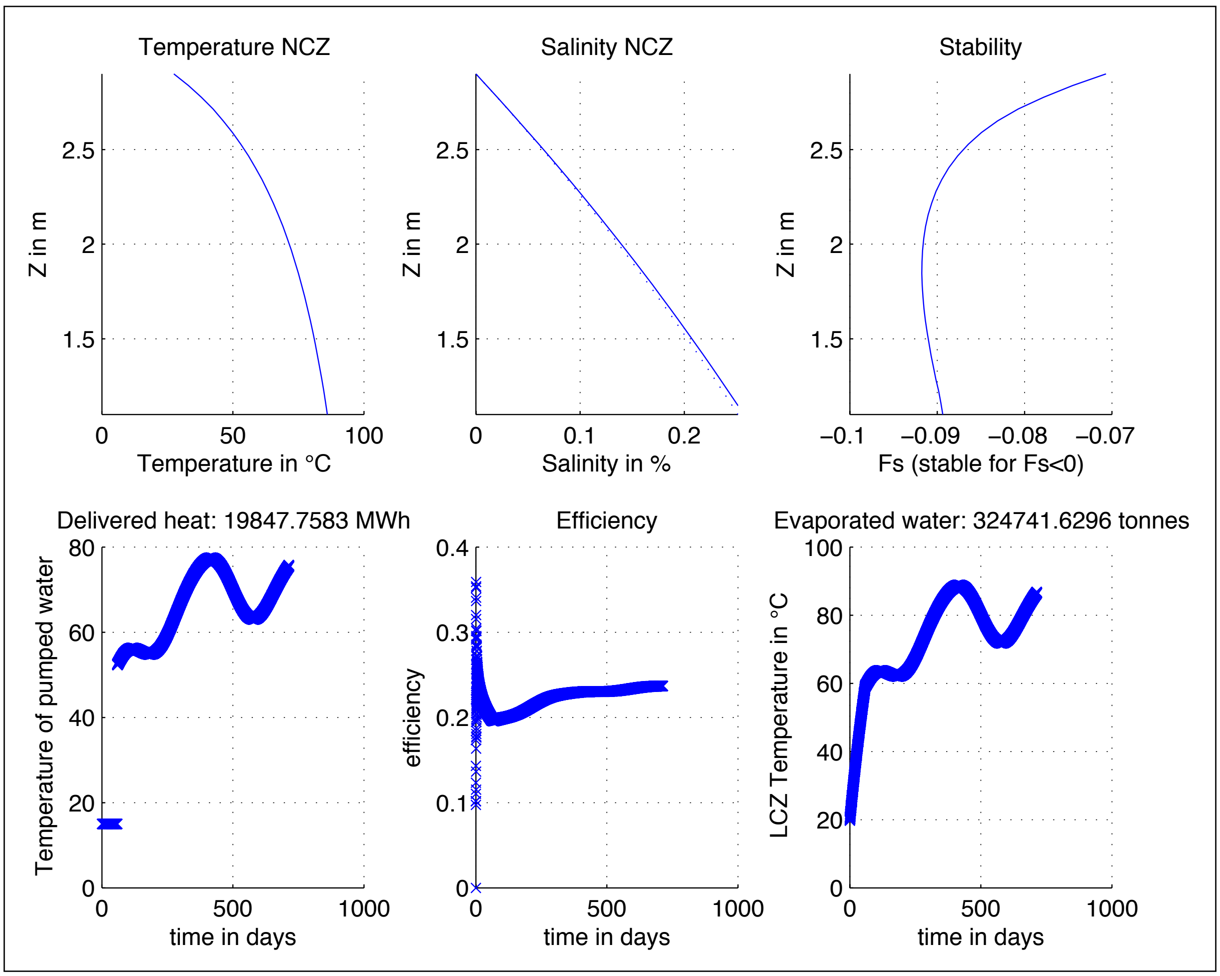

Figure 5.1: Interface created to facilitate the supervision of the simulation runs.

washing, avoiding the need of secondary heat exchangers. The diameter and number of the tubes that compose the mesh were analyzed in order to obtain a technically and economically efficient IHE. Table 7 presents an IHE composed with a 20 PE-100 tubes mesh with different commercial diameters and PE-100 manifolds of 125 mm of diameter:

Table 7: IHE composed by 20 tubes for different diameters

Diameter mm	Reynolds Number	U_{HX} W/m^2 °C	Surface area m^2	Length per tube m	Cost US$	Pressure drop kPa
32	22580	57.76	807	401	24,986	53
50	14472	52.35	890	283	25,902	15
75	9648	17.43	2673	567	83,031	12

The values presented in Table 7 were calculated for a constant flow of 21.45 m^3/h and for a Δ T of at least 48.2°C. The pressure drop has been calculated considering the absolute roughness of PE-100, equal to 7×10^{-6} m and assuming that the discharge and return manifolds are at the same height. It can be noticed that for a smaller diameter tubes (i.e. 32 mm), the required surface area is smaller compared to the other options and hence cheaper. This is due to thinner tube walls and a higher Reynolds number (faster flow) which results in a higher convective heat transfer coefficient. However, a faster flow results and higher pressure drops. On the other hand, a larger diameter (i.e. 50 mm) reduces the length of each of the tubes, avoiding the need of complicated geometries (i.e. coils) to fit the pond and the slower flow results in lesser pressure drops. However, if the diameter is large enough (i.e. 75 mm) the Reynolds number falls into the transitional flow range (between 2,300 and 10,000), where the flow behaves randomly as turbulent or laminar (Cengel, 2003), the heat transfer coefficient is considerably reduced and therefore the required heat exchange surface area increases notably.

A different approach to reduce the flow velocity and thus the pressure drop, is by adding tubes to the mesh instead of increasing the diameter. This would allow the conduction of heat through thinner walls and therefore with a better overall heat transfer coefficient and a more uniform heat withdrawal. Table shows the effect of a larger mesh of tubes of 32 mm of diameter:

Table 8: IHE composed by 20 tubes for different diameters

Number of tubes	Reynolds Number	U_{HX} W/m^2 °C	Surface area m^2	Length per tube m	Cost US$	Pressure drop kPa
20	22580	57.76	807	401	24,986	53
30	15054	57.16	815	270	25,205	25
40	11290	56.61	823	205	25,410	18
44	10264	56.40	826	187	25,509	16
50	9032	17.43	1510	301	43,291	18

From Table 8 it can be seen that the even though the Reynolds number was decreased, it did not affected significantly the overall heat transfer coefficient, and the pressure drop was diminished 3 times by using 44 tubes instead of 20. In comparison, the 44 tubes mesh and 32 mm of diameter is US$400 cheaper than the 20 tube mesh and 50 mm diameter, each tube is 96 m shorter and the overall heat coefficient is 8% higher. To compensate the pressure 18 kPa of pressure drop a power of only 97 W is required. Based on these arguments, it has been decided that the 44 tubes mesh of 32 mm of diameter is the most suitable configuration among the aforementioned.

5.1.2. Determination of the layers thicknesses

In order to maximize the solar radiation absorption in the LCZ, the thickness of the UCZ should be kept as thin as possible. Therefore, the simulations were run assuming a thickness, practical to maintain in a solar pond (Jaefarzadeh and Akbarzadeh, 2002), of 20 cm. The thickness of the NCZ was kept constant due to model restrictions and calculated using equation 4.4.3, the average insolation throughout a year at Spence (215.3 W/m^2) and the average weighted coefficient of direct and diffuse irradiation ($\bar{p}$) was calculated using data obtained from CNE et al. (2008) for the city of Calama, which is the nearest city (62 km, north-east of Spence) with an available registry. Under these conditions, the thickness of optimum NCZ thickness was found to be 1.8 m. On the other hand, the determination of the LCZ thickness required an iterative process in order to find the one that was able to store enough heat to deliver water in the desired range of temperatures. Table 9 presents the effect of the LCZ thickness on its average temperature as well as on its variability.

Table 9: Temperature range of the LCZ after the third year of operation for different thicknesses

Thickness	0.5 m	0.75 m	1 m	1.25	1.5
Min. T	63.5 °C	64.8 °C	66.0 °C	67.0 °C	67.8 °C
Avg. T	75.8 °C	75.8 °C	75.8 °C	75.8 °C	75.8 °C
Max. T	86.8 °C	85.7 °C	84.8 °C	83.9 °C	83.1 °C

It can be noticed that the thickness of the LCZ controls the amplitude of its range of temperature. A thicker LCZ takes longer to heat up and to cool down and therefore, the difference between the extreme bounds of the range is smaller compared to that of a thinner LCZ. The effect of the LCZ thickness on the outlet temperature of the HX is presented in Figure 5.2.

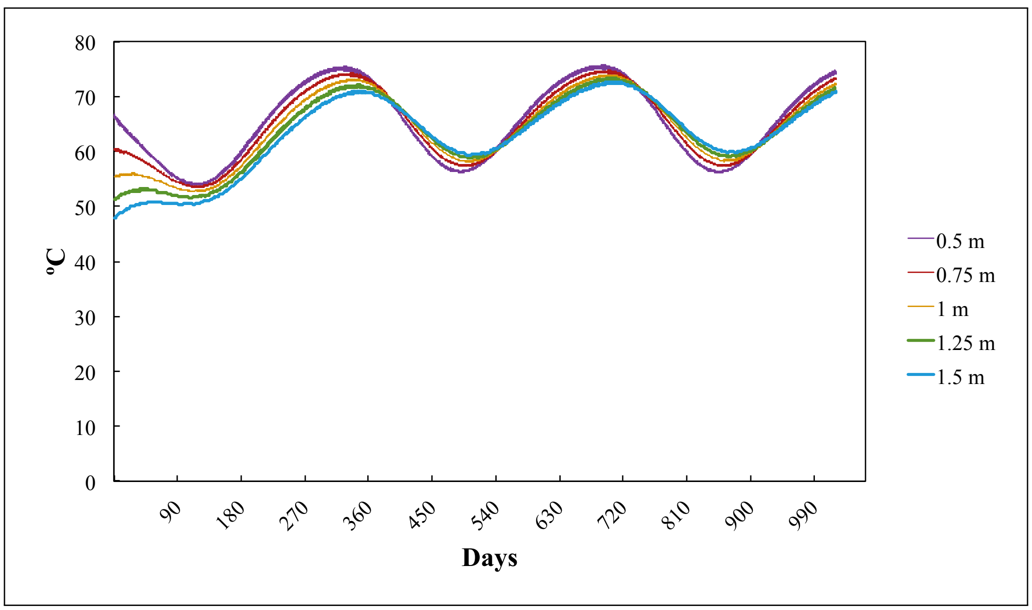

Figure 5.2: Outlet temperature of the water flow for different LCZ thicknesses.

It shows the different temperature amplitude of the heated up flow for the LCZ thicknesses. In order to obtain a flow within the 63.2-78.6 °C range, the amplitude of the flow should not be greater than of 15.4°C. Considering that the amplitude of the temperature curve obtained with a LCZ thickness of 1 m is 15.9 °C and that obtained with a 1.25 thick LCZ is 14.3 °C, then the desired LCZ thickness is within such range. From Figure 5.3 it can be noticed that a thickness of 1.1 m provides such temperature amplitude.

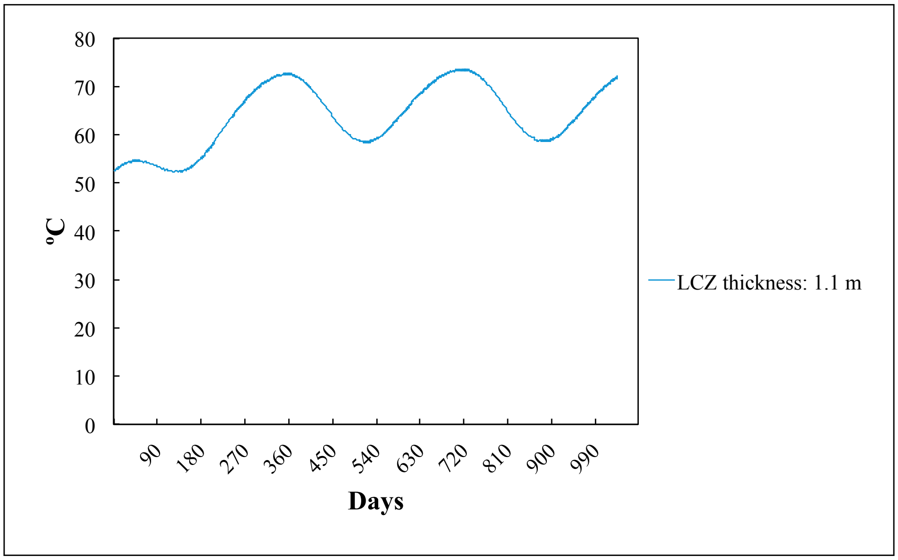

Figure 5.3: Outlet temperature of the water flow for a 1.1 m thick LCZ.

5.1.3. Required effective solar collecting surface area

The collected solar radiation is proportional to the surface area of the LCZ, and therefore, the larger it is, the more energy can be withdrawn from it. Figure 5.4 shows how the outlet temperature of a flow varies with the LCZ surface area:

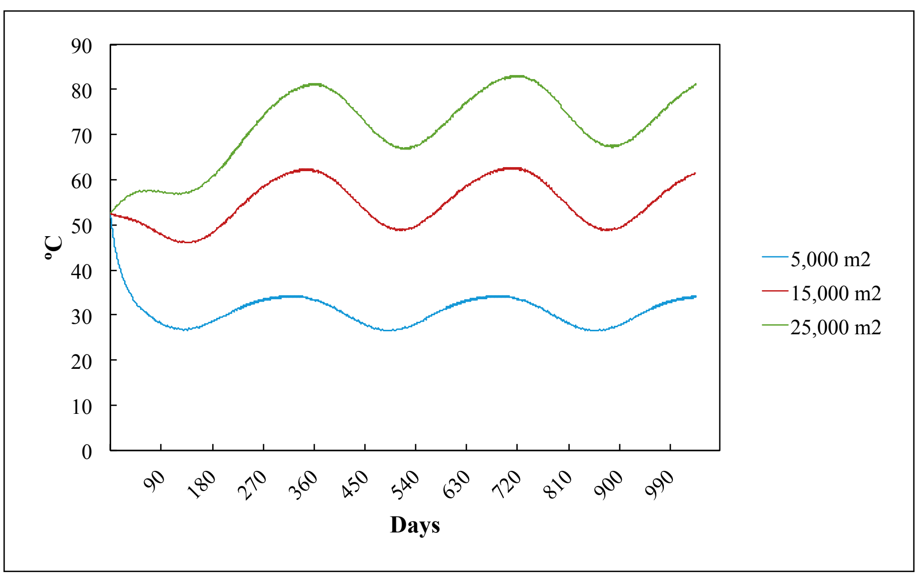

Figure 5.4: Outlet temperature of the water flow for different solar pond surface area.

On the other hand, the site conditions, such as solar radiation, water table depth and ground thermal conductivity, determine the surface area of the solar pond to meet its purpose. At Spence, the average insolation is 215.3 W/m^2, according to ground studies performed by SGA (2009) the water table depth at Spence Mine site varies between 16 and 93 m and the thermal conductivity of the ground is 1 W/(m K) approximately (Arancibia, 2012d). With these conditions, the necessary surface area to deliver the flow of water within the desired temperature range has been determined to be of 24,100 m^2 if the water table is at 16 m and of 22,500 m^2 if the water table is at 93 m of depth (Table 10).

Table 10: Required surface area for different water table depth and outlet temperature for the third year of operation

	Water table depth		
	16 m	55 m	93 m
Surface area	24,100m^2	22,600 m^2	22,500 m^2
Min. T	63.2 °C	63.2 °C	63.3 °C
Avg. T	71.3 °C	71.3 °C	71.5 °C
Max. T	78.8 °C	78.8 °C	78.9 °C

In absence of further information regarding to the depth of the water at the Spence mine facilities, it was assumed that a water table at 55 m below the surface corresponds to the most likely case.

5.1.4. Wall angle

Large solar ponds are usually built with sloping walls (also called banks) of between 1:1 to 1:3 (1 horizontal per 1 vertical) Srinivasan (1993) instead of vertical, for they facilitate the circulation of heavy machinery during construction and maintenance, and to prevent operation accidents, such as the fall of an operator into the hot layer. The slope, however induces instabilities in the NCZ. The wall angle with highest NIP was calculated using equation 4.2.2 for the latitude of Spence Mine (22°48') and its curve is presented in Figure 5.5:

It can be noticed that a vertical wall offers the best stability and that a wall with a 45.3° angle has the highest NIP, therefore the 1:1 slope (45 °) should be avoided whereas the 1:3 slope is 33%

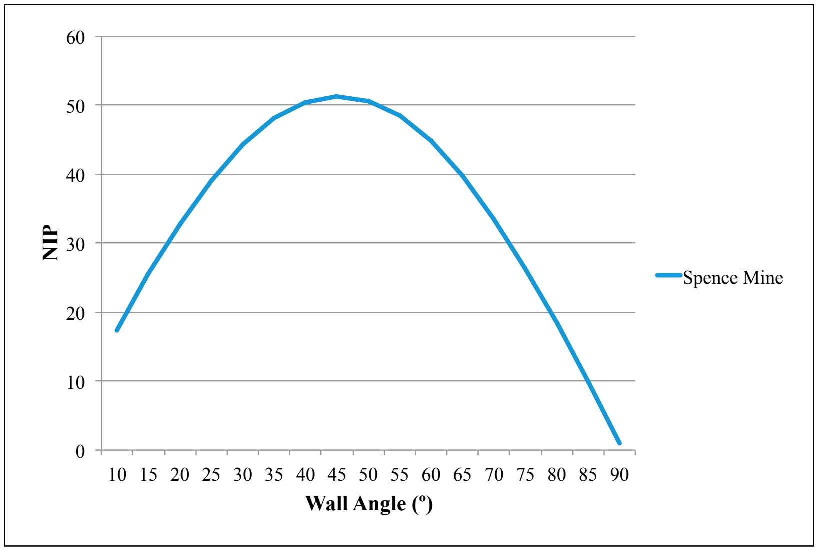

Figure 5.5: Normalized instability potential of solar pond wall angle at Spence

more stable than the 1:2 slope. The wall angle also increase the excavated volume and the wall area respect to that of a solar pond with vertical walls with the same depth and LCZ volume (Table 11) due to the addition of ineffective surface area.

Table 11: Increment of volume and wall area of a solar pond due to slopping walls

Slope	**Pond Volume** m^3	**Wall area** m^2	**Surface area** m^2
Vertical	67,800	1,851	22,600
1:2	70,364	4,205	25,354
1:3	71,657	5,994	26,785

It can be noticed that the total area of the walls increases significantly with the addition of a slope (in 127 and 224%), which undermines the assumption of the model that the heat losses through this interfaces are small compared those through the bottom. In order to include the extra heat losses, the area of the bottom of the pond was increased by the horizontal projection of the total wall area ($cos(\psi)\ A_{wall}$). Then, it was found that by increasing the effective collecting area in 800, 400 or 200 m^2 for a water table at 16, 55 or 93 m of depth respectively, the heat losses due to a 1:3 sloped wall could be compensated.

5.1.5. Thermal insulation

The use of a thermal insulating layer is critical when the water table is close to the surface (< 5 m), whereas in other cases is less significant and an impermeable layer would suffice. In this case, if a 60 cm thermal insulating layer of XPS is added, the required collecting areas for a water table at a depth of 16 m, 55 m and 93 m are reduced to 22,600, 22,200 and 22,100 m^2 respectively.

The described thermal insulation layer would represent an extra investment estimated to be of US$5.25 per square meter (Zhangjiagang Leader Co. Ltd., 2012) and therefore, in order to decide if it would be a significant improvement for the solar pond, it should be contrasted to the benefit of reducing the size of the pond, construction costs and water and salt requirements.

5.2. Proposed solar pond design

The main parameters for a suitable solar pond have already been established. These are the required surface area for a certain water table depth, the effect of the addition of a thermal insulation, the layer thicknesses as well as the IHE characteristics and therefore a design can be presented for the most likely case (Table 12, Appendix C.1).

For the design HDPE liners have been chosen among the other material options, since they are resistant to brine at temperatures found in the LCZ (PDL Staff, 2001). After a literature review, no evidence of premature failure in solar ponds has been reported and are the cheapest alternative. The first liner would be buried under 30 cm of soil to reduce the exposure to solar radiation,

Table 12: Proposed solar pond design, single configuration, water table at 55 m deep

Surface Area		27,213 m^2
Wall Slope		1:3
Layer Thickness	UCZ:	0.2 m
	NCZ:	1.8 m
	LCZ:	1.1 m
Required Salt		15,122 t
Required Water		72,883 m^3
Lining	on the bottom:	1.5 mm HDPE smooth, double layer
	on the walls:	1.5 mm HDPE textured, double layer
IHE		44 PE-100 tube mesh connecting 2 manifolds
Wave Suppression		70 HDPE rings, 15 m of perimeter

whereas the second liner would be placed 30 cm below. A 1:3 slope has been chosen over 1:2, for it has been decided to favor the stability and functionality of the solar pond while ensuring operation safety and ease of maintenance. Filling the pond with the saturated brine would take five days with a 360 m^3/h pump and the establishment of the gradient would take 18 days using two diffusers similar to the one used at the El Paso solar pond. From Figure 5.6 it can be noticed that nearby the electrowinning stage in the Spence mine there are terrains available to locate a solar pond of the mentioned characteristics.

5.2.1. Single versus modular configuration

The occurrence of accidental breakdown of solar pond essential components (i.e. liners) is a permanent threat that conditions the system performance, due to the aggressive thermohaline environment which they are subject to. The repair of liners is difficult and at in case of failure of this, it requires shutdown of the pond and its drainage to replace the liner. The conception of the design as a modular system can increase its reliability, since the simultaneous failure of modules is less likely compared to one pond. It also allows partial maintenance of the system, and therefore, it is better to stop a fraction of the heat production during the procedure rather than the whole plant. The proposed modular array consists of two solar ponds that together are able to provide the same heat supply as that of the single solar pond, since their main parameters, i.e. IHE, lining, wall

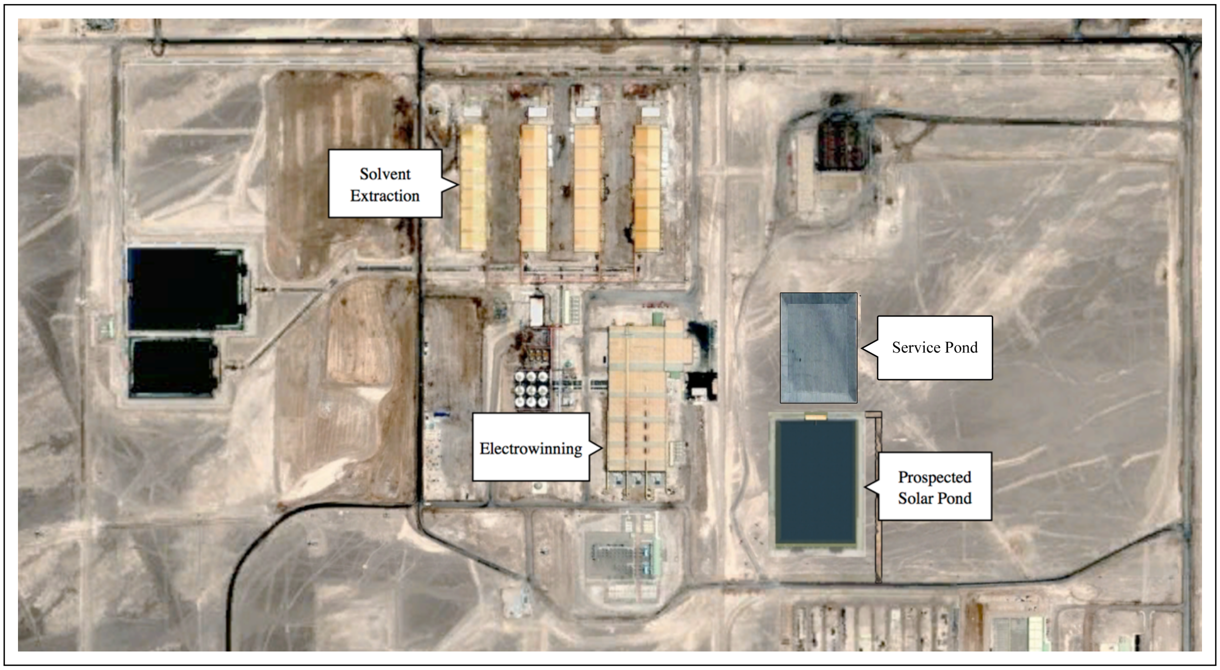

Figure 5.6: Proposed site for construction of a solar pond at Spence mine

slope and the layers thicknesses have been kept as in the former design (Figure 5.7, Appendix C.2).

However the dual array has a larger wall area, hence the effective collecting area had to be adjusted in order to deliver the same heat load of the single array, increasing the sum of the volumes of the two modules in 4% compared to the volume of the single pond.

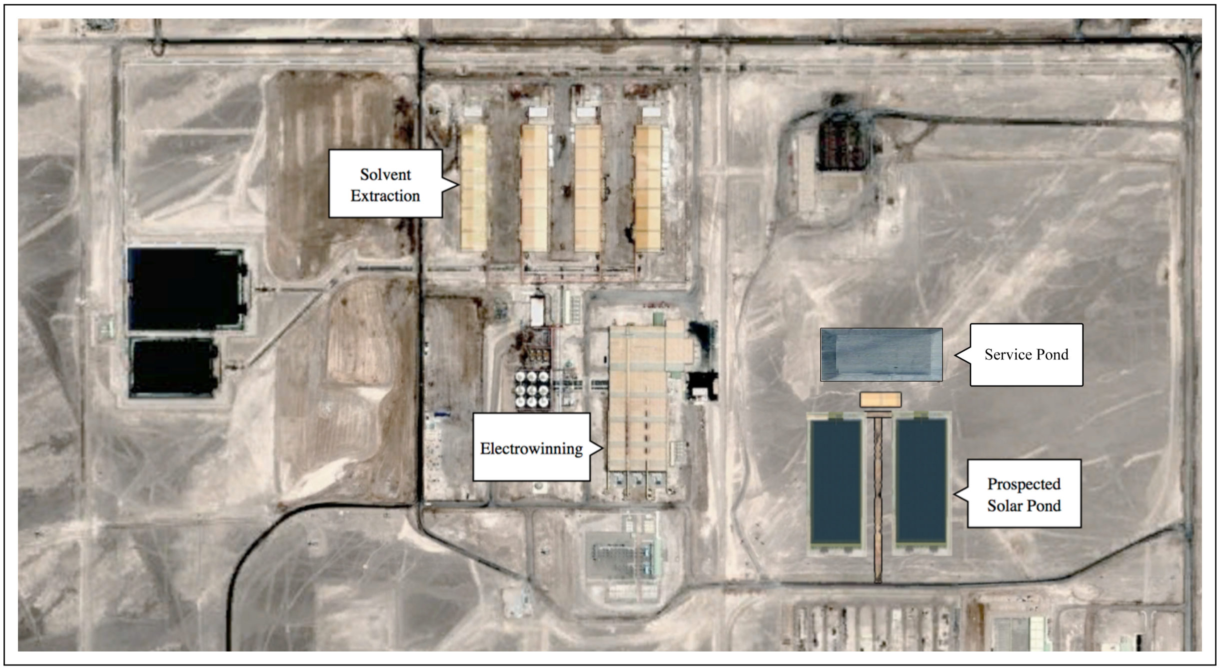

Figure 5.7: Proposed modular setup for the solar pond

6. RESULTS

6.1. Predicted performance

Since the parameters that determine the performance of the solar pond are the same for both configurations, the simulations of uninterrumped operation yielded identical results for both. Performance numbers for a period of seven years are presented in Table 13.

Table 13: Performance of the solar pond design after seven years of operation

Year	Average efficiency	Water temperature (°C) Min	Max	Average
1	21.3%	52.3	75.0	60.1
2	23.3%	63.0	77.5	70.8
3	23.8%	63.2	78.9	71.4
4	24.0%	63.2	79.0	71.4
5	24.1%	63.2	79.1	71.4
6	24.2%	63.2	79.1	71.5
7	24.3%	63.2	79.2	71.5

It can be noticed that the solar pond would be able to deliver process heat with the minimum required temperature (63.2°) from the third year of operation. It can also be seen that the efficiency of the solar pond increases notably during the first three years of operation and less significantly after the fourth, reaching a maximum of 24.3% at the end of the seventh year. At the end of the first year of operation, 7,700 MWh would have been generated, while in the seventh year of operation 12,300 MWh would be delivered, covering 77% of the annual energy demand of the EW cathodes washing process. Therefore, it can be asserted that the solar pond can significantly reduce the diesel consumption in the make up water heating for the copper cathodes washing process, however it cannot completely replace the water heater.

The performance of the modular setup is slightly better if the system operation considers planned shutdowns. In a year that maintenance procedures requiring drainage of the pond take place, the ability of the modular setup to remain partially operative allows it to deliver half of the flow within the temperature range, whereas the single solar pond setup would require the diesel water heater to provide the whole heat supply during such period, which results in 29% of more energy generated by the modular configuration that year. Assuming an operation lifetime of 20 years, in which 2 maintenance procedures would be carried out at beginning of the eighth and sixteenth year, the solar pond would have reduced the diesel consumption in 72% if modular and 71% otherwise of the copper cathode washing process (Figure 6.1).

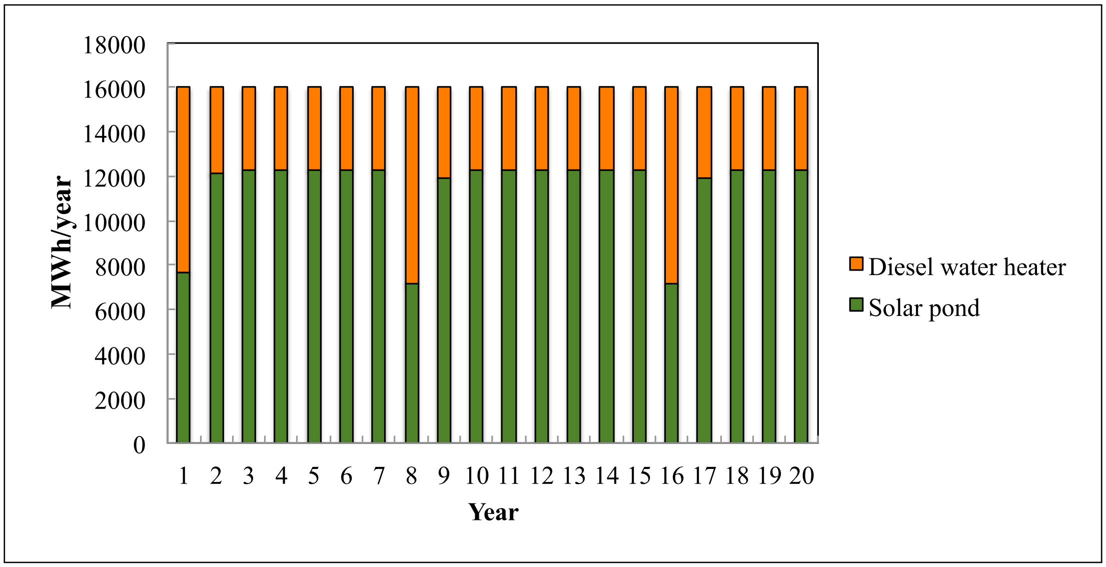

Figure 6.1: Prospected energy supply composition with a dual array solar pond preheating stage during lifetime operation

6.2. Economical analysis

6.2.1. Investment Cost

In order to reduce the cost associated to the construction of the solar pond, it should be carried out by excavating the fraction of depth of the pond that would allow the construction of banks of walls with the volume of removed earth. Considering an excavation cost of US$ 3.1 per cubic meter and banking of walls at US$ 3.9 per cubic meter (Garrido, 2012a) the cost of earthworks of the single pond would be of US$ 300,000 and for the dual array would be of US$ 347,000. If the depth of the pond was achieved by excavating only, the earthworks cost would be around 20% higher for both cases.

The wall and bottom areas of the single solar pond are 5,994 and 21,099 m^2 respectively, whereas those of the dual array these are 9,695 and 20,197 m^2. To estimate the cost of lining of the pond, it was assumed that a 10% larger area was necessary due to overlapping of the sheets for welding, and a price, including installation, of US$ 3.9 per square meter for the bottom liner and US$ 3.0 per square meter for the wall liner. The cost of lining for the single pond would be of US$273,000 and US$ 283,000 for the dual array.

The first load of water and salt were considered part of the initial investment. The water and salt required to fill the pond, generate the salt gradient and layers with the thicknesses of the design would be of 73,000 m^3 and 15,120 t for the single pond or 76,000 m^3 and 15,400 t for the dual array. The cost of filling the pond was estimated considering a cost of water of industrial quality of US$ 2 per cubic meter (Arancibia, 2012c) and a cost of salt of US$ 100 per t (Antou, 2012), which for the single pond would be of US$ 1,658,000 and US$ 1,668,000 for the dual array.

The heat exchanger would be the same for both single and dual array solar ponds, which considers 44 PE-100 tubes (22 per module for the dual array), 2 manifolds and a 100 W circulating pump (Wenzhou Kaixin Pump Co., Ltd., 2012). Then, the cost of the IHE would be of US$ 25,660.

The wave suppression system of the single pond and of the dual array consist of 70 and 73 floating rings respectively made of HDPE (980 kg/m^3), 15 m of perimeter, 74 mm wide and 5 m thick. Assuming a price of US$ 1 per, kg (Qingdao TSD Plastic Co., Ltd., 2012), the cost of the rings for the single pond was estimated to be US$ 27,000 and US$28,000 for the dual array.

The investment in instrumentation equipment was estimated considering a Mettler Toledo DA -100M densitymeter at US$ 8,600 (Mettler Toledo, 2012), a LaMotte 2020wew turbidimeter at US$ 880 (Miller Analytical, 2012), a thermocouple datalogger at US$ 100 (Computing, 2012) and a Global Water variable speed peristaltic pump for water sampling at US$ 630 (Meadows, 2012), which gives a total of US$ 10,210.

The investment cost of a solar pond, in single and dual array ca be seen in Figure 6.2:

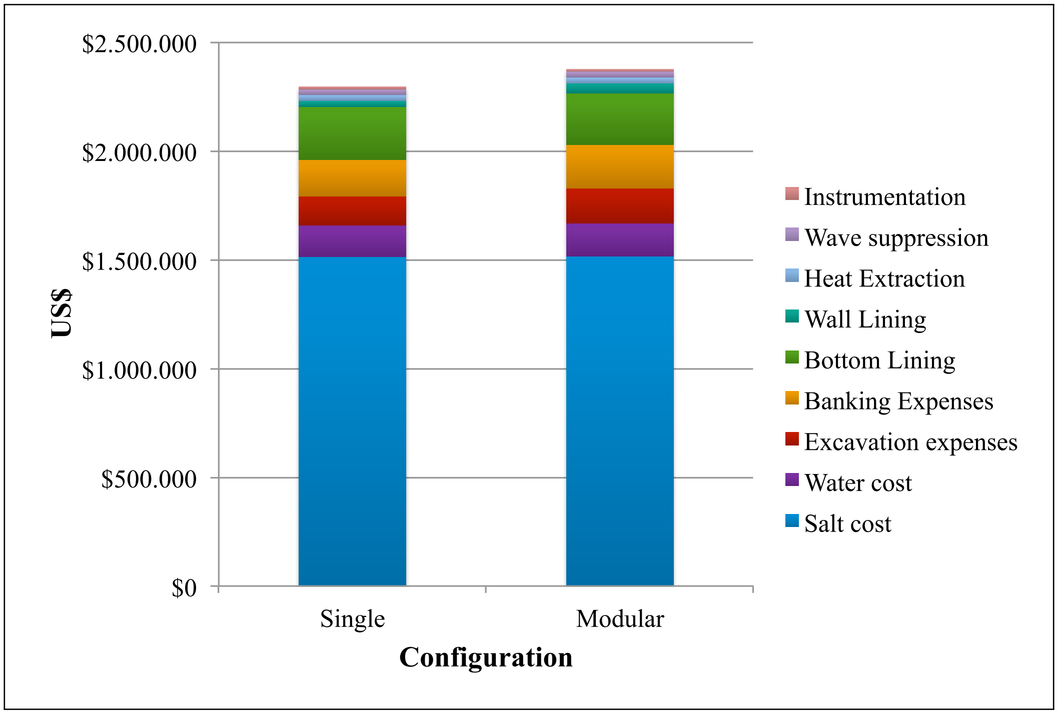

Figure 6.2: Investment cost composition of single and modular solar pond configuration.

It can be seen that the investment of the dual array is 3.6% higher than that of the single pond and that the salt represent around 65% of the cost of the solar pond in both configurations.

The convenience of the use of a thermal insulating layer was verified by comparing the investment cost of a solar smaller solar pond with insulation against one without insulation. The results are presented in the following table:

Table 14: Investment cost of a solar pond with and without thermal insulation for different water table depths

Water table depth	**16 m**	**55 m**	**93 m**
		Investment cost (US$)	
Without XPS layer	2,420,741	2,241,409	2,213,093
With XPS layer	2,373,224	2,332,906	2,322,827

From Table 14 it can be noticed that the inclusion of a thermal insulation layer to the lining scheme represents a benefit only if the solar pond is built over a water table at a depth of 16 m, which represents the worse case scenario.

The choice of a closed salt cycle would require an extra investment destined to the construction of an evaporation pond. The required A_{ep} to recycle the diffused of the single pond would be of 2,160 m^2 and 3,600 m^2 for the dual array, representing an extra investment of US$ 37,500 and US$ 41,500 respectively.

Considering the the participation of salt and water in the initial investment and that the solar pond may have to be drained due to failure of components or maintenance, to avoid discarding the content of the solar pond, the construction of a ”service” pond is proposed, which would serve as storage for the brine while the pond is repaired or maintained. This service pond would have to have the volume of the single pond or that of one of the modules of the dual array. The drainage of the pond would require a 400 m^3/h anti-corrosion centrifugal pump (75 kW of power consumption with 77% of efficiency) at US$ 5,000 (Zehjiang YonJou Technology Co. Ltd., 2012). In order to estimate the extra investment that this would represent, the costs of earthworks were assumed to be the same to those of the single pond or of one of the modules, and that a single layer of lining would suffice. Then, the extra investment due to the inclusion of a service pond would be of US$ 463,000 for the single pond and US$ 274,000 for the dual array, plus the cost of the pump.

6.2.2. Maintenance costs

The maintenance of the density gradient requires of make up water to compensate the water loss due to surface evaporation and overflow, i.e. a salt concentration of 2.5% on top for the the single solar pond setup would be of 44,400 m^3 per year whereas from the dual array it would be of 49,000 m^3 per year. Assuming a water cost of US$ 2 per cubic meter, then the cost of water make up would be of US$ 88,800 for the single pond and US$ 98,000 for the dual array. Whereas in the bottom, the restitution of salt in the LCZ lost due to diffusion to the upper layers is necessary to maintain near saturation concentrations, which for the single solar pond would be of 93,200 kg per year and for the dual array 103,250 kg per year. If a closed salt cycle is chosen, then make up salt is required only for the first year of operation and from the second year, the evaporation pond would provide the salt.

Following the water clarity maintenance proposed by Hull (1990), the required chlorine and alum would be of 76 and 136 kg, respectively, for the single solar pond whereas for the modular setup 84 kg of chlorine and 150 kg of alum would be necessary. With a cost of US$ 6 per kg of chlorine (55%) (Gasulla et al., 2011) US$ and 5.4 per kg of non-ferrous alum sulfate, the turbidity control would represent an annual cost of US$ 1,192 and US$ 1,317 for the single and dual setup, respectively.

Less frequent maintenance were also considered. These would consist in the drainage of the pond, the removal of deposited contaminants by replacing 15 cm of the solar pond bottom, the replacement of the top liner and re-establishment of the salt gradient. It was assumed that the whole procedure would be carried out after seven years of operation, that would cost US$ 142,000 and take two months for the single pond (one week to drain the pond, one month to do the maintenance and three weeks to fill the pond and re-establish the density gradient) whereas for the dual array it would cost US$ 69,000 and take one month per module for the dual array (three days to drain the pond, two weeks to do the maintenance and two weeks the fill and re-establish the density gradient). The cost of the electricity used to drain and fill the single pond would be of US$ 4,000 whereas for the dual array it would be US$ 4,500.

6.2.3. Operational costs

The operation of the solar pond would require of technicians responsible for the proper functioning of the pond. Considering that solar ponds as large as the Beith'Ha Arava solar pond were operated by only two persons, it was assumed that such workforce is enough for the one proposed.

The control of the temperature gradient would be performed with T-type thermocouples, which were assumed to have a lifetime of 1 week, and therefore 52 thermocuoples, at US$ 30 (Micro-

DAQ, 2012) each, would be required per year. The control of the clarity of the water would require of 30 test vials, whose lifetime was assumed to be of 1 year, being cost of a pack of six of US$ 28 (Miller Analytical, 2012).

The circulation of the water flow through the IHE would require an energy supply of 850 kWh per year. The cost of the electricity at the Spence mine was assumed to be US$ 0.12 per kWh (CNE, 2012). Since the diesel water heater would still be necessary to supply part of the energy demand, the cost of the consumed fuel was also considered, at US$ 0.88 per cubic meter (Arancibia, 2012b).

6.2.4. Discounted cash flows

The purpose of the analysis herein presented was to verify if the inclusion of the solar pond technology to the current setup at the Spence mine (base case) represented an opportunity of reducing its costs. It was carried out using the Discounted Cash flows (DCF) method, common in the decision making, which presents the worth of the project today. Since the water heating process for the copper cathodes washing is an intermediate process without added value to the final product, no direct incomes are perceived and therefore it was not possible to use the Net Present Value method, but instead the investment, operational and maintenance costs were considered for the calculation of the Life Cycle Cost of each (LCC), assuming a constant energy demand, planned shut downs for maintenance every 8 years in a horizon of time of 20 years and a discount rate of 10% (Appendix D). The DCF for each alternative are presented in Table 15:

Table 15: Life cycle and energy cost of of the current process and with solar pond preheating

Alternative	**LCC US$**	**Cost of Energy US$/MWh**
Base case	16,011,000	47.7
Single solar pond, open salt cycle	10.067.500	30.0
Single solar pond, closed salt cycle	10,029,709	29.9
Modular solar pond, open salt cycle	10,027,727	29.8
Modular solar pond, closed salt cycle	9,992,345	29.7

It can be noticed that the solar pond reduces the cost of operation of the water heating process in around 38%, because the cost of the MWh delivered by the solar pond is of US$ 18. The use of a closed salt cycle reduces the cost of operation in US$ 35,000. Even though the conception of the solar pond as a dual setup would have higher investment cost it would still reduce the LCC in US$ 37,300, mainly due to a lower contribution of the diesel water heater and a smaller service pond. Therefore, the dual array with a closed salt cycle should be preferred.

The estimated cost of the energy delivered by the prospected solar pond corresponds to half the cost of the energy produced by the Pyramid Hill solar pond (Leblanc et al., 2011). However, at Pyramid Hill solar pond is located over a water table at 3 m of depth. In order to verify the reliability of the estimated cost of energy, a similar calculation was done for a dual array solar pond with closed salt cycle, over a water table of 3 m deep, and determined to be of US$ 38.8 per MWh, which is similar to the value of the Pyramid Hill solar pond.

6.2.5. Sensitivity analysis

In the previous calculations of the LCC, the prices of inputs were assumed to be invariant in time. Since the main input of a solar pond with closed salt cycle is water, a scenario in which water becomes increasingly scarce and hence more expensive would represent a threat to the economic performance. Therefore a sensitivity analysis was carried out by increasing the price of water in a constant percentage after the third year of operation (Figure 6.3).

Figure 6.3 shows that even for a 10% of annual growth, scenario in which the cost of water at the 20th year would be more than five times the current cost, the implementation of the solar pond would still be profitable for the company. Another factor that could diminish the solar pond performance is the frequency of shut downs. For the LCC calculations it was assumed that the solar pond is stopped only every 8 years, and therefore the components can withstand such period of time. However, if by any chance the lifetime of e.g. the liners was less than expected, it would reduce the participation of the pond in the heat supply and would increase the maintenance costs. Figure 6.4 shows the LCC of a solar pond that remains operative 7, 3 and 1 year before the next

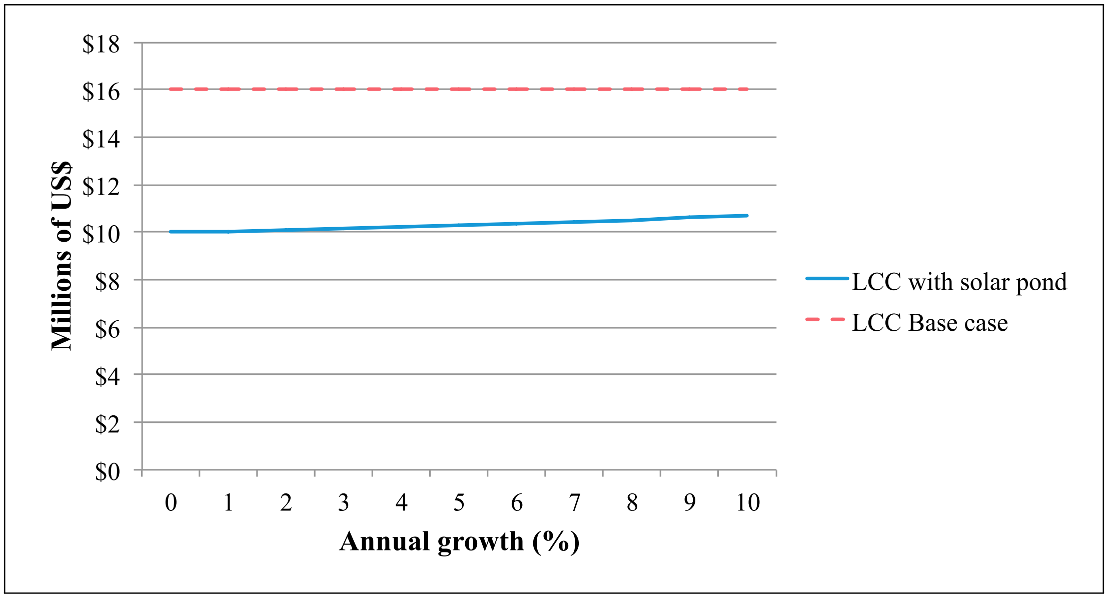

Figure 6.3: LCC of the heating stage with solar pond for different scenarios of water price annual growth

liner replacement. It can be seen that if the liner lifetime is of 1 year, scenario in which 55% of the heat would be supplied by the solar pond, it would still be profitable for the company.

So far, it has been assumed that the operation of the solar pond starts right after the construction is finished, it is carried out by trained technician and therefore, do not require a learning stage. Such scenario is likely for commercially available and mature technologies, where the operation is usually taught by the supplier. Whereas in the case of solar ponds, no technology supplier exist yet and therefore, the operational experience could be gained by having the operators trained by experts at one of the few operative a projects, by learning from advice of experts but without access to their facilities, or through a longer, independent learning process.

To estimate the impact of each scenario in the LCC, it was assumed that the construction of the dual array solar pond begins during the last year of training. The first scenario would not require the construction of a pilot pond, and the learning stage would be completed in year zero whereas the second and third scenario requires the construction of a pilot pond and take 2 and 4 years respectively. During the learning stage, the pilot solar pond would not generate useful energy and therefore the diesel water heater would supply the demand. It was assumed that the training solar pond has the same layer thicknesses that the designed pond and a surface area such that it could be

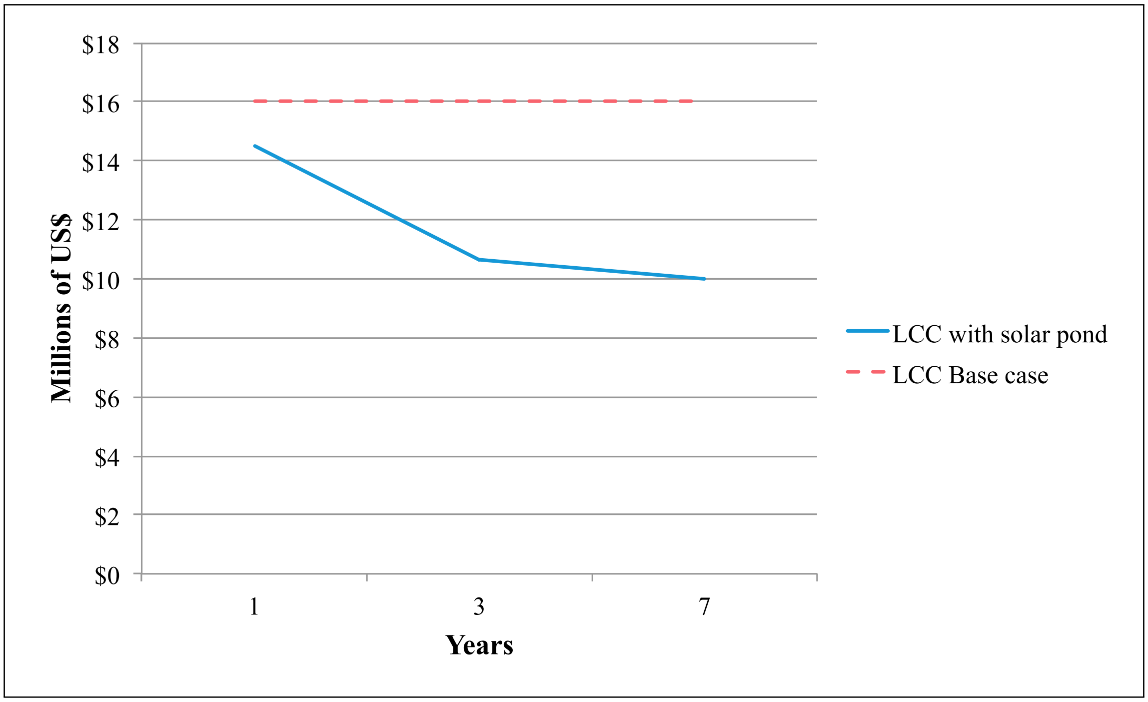

Figure 6.4: LCC of the heating stage with solar pond for different scenarios of liner replacement frequency.

used later as the evaporation pond for the salt recycling process.

The cost of the pilot, including instrumentation, has been estimated to be US$ 147,200, the operational cost would be US$ 73,800 and the maintenance. The LCC for different learning stage lengths is presented in Figure 6.5:

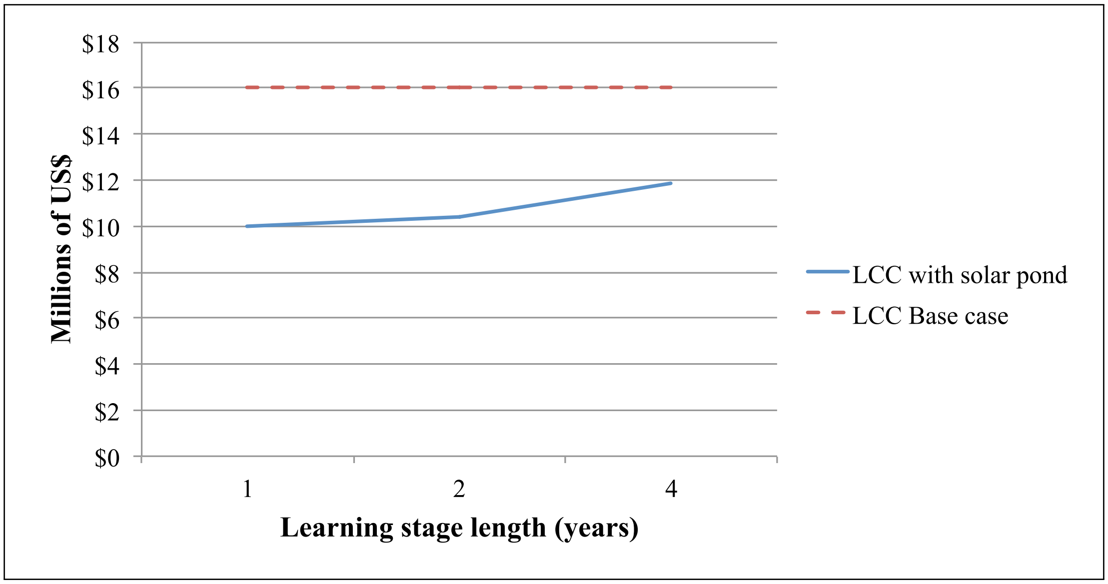

Figure 6.5: LCC of the heating stage with solar pond for different learning stage lengths.

It can be noticed that a learning stage of four years would increase the cost of the generated energy in US$ 5 being per MWh, nonetheless it would be still below the US$ 47.7 per MWh currently paid. Therefore a development program of a solar pond project would be still profitable for the company.

7. CONCLUSIONS

The copper mining industry in Chile is one of the main energy consumers, which relies on a matrix dominated by fossil fuels due to limited energy sources. In the last years it has experienced a significant increase in their green house gasses emissions caused by a forced migration from natural gas to diesel and coal, which in a climate change context seems to be little sustainable. However during the year, announcements made by important industry players gave signals of diversification towards less conventional energy sources. More specifically, taking advantage of the favorable insolation conditions, these companies have opted for the use of solar collectors (parabolic through and flat panels) to reduce their diesel consumption in the heat supply for the electrowinning stage of the hydrometallurgic process. In this thesis, a different type of solar collector was studied and proposed. A design, as well as its predicted performance, were provided for the preheating of water used in the copper cathodes washing step at the end of the electrowinning stage.

Solar ponds are a body of stratified brine that collect and store the solar radiation as thermal energy in the bottom, from where the heat can be withdrawn providing temperatures that range between 50 and 80°C making it suitable for the requirements of the target process. The buoyancy of the heated water at the bottom is prevented by the artificial formation of a density gradient by adding salt in the bottom, and maintaining negligible salt concentrations at the top. Its simple working principle was discovered by chance at the beginning of the XX century and it has been studied in depth, both analytically and experimentally, since the 1970s in Israel, USA and Australia among others. However this technology is still in an experimental condition and therefore several practical aspects remain unclear and open for improvements.

The performance of a solar pond varies, both with its design and location where it is placed. Therefore, a mathematical model was put together based on scattered sources, was solved numerically for the non convective zone and weather measures obtained at Spence mine were used to predict the behavior of the prospected pond for different design parameters, in order to obtain a suitable combination. The validation of the estimated parameters against operational records obtained from a solar pond shows that despite the limitations of an uni-dimensional model, it generated values that resembled the empirical data with acceptable accuracy.

It was determined that the conception of the solar pond design in a modular setup would increase the reliability of the system and reduce the participation of the diesel water heater in the supply of the energy demand. Therefore, the proposed design consists on a dual array of solar ponds of 15,574 m^2 each, with 1:3 slopping banks made out of the removed earth to level the ground would collect solar radiation with an efficiency of 24.% to provide a flow of 21.45 m^3/h in a temperature range of 63.2 and 78.9 °C after the third year of operation, 24 hours per day, no matter the depth of the water table. However, a layer of thermal insulation would be necessary if the water table is at 16 m deep to keep a similar surface area. The required salt to establish the density gradient would be 15,386 t of sodium chloride, which represents 67% of the investment cost. Salt diffuses to upper regions of the pond, and therefore the maintenance of the gradient requires the re-injection of saturated brine at the bottom and flushing of the upper convective zone. It was found that the recycling of the salt by means of an evaporation pond that re-concentrates the brine is cheaper than discarding and make-up for the diffused salt.

The proposed design addresses stability of the gradient as the main issues in the operation of the solar pond. Therefore, a simple in-pond heat exchanger composed by a corrosion resistant polyethylene tubes mesh located in the lower convective zone was chosen over the extraction and re-injection of the hot brine. The chosen liner material was HDPE over clay based liners for no evidence of premature failure associated to their use was found and they are also cheaper.

The cost of the heat supplied by the proposed solar pond, estimated based on its predicted performance at site conditions, would be of US$ 18 per MWh. Then, the inclusion of the solar pond preheating stage could reduce the cost of the thermal kilowatt-hour in 37.7% and in 77% the diesel consumption by the water heater after 20 years of operation, resulting in the avoidance of 62,000 t of CO_2 at the end of the pond lifetime. These results were sensitized in scenarios of increasingly expensive water, frequent shutdowns and the requirement of operation learning stage prior the adoption of the technology, and none of these affected the life cycle cost of the system with a solar pond preheating stage in a way that would make the current setup preferable.

In order to get a better understanding of the behavior of a solar pond under the environmental conditions found at Spence mine, and therefore refine the results herein presented, the measurement of weather data for a longer period of time (more than 1 year) would be required. A model of a solar pond that considers the convective layers, with its temperature gradients and motions should be implemented. This however, requires of a 3 dimensional analysis of the solar pond and the use of complex physics and mathematics that are beyond the scope of the present thesis. The implementation of a small pilot in the site would be of most utility. It could help to gain experience in the operation of a solar pond, it would provide empirical data to contrast those generated by the model, would help in the study of variables such as biological growth and solar radiation attenuation and also, how ground vibrations generated by explosives detonations could affect the stability of the density gradient. The latter has not been addressed by any research up to date.

BIBLIOGRAPHY

Abdel-Salam, H. E. A. and Probert, S. D. (1986). Solar ponds: Design and prospects. *Applied Energy*, 24:91–126.

Akbarzadeh, A. (1988). Convective layers generated by side walls in solar ponds. *Solar Energy*, 41(6):521–529.

Akbarzadeh, A. (1989). Convective layers generated by side walls in solar ponds: observations. *Solar Energy*, 43(1):17–23.

Akbarzadeh, A. and Ahmadi, G. (1980). Computer simulation of the performance of a solar pond in the southern part of Iran. *Solar Energy*, 24:143–151.

Akbarzadeh, A. and Ahmadi, G. (1981). On the development of the salt concentration profile in a solar pond. *Energy*, 6:369–382.

Akbarzadeh, A. and Golding, P. (1992). The importance of wall angle for stability in solar ponds. *Solar Energy*, 49(2):123–126.

Akbarzadeh, A., MacDonald, W. G., and Wang, Y. F. (1983). Reduction of surface mixing in solar ponds by floating rings. *Solar Energy*, 31(4):377–380.

Alagao, F. B. (1996). Simulation of the transient behavior of a closed-cycle salt-gradient solar pond. *Solar Energy*, 56(3):245–260.

Alagao, F. B., Akbarzadeh, A., and Johnson, P. W. (1994). The design, construction and initial operation of a closed-cycle salt-gradient solar pond. *Solar Energy*, 53(4):343–351.

ANCID (2004). Bentonite treatments. http://www.irrigation.org.au/seepage/4_2_5_bentonite.html.

Angeli, C. and Leonardi, E. (2005). The effect of thermodiffusion on the stability of a salt gradient solar pond. *International Journal of Heat and Mass Transfer*, 48:4633–4639.

Antou, Z. (2012). Sodium chloride/industrial salt price. http://www.alibaba.com/product-gs/608280459/Sodium_Chloride_industrial_salt_price.html.

Arancibia, F. (2012a). Copper cathods washing process at Spence mine. Personal Communication.

Arancibia, F. (2012b). Cost of diesel at spence mine. Personal Communication.

Arancibia, F. (2012c). Cost of water at spence mine. Personal Communication.

Arancibia, F. (2012d). Thermal conductivity of the ground at spence mine. Personal Communication.

ASHRAE (2009). *Handbook - Fundamentals (SI Edition)*. American Society of Heating, Refrigerating and Air-Conditioning Engineers, Inc.

Beniwal, R. S. and Singh, R. (1987). Calculation of efficiency of salt gradient solar ponds. *Heat Recovery Systems & CHP*, 7(6):497–516.

Busquets, E., Kumar, V., Mota, J., Chacon, R., and Lu, H. (2012). Thermal analysis of a solar pond prototype to study the non-convective zone salt gradient stability. *Solar Energy*, 86(5):1366–1377.

Cavalli, P. (2012). ”Minera construye planta termosolar más grande de su tipo”. *El Mercurio*.

Cengel, Y. A. (2003). *Heat Transfer: A Practical Approach*. McGraw-Hill.

Chen, C. F. and Skok, M. W. K. (1974). Cellular convection in a salinity gradient along a heated inclined wall. *International Journal of Heat and Mass Transfer*, 17:51–60.

CNE (2009). Modelación del recurso solar y eólico en el norte de chile.

CNE (2012). Serie precio medio de mercado sistema interconectado del Norte Grande (PMM SING). http://www.cne.cl/tarificacion/electricidad/precios-de-nudo-de-corto-plazo/467-pmm-sing.

CNE, PNUD, and UTFSM (2008). *Irradiancia solar en territorios de la República de Chile: Registro solarimétrico*.

Computing, M. (2012). Battery-powered remote thermocouple data logger with lcd. http://www.mccdaq.com/usb-data-acquisition/usb-501-tc-lcd.aspx.

Dah, M. M. O., Ouni, M., Guizani, A., and Belghith, A. (2005). Study of thermal salinity profiles development of solar pond in laboratory. *Desalination*, 183(1-3):179–185.

Davenport, W. G., King, M., Schlesinger, M., and Biswas, A. (2002). *Extractive Metallurgy of Copper*. Elsevier, fourth edition.

Davis, J. R. (2001). *ASM Specialty Handbook: Copper and Copper Alloys*. Asm International.

Duffie, J. A. and Beckman, W. A. (2006). *Solar Engineering of Thermal Processes*. Wiley, third edition.

El Mercurio (2012). Codelco adjudica a consorcio chileno–danés construcción y operación de mayor planta solar térmica del mundo para la minería.

García, J. H. (2012). Weather measurements record at spence for year 2010. Personal Communication.

Garrido, C. (2012a). Costs of excavation, earth movements, and banking. Personal Communication.

Garrido, C. (2012b). Properties and costs of liners. Personal Communication.

Gasulla, N., Yaakob, Y., Leblanc, J., Akbarzadeh, A., and Cortina, J. L. (2011). Brine clarity maintenance in salinity-gradient solar ponds. *Solar Energy*, 85:2894–2902.

Gómez, D. R. and Watterson, J. D. (2006). *Guidelines for National Greenhouse Gas Inventories*, volume 2. Intergovernmental Panel on Climate Change.

Green, D. W. and Perry, R. H. (2008). *Perry's Chemical Engineers' Handbook*. McGraw-Hill, 8th edition.

Guajardo, J. (2011). Situacion actual y perspectivas para la mineria en chile.

Hassairi, M., Safi, M. J., and Chibani, S. (2001). Natural brine solar pond: An experimental study. *Solar Energy*, 70(1):45–50.

Henningson, D. S. and Berggren, M. (2005). *Fluid Dynamics: Theory and Computation*. Department of Mechanics and the department of Numerical Analysis and Computer Science, Royal Institute of Technology (KTH), Sweden.

Hull, J. R. (1980). Computer simulation of solar pond thermal behavior. *Solar Energy*, 25:33–40.

Hull, J. R. (1990). Maintenance of brine transparency in salinity gradient solar ponds. *Journal of Solar Energy Enegineering*, 112:65–69.

IEA (2011). Energy statistics for Chile: Electricity generation by fuel. http://www.iea.org/stats/pdf_graphs/CLELEC.pdf.

International Copper Study Group (2010). World copper fact book 2010.

Jaefarzadeh, M. R. (2004). Thermal behavior of a small salinity-gradient solar pond thermal behavior of a small salinity-gradient solar pond with wall shading effect. *Solar Energy*, 77:281–290.

Jaefarzadeh, M. R. (2006). Heat extraction from a salinity-gradient solar pond using in pond heat exchanger. *Applied Thermal Engineering*, 26:1858–1865.

Jaefarzadeh, M. R. and Akbarzadeh, A. (2002). Towards the design of low maintenance salinity gradient solar ponds. *Solar Energy*, 73(5):375–384.

Jones, G. F., Meyer, K. A., Hedstrom, J. C., Jones, G. F., Meyer, K. A., Hedstrom, J. C., Dreicer, J. S., and Grimmer, D. P. (1983). Design, construction and initial operation of The Los Alamos Laboratory salt-gradient solar pond. ASME Solar Energy Division.

Karim, C., Slim, Z., Kais, C., Jomâa, S. M., and Akbarzadeh, A. (2010). Experimental study of the salt gradient solar pond stability. *Solar Energy*, 84(1):24–31.

Kaushika, N. D. (1984). Solar ponds: A review. *Energy Conversion & Management*, 24(4):353–376.

Kern, D. Q. (1950). *Process Heat Transfer*. McGraw-Hill Book.

Kishore, V. V. N. and Joshi, V. (1984). A practical collector efficiency equation for nonconvecting solar ponds. *Solar Energy*, 33(5):391–395.

Kumar, A. and Kishore, V. V. N. (1999). Construction and operational experience of a 6,000 m2 solar pond at Kutch, India. *Solar Energy*, 65(4):237–249.

Kurt, H., Halici, F., and Binark, A. K. (2000). Solar pond conception-experimental and theoretical studies. *Energy Conversion & Management*, 41:939–951.

Leblanc, J., Akbarzadeh, A., Andrews, J., Lu, H., and Golding, P. (2011). Heat extraction methods from salinity-gradient solar ponds and introduction of a novel system of heat extraction for improved efficiency. *Solar Energy*, 85(12):3103–3142.

Li, N., Yin, F., Sun, W., Zhang, C., and Shi, Y. (2010). Turbidity study of solar ponds utilizing seawater as salt source. *Solar Energy*, 84:289–295.

Liao, Y. (1987). Gradient stability and injection analysis for the el paso solar pond. Master's thesis, The University of Texas at El Paso.

Liew, F. (2008). Tes-amm analysis: Pyrometallurgy versus hydrometallurgy. Technical report, TES-AMM Singapore Engineering Department.

Lobos, A. (2007). Aereal view of spence mine. http://www.flickr.com/photos/armandolobos/1664601542/.

Lu, H., Swift, A. H. P., Hein Jr., H. D., and Walton, J. C. (2004). Advancement in salinity gradient solar pond technology based on sixteen years of operational experience. *Solar Energy Engineering*, 126:759–767.

Mamaev, O. I. (1975). *Temperature-Salinity Analysis of World Ocean Waters*. Elsevier Oceanography Series. Elsevier Scientific Publishing.

Mansour, R. B., Nguyen, C. T., and Galanis, N. (2004). Numerical study of transient heat and mass transfer and stability in a salt-gradient solar pond. *International Journal of Thermal Sciences*, 43:779–790.

Meadows, B. (2012). Global water instrumentation variable speed peristaltic pump. http://www.benmeadows.com/global-water-instrumentation-variable-speed-peristaltic-pump_s_129093/#mainProductBottom.

Mehta, A. S., Pathak, N., Shah, B. M., and Gomkale, S. D. (1988). Performance analysis of a bittern-based solar pond. *Solar Energy*, 40(5):469–475.

Menon, E. and Menon, P. (2010). *Working Guide to Pumps and Pumping Stations - Calculations Working Guide to Pumps and Pumping stations - Calculations and Simulations*. Elsevier.

Mettler Toledo (2012). Mettler toledo da - 100m benchtop density meter built in peltier thermostat, 0.001 g/cm3 accuracy. http://www.amazon.com/Mettler-Toledo-DA-Benchtop-Thermostat/dp/B003P9WRAO.

MicroDAQ (2012). Mineral insulated thermocouples. http://www.microdaq.com/thermocouples/mineral-insulated.php.

Miller Analytical (2012). Lamotte turbidimeter price. http://www.milleranalytical.com/Turbidimeters.htm.

Mills, D. (2001). *Solar energy: the state of the art : ISES position papers*, chapter 11. Solar thermal electricity, pages 628–637. Jamas & James (Science Publishers) Ltd.

Mining Technology (2011). Spence copper cathode mine, Chile. http://www.mining-technology.com/projects/spence_copper.

Morris, W. S., Haggard, K. W., Bahm, R. J., and Fosdick, E. K. (1985). New Mexico climate manual: solar and weather data. Technical Report 2-72-4523, New Mexico Energy, Minerals and Natural Resources Department.

Ocaranza, J. (2011). *Estadísticas del cobre y otros minerales: 1991 - 2010*. Comisión Chilena del Cobre.

Ouni, M., Guizani, A., Lu, H., and Belghith, A. (2003). Simulation of the control of a salt gradient solar pond in the south of Tunisia. *Solar Energy*, 75:95–101.

Pande, R. N. and Chaudhary, D. R. (1984). Stability, effective insulation and heat loss of a salt-stability, effective insulation and heat loss of a salt-gradient solar pond. *Applied Energy*, 17(117-131).

PDL Staff (2001). *Chemical Resistance of Plastics and Elastomers (3rd Electronic Edition)*. William Andrew Publishing/Plastics Design Library.

Peacey, J., Xian-jian, G. U. O., and Robles, E. (2004). Copper hyidrometallurgy -current status, preliminary economics, future directions and positioning versus smelting. *The Chinese Journal of Nonferrus Metals*, 14(3):560–568.

Peinan, M. and Hongfei, Z. (1994). Optimum thickness of the gradient layer and maximum energy gains of a solar pond. *Energy*, 19(8):901–904.

Perez, V. (2010). Demanda de energía eléctrica en la minería del cobre y perspectivas de seguridad en su abastecimiento.

Pimentel, S. (2010). *Consumo de energía y emisiones de gases de efecto invernadero asociadas a la minería del cobre de Chile. Año 2009*. Comision Chilena del Cobre.

Prasad, R. and Rao, D. P. (1996). Estimation of the thickness of the lower convective layer of solar ponds. *Renewable Energy*, 7(4):401–407.

Punyasena, M. A., Amarasekara, C. D., Jayakody, J. R. P., and Perera, P. A. A. (2003). An investigation of rain and wind effects on thermal stability of large-area saltpan solar ponds. *Solar Energy*, 74:447–451.

Qingdao TSD Plastic Co., Ltd. (2012). High density polyethylene sheet. http://www.alibaba.com/product-gs/367207590/High_Density_Polyethylene_Sheet.html.

Rabl, A. and Nielsen, C. (1975). Solar ponds for space heating. *Solar Energy*, 17(1):1–12.

Raman, P. and Kishore, V. V. N. (1990). An alternate lining scheme for solar ponds– Results of a liner test rig. *Solar Energy*, 45(4):193–199.

Rezachek, D. (1993). Development of a solar pond system design computational model. In *Proceedings of the 3rd International Conference PROGRESS IN SOLAR PONDS*. University of Texas - El Paso.

Rubin, H. and Benedict, B. A. (1984). Modeling the performance of a solar pond as a source of thermal energy. *Solar Energy*, 33(5):391–395.

Sabetta, F., Pacetti, M., and Principi, P. (1985). An internal heat extraction system for solar ponds. *Solar Energy*, 34(4/5):295–302.

Saxena, A. K., Sugandhi, S., and Husain, M. (2009). Significant depth of ground water table for thermal performance of salt gradient solar pond. *Renewable Energy*, 34:790–793.

SGA (2009). Declaración de impacto ambiental: “modificaciones menores en Minera Spence”.

Sherman, B. S. and Imberger, J. (1991). Control of a solar pond. *Solar Energy*, 46(2):71–81.

Shigeta, M., Watanabe, T., Izawa, S., and Fukunishi, Y. (2009). Incompressible SPH simulation of double-diffusive convection phenomena. *International Journal of Emerging Multidisciplinary Fluid Sciences*, 1(1):1–18.

Shladow, S. G. (1984). The upper mixed zone of a salt gradient solar pond: Its dynamics, prediction and control. *Solar Energy*, 33(5):417–426.

Silva, G. and Almanza, R. (2009). Use of clays as liners in solar ponds. *Solar Energy*, 83:905–919.

Simona AG (2011a). Bruttopreisliste rohre, formteile, armaturen Pe 100, Pe 80, Pe-el.

Simona AG (2011b). Bruttopreisliste rohre, formteile, armaturen PP, PPs, PVDF, E-CTFE.

Sodha, M. S., Kaushik, N. D., and Rao, S. K. (1981). Thermal analysis of three zone solar pond. *Energy Research*, 5:321–340.

Srinivasan, J. (1993). Solar pond technology. *Sadhana*, 18:39–55.

Srithar, K. and Velmurugan, V. (2008). Prospects and scopes of solar pond: A detailed review. *Renewable & Sustainable Energy Reviews*, 12:2253–2263.

Tabor, H. (1980). Non-convecting solar ponds. *Philosophical Transactions of the Royal Society of London. Series A, Mathematical and Physical Sciences*, 295(1414):423–433.

Tabor, H. (1981). Solar ponds. *Solar Energy*, 27(3):181–194.

Tabor, H. and Doron, B. (1990). The Beith Ha'Arava solar pond power plant (SPPP) – Progress report. *Solar Energy*, 45(4):247–253.

Tang, I. A. and Hassab, M. A. (1990). Performance of solar ponds with wind suppressors. *Solar & wind technology*, 7(4):367–377.

U.S. Geological Survey (2010). Copper statistical compendium. http://minerals.usgs.gov/minerals/pubs/commodity/copper/stat/.

Valderrama, C., Gibert, O., Arcal, J., Solano, P., Akbarzadeh, A., Larrotcha, E., and Cortina, J. L. (2011). Solar energy storage by salinity gradient solar pond: Pilot plant construction and gradient control. *Desalination*, 279:445–450.

Viskanta, R. and Tabor, J. S. (1978). Absorption of solar radiation in ponds. *Solar Energy*, 21:17–25.

Wang, J. and Seyed-Yagoobi, J. (1995). Effect of water turbidity on thermal performance of a salt-gradient solar pond. *Solar Energy*, 54(5):301–308.

Wang, Y. F. and Akbarzadeh, A. (1983). A parametric study on solar ponds. *Solar Energy*, 30(6):555–562.

Weather Underground (2012). Weather history for Los Alamos, NM. http://www.wunderground.com/history/.

Weinberger, H. (1964). The physics of the solar pond. *Solar Energy*, 8(2):45–56.

Wenzhou Kaixin Pump Co., Ltd. (2012). 25pg14-5 shield booster circulation pump. http://www.alibaba.com/product-gs/605485856/25PG14_5_Shield_Booster_Circulation_Pump.html.

Zangrando, F. (1980). A simple method to establish salt gradient solar ponds. *Solar Energy*, 25:467–470.

Zehjiang YonJou Technology Co. Ltd. (2012). Is,ih anti-corrosion multistage pump. http://goodpump.en.alibaba.com/product/534727230-200149155/IS_IH_Anti_corrosion_Multistage_Pump.html.

Zhang, Z. M. and Wang, Y. F. (1990). A study on thermal storage of the ground beneath solar ponds by computer simulation. *Solar Energy*, 44(5):243–248.

Zhangjiagang Leader Co. Ltd. (2012). XPS / extruded polystyrene foam board. http://www.alibaba.com/product-gs/641608569/Thermal_Insulation_Boards_XPS.html.

APPENDICES

A Chilean electrical generation matrix between years 2000 and 2009

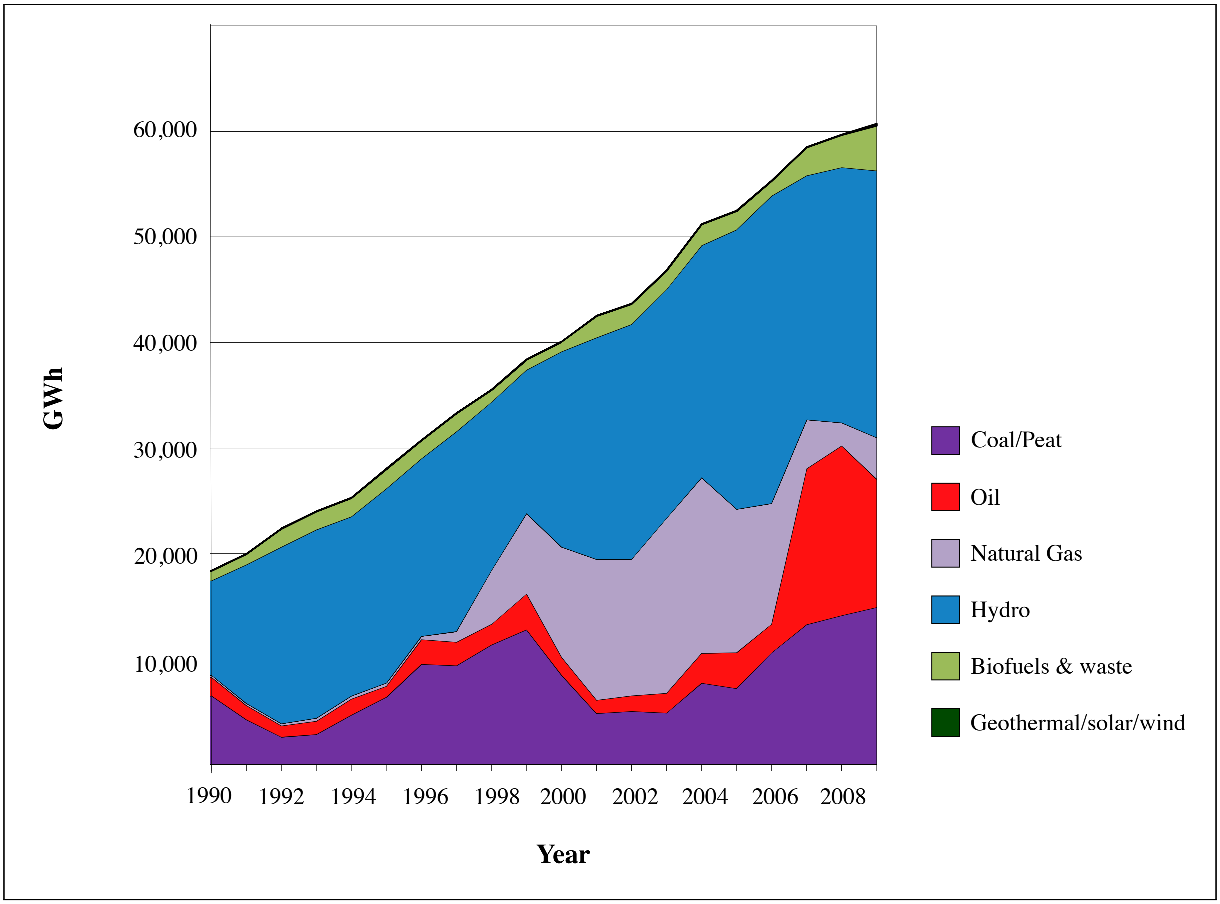

Figure A.1: Evolution of the Chilean electrical generation matrix between years 2000 and 2009 (IEA, 2011)

B In-pond heat exchanger configuration variations

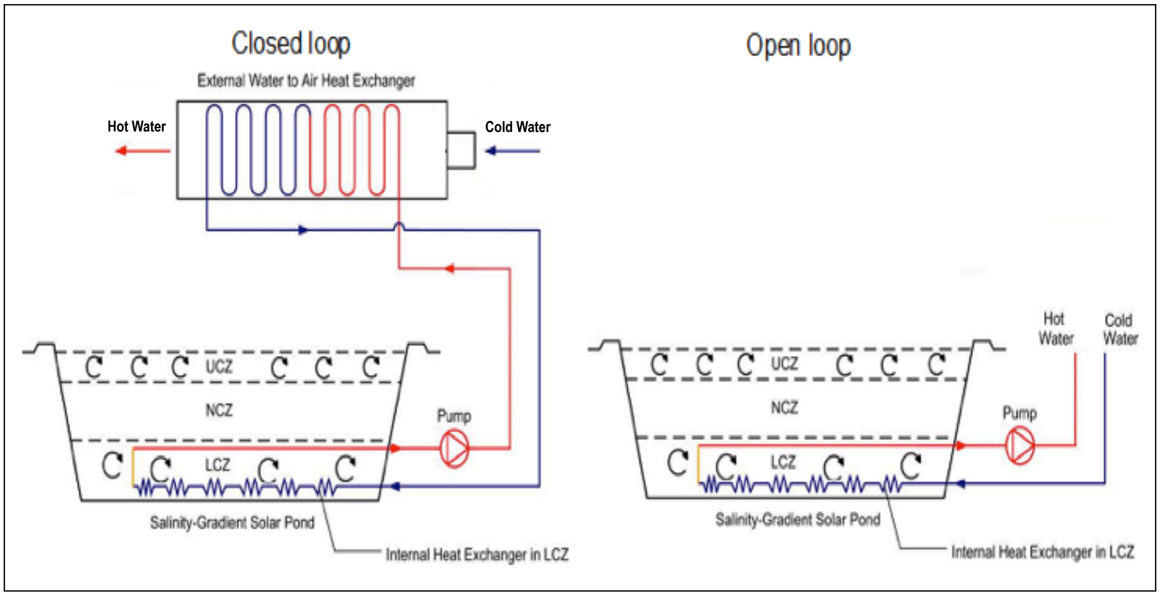

Figure B.1: Closed and open cycle configurations for in-pond heat extraction method (Leblanc et al., 2011)

C Solar pond designs

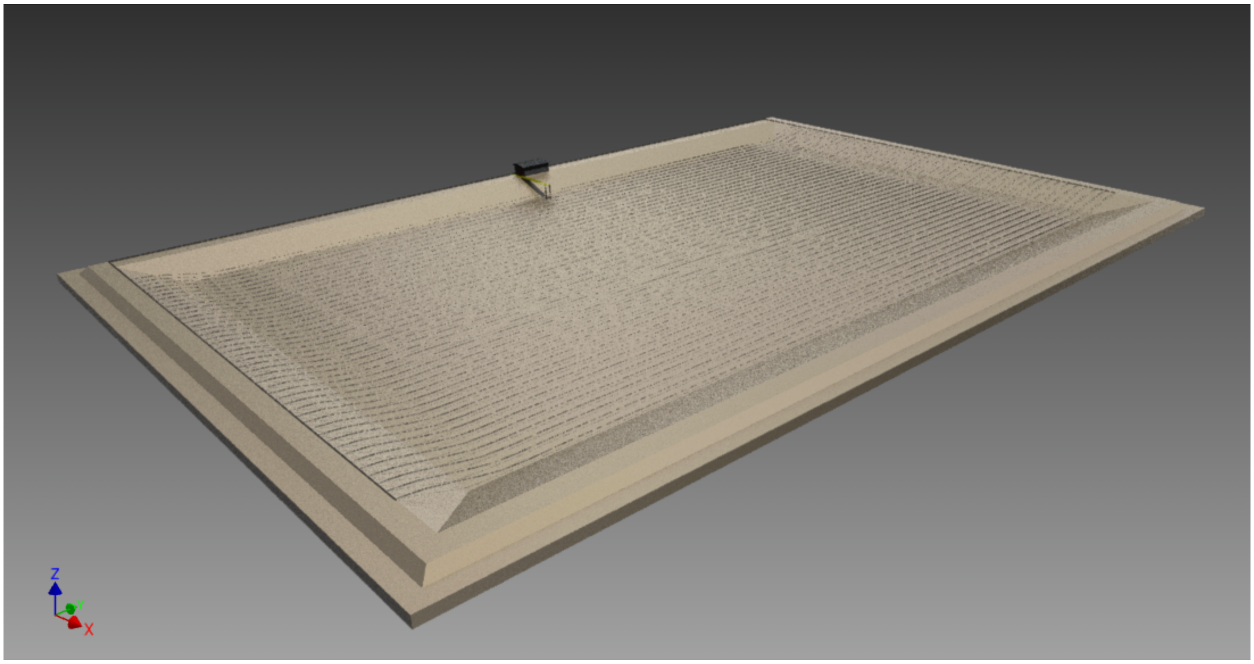

Figure C.1: Solar pond design, single configuration, drained.

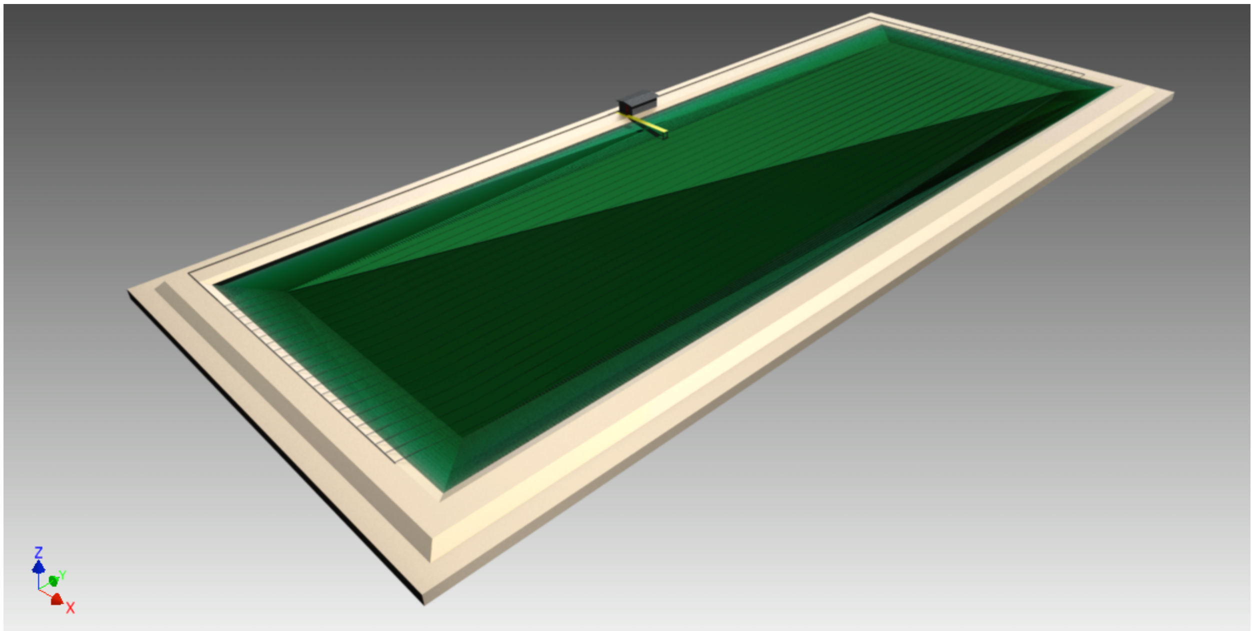

Figure C.2: Solar pond design, modular configuration, filled.

D Discounted cash flows calculation

Table 16: Base case DCF calculation.

	YEAR	0	1	2	3	4	5	6	7	8
PROJECTIONS										
Energy demand	(MWh)		13880	13880	13880	13880	13880	13880	13880	13880
Diesel Consumption	(t)		1159,4	1159,4	1159,4	1159,4	1159,4	1159,4	1159,4	1159,4
COSTS										
Operational										
Diesel	(US$ 0.88 /L)		$1.226.258	$1.226.258	$1.226.258	$1.226.258	$1.226.258	$1.226.258	$1.226.258	$1.226.258
CASH FLOW		$0	$-1.226.258	$-1.226.258	$-1.226.258	$-1.226.258	$-1.226.258	$-1.226.258	$-1.226.258	$-1.226.258

	9	10	11	12	13	14	15	16	17	18	19	20
Energy demand	13880	13880	13880	13880	13880	13880	13880	13880	13880	13880	13880	13880
Diesel Consumption	1159,4	1159,4	1159,4	1159,4	1159,4	1159,4	1159,4	1159,4	1159,4	1159,4	1159,4	1159,4
Diesel	$1.226.258	$1.226.258	$1.226.258	$1.226.258	$1.226.258	$1.226.258	$1.226.258	$1.226.258	$1.226.258	$1.226.258	$1.226.258	$1.226.258
CASH FLOW	$-1.226.258	$-1.226.258	$-1.226.258	$-1.226.258	$-1.226.258	$-1.226.258	$-1.226.258	$-1.226.258	$-1.226.258	$-1.226.258	$-1.226.258	$-1.226.258
											PV	**$-10.439.827**

Table 17: Single solar pond, open salt cycle DCF calculation.

	YEAR	0	1	2	3	4	5	6	7	8
PROJECTIONS										
Energy demand	(MWh)		13880	13880	13880	13880	13880	13880	13880	13880
SP thermal generation	(MWh)		7697	12125	12281	12287	12288	12288	12288	5589
Diesel Consumption	(t)		516	147	134	133	133	133	133	693
COSTS										
Investment										
Solar Pond		$2.293.487	$0	$0	$0	$0	$0	$0	$0	$0
Service Pond		$0	$0	$0	$0	$0	$0	$0	$468.325	$0
Operational										
Solar pond operators salary	(2 employees)	$0	$72.000	$72.000	$72.000	$72.000	$72.000	$72.000	$72.000	$72.000
Electricity	(cUS$ 12 /kWh)	$0	$102	$102	$102	$102	$102	$102	$102	$102
Thermocouples	(1 per week)	$0	$1.560	$1.560	$1.560	$1.560	$1.560	$1.560	$1.560	$1.560
Test Vials	(30 per year)	$140	$140	$140	$140	$140	$140	$140	$140	$140
Diesel	(US$ 0.88 /l)	$0	$546.240	$155.055	$141.309	$140.699	$140.646	$140.646	$140.611	$732.482
Maintenance										
Diffusion make-up salt	(US$ 100 /MT)	$0	$9.321	$9.321	$9.321	$9.321	$9.321	$9.321	$9.321	$9.321
Evaporation make-up water	(US$ 2 /m^3)	$0	$375.539	$375.539	$375.539	$375.539	$375.539	$375.539	$375.539	$375.539
Flushing water	(US$ 2 /m^3)	$0	$14.224	$14.224	$14.224	$14.224	$14.224	$14.224	$14.224	$14.224
Clarity treatment		$0	$1.192	$1.192	$1.192	$1.192	$1.192	$1.192	$1.192	$1.192
Bottom maintenance		$0	$0	$0	$0	$0	$0	$0	$0	$146.108
CASH FLOW		$-2.293.487	$-1.020.319	$-629.134	$-615.387	$-614.777	$-614.724	$-614.724	$-1.083.014	$-1.352.668

	9	10	11	12	13	14	15	16	17	18	19	20
PROJECTIONS												
Energy demand	13880	13880	13880	13880	13880	13880	13880	13880	13880	13880	13880	13880
SP thermal generation	12159	12128	12287	12288	12288	12288	12289	5589	12038	12299	12311	12311
Diesel Consumption	144	146	133	133	133	133	133	693	154	132	131	131
COSTS												
Investment												
Solar Pond	$0	$0	$0	$0	$0	$0	$0	$0	$0	$0	$0	$0
Service Pond	$0	$0	$0	$0	$0	$0	$0	$0	$0	$0	$0	$0
Operational												
Solar pond operators salary	$72.000	$72.000	$72.000	$72.000	$72.000	$72.000	$72.000	$72.000	$72.000	$72.000	$72.000	$72.000
Electricity	$102	$102	$102	$102	$102	$102	$102	$102	$102	$102	$102	$102
Thermocouples	$1.560	$1.560	$1.560	$1.560	$1.560	$1.560	$1.560	$1.560	$1.560	$1.560	$1.560	$1.560
Test Vials	$140	$140	$140	$140	$140	$140	$140	$140	$140	$140	$140	$140
Diesel	$152.016	$154.773	$140.708	$140.664	$140.637	$140.620	$140.593	$732.473	$162.697	$139.657	$138.649	$138.596
Maintenance												
Diffusion make-up salt	$9.321	$9.321	$9.321	$9.321	$9.321	$9.321	$9.321	$9.321	$9.321	$9.321	$9.321	$9.321
Evaporation make-up water	$375.539	$375.539	$375.539	$375.539	$375.539	$375.539	$375.539	$375.539	$375.539	$375.539	$375.539	$375.539
Flushing water	$14.224	$14.224	$14.224	$14.224	$14.224	$14.224	$14.224	$14.224	$14.224	$14.224	$14.224	$14.224
Clarity treatment	$1.192	$1.192	$1.192	$1.192	$1.192	$1.192	$1.192	$1.192	$1.192	$1.192	$1.192	$1.192
Bottom maintenance	$0	$0	$0	$0	$0	$0	$0	$146.108	$0	$0	$0	$0
CASH FLOW	$-626.094	$-628.851	$-614.786	$-614.742	$-614.716	$-614.698	$-614.671	$-1.352.659	$-636.775	$-613.735	$-612.728	$-612.675
											PV	**$-8.667.132**

Table 18: Single solar pond, closed salt cycle DCF calculation.

	YEAR	0	1	2	3	4	5	6	7	8
PROJECTIONS										
Energy demand	(MWh)		13880	13880	13880	13880	13880	13880	13880	13880
SP thermal generation	(MWh)		7702,4	12150,6	12304,2	12310,8	12311,2	12311,4	12311,4	5589
Diesel Consumption	(t)		516	147	134	133	133	133	133	693
COSTS										
Investment										
Solar Pond		$2.293.487	$0	$0	$0	$0	$0	$0	$0	$0
Evaporation Pond		$8.507	$0	$0	$0	$0	$0	$0	$0	$0
Service Pond		$0	$0	$0	$0	$0	$0	$0	$468.325	$0
Operational										
Solar pond operators salary	(2 employees)	$0	$72.000	$72.000	$72.000	$72.000	$72.000	$72.000	$72.000	$72.000
Electricity	(cUS$ 1 /kWh)	$0	$102	$102	$102	$102	$102	$102	$102	$102
Thermocouples	(1 per week)	$0	$1.560	$1.560	$1.560	$1.560	$1.560	$1.560	$1.560	$1.560
Test Vials	(30 per year)	$0	$140	$140	$140	$140	$140	$140	$140	$140
Diesel	(US$ 0.88 /l)	$0	$546.240	$155.055	$141.309	$140.699	$140.646	$140.646	$140.611	$732.482
Maintenance										
Diffusion make-up salt	(US$ 100 /MT)	$0	$9.321	$0	$0	$0	$0	$0	$0	$0
Evaporation make-up water	(US$ 2 /m^3)	$0	$375.539	$375.539	$375.539	$375.539	$375.539	$375.539	$375.539	$375.539
Flushing water	(US$ 2 /m^3)	$0	$14.224	$6.528	$6.528	$6.528	$6.528	$6.528	$6.528	$6.528
Clarity treatment		$0	$1.173	$1.173	$1.173	$1.173	$1.173	$1.173	$1.173	$1.173
Bottom maintenance		$0	$0	$0	$0	$0	$0	$0	$0	$146.108
CASH FLOW		$-2.301.995	$-1.020.300	$-612.098	$-598.351	$-597.742	$-597.689	$-597.689	$-1.065.978	$-1.335.632

	9	10	11	12	13	14	15	16	17	18	19	20
Energy demand	13880	13880	13880	13880	13880	13880	13880	13880	13880	13880	13880	13880
SP thermal generation	12038,4	12299,2	12310,6	12311,2	12311,4	12311,6	12311,9	5589	12038,4	12299,2	12310,6	12311,2
Diesel Consumption	144	146	133	133	133	133	133	693	154	132	131	131
Solar Pond	$0	$0	$0	$0	$0	$0	$0	$0	$0	$0	$0	$0
Evaporation Pond	$0	$0	$0	$0	$0	$0	$0	$0	$0	$0	$0	$0
Service Pond	$0	$0	$0	$0	$0	$0	$0	$0	$0	$0	$0	$0
Solar pond operators salary	$72.000	$72.000	$72.000	$72.000	$72.000	$72.000	$72.000	$72.000	$72.000	$72.000	$72.000	$72.000
Electricity	$102	$102	$102	$102	$102	$102	$102	$102	$102	$102	$102	$102
Thermocouples	$1.560	$1.560	$1.560	$1.560	$1.560	$1.560	$1.560	$1.560	$1.560	$1.560	$1.560	$1.560
Test Vials	$140	$140	$140	$140	$140	$140	$140	$140	$140	$140	$140	$140
Diesel	$152.016	$154.773	$140.708	$140.664	$140.637	$140.620	$140.593	$732.473	$162.697	$139.657	$138.649	$138.596
Diffusion make-up salt	$0	$0	$0	$0	$0	$0	$0	$0	$0	$0	$0	$0
Evaporation make-up water	$375.539	$375.539	$375.539	$375.539	$375.539	$375.539	$375.539	$375.539	$375.539	$375.539	$375.539	$375.539
Flushing water	$6.528	$6.528	$6.528	$6.528	$6.528	$6.528	$6.528	$6.528	$6.528	$6.528	$6.528	$6.528
Clarity treatment	$1.173	$1.173	$1.173	$1.173	$1.173	$1.173	$1.173	$1.173	$1.173	$1.173	$1.173	$1.173
Bottom maintenance	$0	$0	$0	$0	$0	$0	$0	$146.108	$0	$0	$0	$0
CASH FLOW	$-609.059	$-611.815	$-597.750	$-597.706	$-597.680	$-597.662	$-597.636	$-1.335.623	$-619.740	$-596.699	$-595.692	$-595.639
											PV	**$-8.546.075**

Table 19: Modular solar pond, open salt cycle DCF calculation.

	YEAR	0	1	2	3	4	5	6	7	8
PROJECTIONS										
Energy demand	(MWh)		13880	13880	13880	13880	13880	13880	13880	13880
SP thermal generation	(MWh)		7697	12125	12281	12287	12288	12288	12288	7201
Diesel Consumption	(t)		516	147	134	133	133	133	133	558
COSTS										
Investment										
Solar Pond		$2.337.928	$0	$0	$0	$0	$0	$0	$0	$0
Service Pond		$0	$0	$0	$0	$0	$0	$0	$278.492	$0
Operational										
Solar pond operators salary	(2 employees)	$0	$72.000	$72.000	$72.000	$72.000	$72.000	$72.000	$72.000	$72.000
Electricity	(cUS$ 12 /kWh)	$0	$102	$102	$102	$102	$102	$102	$102	$102
Thermocouples	(1 per week)	$0	$1.560	$1.560	$1.560	$1.560	$1.560	$1.560	$1.560	$1.560
Diesel	(US$ 0.88 /l)	$0	$546.240	$155.055	$141.309	$140.699	$140.646	$140.646	$140.611	$590.060
Maintenance										
Diffusion make-up salt	(US$ 100 /MT)	$0	$9.321	$9.321	$9.321	$9.321	$9.321	$9.321	$9.321	$9.321
Evaporation make-up water	(US$ 2 /m^3)	$0	$415.090	$415.090	$415.090	$415.090	$415.090	$415.090	$415.090	$415.090
Flushing water	(US$ 2 /m^3)	$0	$14.224	$14.224	$14.224	$14.224	$14.224	$14.224	$14.224	$14.224
Clarity treatment		$0	$1.317	$1.317	$1.317	$1.317	$1.317	$1.317	$1.317	$1.317
Bottom maintenance		$0	$0	$0	$0	$0	$0	$0	$0	$142.188
CASH FLOW		$-2.337.928	$-1.059.854	$-668.669	$-654.923	$-654.313	$-654.260	$-654.260	$-932.717	$-1.245.861

	9	10	11	12	13	14	15	16	17	18	19	20
Energy demand	13880	13880	13880	13880	13880	13880	13880	13880	13880	13880	13880	13880
SP thermal generation	11948	12272	12287	12288	12288	12288	12289	7201	11948	12272	12287	12288
Diesel Consumption	161	134	133	133	133	133	133	558	161	134	133	133
Solar Pond	$0	$0	$0	$0	$0	$0	$0	$0	$0	$0	$0	$0
Service Pond	$0	$0	$0	$0	$0	$0	$0	$0	$0	$0	$0	$0
Solar pond operators salary	$72.000	$72.000	$72.000	$72.000	$72.000	$72.000	$72.000	$72.000	$72.000	$72.000	$72.000	$72.000
Electricity	$102	$102	$102	$102	$102	$102	$102	$102	$102	$102	$102	$102
Thermocouples	$1.560	$1.560	$1.560	$1.560	$1.560	$1.560	$1.560	$1.560	$1.560	$1.560	$1.560	$1.560
Diesel	$170.657	$142.024	$140.726	$140.646	$140.646	$140.620	$140.505	$590.060	$170.657	$142.024	$140.726	$140.646
Diffusion make-up salt	$9.321	$9.321	$9.321	$9.321	$9.321	$9.321	$9.321	$9.321	$9.321	$9.321	$9.321	$9.321
Evaporation make-up water	$415.090	$415.090	$415.090	$415.090	$415.090	$415.090	$415.090	$415.090	$415.090	$415.090	$415.090	$415.090
Flushing water	$14.224	$14.224	$14.224	$14.224	$14.224	$14.224	$14.224	$14.224	$14.224	$14.224	$14.224	$14.224
Clarity treatment	$1.317	$1.317	$1.317	$1.317	$1.317	$1.317	$1.317	$1.317	$1.317	$1.317	$1.317	$1.317
Bottom maintenance	$0	$0	$0	$0	$0	$0	$0	$142.188	$0	$0	$0	$0
CASH FLOW	$-684.271	$-655.638	$-654.340	$-654.260	$-654.260	$-654.234	$-654.119	$-1.245.861	$-684.271	$-655.638	$-654.340	$-654.260
											PV	**$-8.856.251**

Table 20: Modular solar pond, closed salt cycle DCF calculation.

	YEAR	0	1	2	3	4	5	6	7	8
PROJECTIONS										
Energy demand	(MWh)		13880	13880	13880	13880	13880	13880	13880	13880
SP thermal generation	(MWh)		7702	12151	12304	12311	12311	12311	12311	5969
Diesel Consumption	(t)		516	147	134	133	133	133	133	558
COSTS										
Investment										
Solar Pond		$2.337.928	$0	$0	$0	$0	$0	$0	$0	$0
Evaporation Pond		$9.396	$0	$0	$0	$0	$0	$0	$0	$0
Service Pond		$0	$0	$0	$0	$0	$0	$0	$278.492	$0
Operational										
Solar pond operators salary	(2 employees)	$0	$72.000	$72.000	$72.000	$72.000	$72.000	$72.000	$72.000	$72.000
Electricity	(cUS$ 1 /kWh)	$0	$102	$102	$102	$102	$102	$102	$102	$102
Thermocouples	(1 per week)	$0	$1.560	$1.560	$1.560	$1.560	$1.560	$1.560	$1.560	$1.560
Test vials	(30 per year)	$0	$140	$140	$140	$140	$140	$140	$140	$140
Diesel	(US$ 0.88 /l)	$0	$546.240	$155.055	$141.309	$140.699	$140.646	$140.646	$140.611	$590.060
Maintenance										
Diffusion make-up salt	(US$ 102 /MT)	$0	$10.325	$0	$0	$0	$0	$0	$0	$0
Evaporation make-up water	(US$ 2 /m^3)	$0	$415.090	$415.090	$415.090	$415.090	$415.090	$415.090	$415.090	$415.090
Flushing water	(US$ 2 /m^3)	$0	$14.224	$7.232	$7.232	$7.232	$7.232	$7.232	$7.232	$7.232
Clarity treatment		$0	$1.287	$1.287	$1.287	$1.287	$1.287	$1.287	$1.287	$1.287
Bottom maintenance		$0	$0	$0	$0	$0	$0	$0	$0	$142.188
CASH FLOW		$-2.347.324	$-1.060.969	$-652.467	$-638.720	$-638.111	$-638.058	$-638.058	$-916.514	$-1.229.659

	9	10	11	12	13	14	15	16	17	18	19	20
Energy demand	13880	13880	13880	13880	13880	13880	13880	13880	13880	13880	13880	13880
SP thermal generation	12072	12296	12311	12311	12311	12312	12312	5969	12072	12296	12311	12311
Diesel Consumption	161	134	133	133	133	133	133	558	161	134	133	133
Solar Pond	$0	$0	$0	$0	$0	$0	$0	$0	$0	$0	$0	$0
Evaporation Pond	$0	$0	$0	$0	$0	$0	$0	$0	$0	$0	$0	$0
Service Pond	$0	$0	$0	$0	$0	$0	$0	$0	$0	$0	$0	$0
Solar pond operators salary	$72.000	$72.000	$72.000	$72.000	$72.000	$72.000	$72.000	$72.000	$72.000	$72.000	$72.000	$72.000
Electricity	$102	$102	$102	$102	$102	$102	$102	$102	$102	$102	$102	$102
Thermocouples	$1.560	$1.560	$1.560	$1.560	$1.560	$1.560	$1.560	$1.560	$1.560	$1.560	$1.560	$1.560
Test vials	$140	$140	$140	$140	$140	$140	$140	$140	$140	$140	$140	$140
Diesel	$170.657	$142.024	$140.726	$140.646	$140.646	$140.620	$140.505	$590.060	$170.657	$142.024	$140.726	$140.646
Diffusion make-up salt	$0	$0	$0	$0	$0	$0	$0	$0	$0	$0	$0	$0
Evaporation make-up water	$415.090	$415.090	$415.090	$415.090	$415.090	$415.090	$415.090	$415.090	$415.090	$415.090	$415.090	$415.090
Flushing water	$7.232	$7.232	$7.232	$7.232	$7.232	$7.232	$7.232	$7.232	$7.232	$7.232	$7.232	$7.232
Clarity treatment	$1.287	$1.287	$1.287	$1.287	$1.287	$1.287	$1.287	$1.287	$1.287	$1.287	$1.287	$1.287
Bottom maintenance	$0	$0	$0	$0	$0	$0	$0	$142.188	$0	$0	$0	$0
CASH FLOW	$-668.069	$-639.436	$-638.137	$-638.058	$-638.058	$-638.031	$-637.916	$-1.229.659	$-668.069	$-639.436	$-638.137	$-638.058
											PV	**$-8.743.449**